# ENVIRONMENTAL AND OROGRAPHIC INFLUENCES ON GREAT SALT LAKE-EFFECT PRECIPITATION

by

Trevor Iain Alcott

A dissertation submitted to the faculty of
The University of Utah
in partial fulfillment of the requirements for the degree of

Doctor of Philosophy

Department of Atmospheric Sciences

The University of Utah

August 2012

**The University of Utah Graduate School**

# STATEMENT OF DISSERTATION APPROVAL

The dissertation of **Trevor Iain Alcott**

has been approved by the following supervisory committee members:

| | | |
|---|---|---|
| **W. James Steenburgh** | , Chair | **5-9-12** Date Approved |
| **John D. Horel** | , Member | **5-9-12** Date Approved |
| **Steven Krueger** | , Member | **5-9-12** Date Approved |
| **Lawrence Dunn** | , Member | **5-9-12** Date Approved |
| **Neil Laird** | , Member | **5-18-12** Date Approved |

and by **Kevin D. Perry** , Chair of the Department of **Atmospheric Sciences**

and by Charles A. Wight, Dean of The Graduate School.

ABSTRACT

This dissertation examines the influence of environmental conditions and orographic barriers on the frequency, occurrence, and morphology of Great Salt Lake-Effect (GSLE) precipitation. The analysis consists of the development of an updated event climatology, statistical examination of the factors necessary for events, and two case studies that employ numerical modeling to investigate orographic influences.

For the climatology, events were identified using cool season (16 Sep – 15 May) WSR-88D radar imagery, radiosonde soundings, and MesoWest surface observations from 1997/98 – 2009/10. During this period, the frequency of GSLE events features considerable interannual variability that is more strongly correlated to large-scale circulation changes than lake-area variations. Events are most frequent in fall and spring, with a minimum in January when the climatological lake-surface temperature is lowest. Although forecasters commonly use a 16°C lake–700-hPa temperature difference ($\Delta T$) as a threshold for GSLE occurrence, a seasonally varying threshold based on a quadratic fit to the monthly minimum $\Delta T$ values during GSLE events is more appropriate than a single value. A probabilistic forecast method based on the difference between $\Delta T$ and this seasonally varying threshold, 850–700-hPa relative humidity, and 700-hPa wind direction offers substantial improvement over existing methods. An important consideration for forecasting because of their higher precipitation rates, banded features—with a horizontal aspect ratio of 6:1 or greater—dominate only 20% of the time that GSLE is occurring,

while widespread, nonbanded precipitation is much more common.

The two events examined in the second part of the study (27 Oct 2010 and 5 Nov 2011) produce synergistic interactions between lake-effect and orographic processes. A dramatic decrease in precipitation intensity and coverage occurs in numerical simulations when either the lake or terrain forcings are removed. A foehn-like flow over upstream orography reduces the relative humidity of the incipient low-level airmass and limits the intensity of both events. A convergence zone in the lee of isolated upstream topography is positioned over the north arm of the GSL, and may play a role in organizing the 27 Oct 2010 lake-effect band. Downstream orographic influences are large in both events, and include (1) overlake convergence due to flow stagnation along and/or blocking by the Wasatch Mountains, (2) enhancement of blocking effects due to a horizontal moisture gradient, (3) flow deflection around the Oquirrh Mountains into an orographic concavity, and (4) hydrometeor transport into high terrain. These influences are not unique to the GSL region, and our results suggest applicability to other areas where lake-effect occurs in close proximity to mountain barriers, particularly in the case of small water bodies.

TABLE OF CONTENTS

LIST OF TABLES

ACKNOWLEDGEMENTS

I thank committee members Drs. Jim Steenburgh, John Horel, Steve Krueger, Neil Laird and Larry Dunn for their guidance during the writing of this dissertation, and particularly Jim for his outstanding advising over the past five years. I also appreciate the wealth of input offered by Science Operations Officer Randy Graham of the National Weather Service Forecast Office in Salt Lake City. Fellow graduate students were a perpetual source of advice and suggestions, were instrumental in the SOLPEX field campaign, and made the entire graduate school experience more survivable than I would have ever thought. I gratefully acknowledge the provision of datasets, software and/or computer time and services provided by NCDC, NCEP, NCAR, Unidata, the University of Wyoming, and the University of Utah Center for High Performance Computing. Hobart and William Smith College undergrads Benjamin Albright and Jessica Popp performed the initial lake-effect event identification. Comments from three anonymous reviewers improved the manuscript of Chapter 2 following its submittal as an article to *Weather and Forecasting*. This research is based in part on work supported by a series of grants provided by the NOAA/National Weather Service CSTAR program and grant AGS-0938611 from the National Science Foundation. Any opinions, findings, conclusions or recommendations expressed in this dissertation are those of the author and do not necessarily reflect the views of NOAA, the National Weather Service, or the National Science Foundation.

# CHAPTER 1

# INTRODUCTION

Lake-effect snowstorms associated with the Laurentian Great Lakes have been extensively studied over the past century. Cold-season troughs passing over these large water bodies initiate or enhance convective systems that are often understood and forecasted within a framework of well-established conceptual models. The situation is quite different in northern Utah, where the Great Salt Lake covers an area one-fifth that of Lake Ontario, the smallest of the Great Lakes, yet can produce intense snowstorms impacting transportation along a densely populated urban corridor. Tall and steep mountain ranges flank the shores of the Great Salt Lake (GSL), dwarfing the modest topography of the Midwest and Northeast and contributing to orographic-convective interactions that greatly complicate the forecast process. The role of this or any orographic environment on the evolution of lake-effect precipitation is a topic nearly absent from peer-reviewed literature. This work combines an updated radar climatology with real and idealized numerical modeling to improve our understanding of Great Salt Lake-effect events and the influence of regional orography on their evolution.

The terms “lake effect”, “sea effect” and “ocean effect” (hereafter collectively referred to as lake effect) describe convective precipitation that is initiated or enhanced by the advection of a cold airmass over a relatively warm water body. Lake effect has been documented across the globe on a wide range of spatial scales, from the Sea of

Japan (e.g., Kusunoki et al. 2004), North Channel (Browning 1985) and Laurentian Great Lakes (e.g., Braham and Dungey 1984; Niziol 1987) to smaller water bodies such as the Great Salt Lake (e.g., Carpenter 1993; Steenburgh et al. 2000), Lake Champlain (Payer et al. 2007; Laird et al. 2009a) and the Finger Lakes in New York state (Laird et al. 2009b, 2010). Although interest in small lakes has seen a recent increase, the bulk of the lake-effect literature from the past half century has dealt with the Laurentian Great Lakes, where lake effect is frequent and plays a large role in the regional hydroclimate (Wilson 1977; Braham and Dungey 1984).

The phenomenon of lake-effect over the Great Lakes was studied extensively decades before the advent of radar and numerical modeling. Deducing the process from visual observations, Mitchell (1921; pp 502–503) hypothesized that in the presence of cold air advecting over the relatively warm waters of Lake Michigan, a warm air layer develops over the lake surface and, 'convectional currents and turbulence set in, manifesting themselves in the form of vapor near the western shore… clouds farther out in the lake and, eventually, precipitation in the form of snow flurries where convection and turbulence are sufficient to produce it.'

As cold arctic or polar continental air masses advance into the Great Lakes region, sensible and latent heat fluxes from the warmer water surface create convective instability, typically when the incipient airmass is conditionally stable. Lake-effect snows in the Great Lakes peak in early winter (Niziol et al. 1995), but significant events can occur further into the cool season even when the lakes become largely ice-covered (e.g., Cordeira and Laird 2008). Snow accumulations can exceed 2 m in single events, notably in the Tug Hill Plateau region of western New York, where an average of 450 cm

of snow falls annually. In the various lake-effect snowbelts of the Midwest, lake-atmospheric interactions may be responsible for one-third or more of the annual snowfall (Eichenlaub 1970).

Lake effect is not a uniquely North American phenomenon. Cold air from the Asian continent advecting over the warm waters of the Sea of Japan can yield organized convective bands known for producing large snowfalls in the mountainous Hokkaido and Hokuriko regions of Japan (e.g., Kusunoki et al. 2004). The orographic modification of these bands, which are observed most frequently in December and January, is a subject of discussion in a later section. Individual events, such as occurred on 16 Jan 2001 in the eastern Hokuriku district, have produced 50 cm snow in 12 h (Eito et al. 2005). Lake effect has also been known to occur in association with the Black Sea (e.g. Kindap 2010), and in other regions of the globe where cold air outbreaks interact with warm lake or ocean waters.

Lake effect associated with lakes smaller than the Great Lakes has received increasing attention over the past two decades. Carpenter (1993) used forecaster notes from the Salt Lake City National Weather Service office to create a climatology of lake-effect on the GSL. Carpenter identified 28 Great Salt Lake-effect (GSLE) events from 1971–1988, 9 of which produced more than 30 cm of snowfall. Noting a lack of radar information in the Carpenter (1993) study, Steenburgh et al. (2000) used the KMTX Weather Surveillance Radar 88-Doppler (installed in 1994) to identify 16 "well-defined" and 18 "marginal" GSLE events from September 1994 through May 1998 (8.5 $y^{-1}$), with a mid-winter peak in event frequency. On the still smaller (1127-$km^2$) Lake Champlain, Laird et al. (2009) identified 67 events from the 1997-98 through 2005-06 cold seasons

($7.4\ y^{-1}$). Even Otisco Lake, one of the smaller of the Finger Lakes in central New York at 7.6 $km^2$, has been shown to produce lake-effect snow bands (Laird et al. 2010a). Although typically of smaller spatial extent and shorter duration than Great Lakes storms, events on small lakes can be responsible for large snowfalls, notably 53 cm in 2 days in a Lake Tahoe event and 129 cm downstream from the Great Salt Lake in Bountiful, UT on 25–27 Feb 1998 (N. Laird, personal communication; Steenburgh et al. 2000).

The GSL presents a rare combination of high salt content, small and variable area, complex regional topography and a densely populated downstream shore, together generating a wealth of lake-effect related research questions. The GSL is a terminal lake and has a salt content sufficiently high that, with the exception of small areas adjacent to freshwater inlets, it remains ice-free throughout the winter. Partly due to the lack of ice cover, GSLE events occur throughout the cold season from September through May (Steenburgh et al. 2000). The salt content of the lake, which ranges from 6–15% (by mass) in Gilbert Bay to 27% farther north in Gunnison Bay, yields reductions in saturation vapor pressure of up to 32% relative to fresh water (Dickson et al. 1965). Onton and Steenburgh (2001) found precipitation totals in a numerical simulation of a 7 Dec 1998 GSLE event were 15% lower for actual GSL salt contents than for a fresh water simulation.

As of the time of writing, the GSL is at an elevation of 1279.9 m, with the main body of the lake approximately 40 km from west to east and 125 km from north to south. The elevation of the GSL has fluctuated between 1278 and 1284 m since the mid-19$^{th}$ century, with an area ranging widely from 2460 to 8550 $km^2$ (USGS 2012). An extensive examination has not been conducted regarding the role of lake area in the interannual

variability of lake-effect storm frequency and intensity. The maximum fetch distance is aligned at ~325° from the northwest corner of Gunnison Bay to the Salt Lake Valley on the southeast shore. Correspondingly, the majority of GSLE events occur with a 700-hPa wind direction between 285° and 345° (Steenburgh et al. 2000). Despite large variability in lake area, the maximum fetch distance exhibits only modest variability from ~120 km at the record minimum lake level to ~135 km at the record maximum. Recent lake-effect climatologies for small lakes (e.g., Steenburgh et al. 2000, Laird et al. 2009; 2010a) suggest that the occurrence of lake effect is not entirely dependent on having a Great-Lakes-scale fetch distance of ~200–400 km, and in fact Phillips (1972) shows that greater than 50% of the lake-induced lower atmosphere modification takes place over the first 10–20 km of open water.

The conditions characteristic of GSLE events are similar to those associated with events on the Great Lakes and on small eastern lakes. Steenburgh et al. (2000) found that well-defined GSLE events occurred exclusively with a lake–700-hPa temperature difference ($\Delta T$) of 16°C or greater. This value is analogous to the 13°C lake–850-hPa temperature difference ($\Delta T_{850}$) considered a minimum for lake effect on the Great Lakes (Niziol 1987), in that both situations approximately correspond to a dry-adiabatic lapse rate. Nearly all of the studied Lake Champlain (Laird et al. 2009) and Finger Lakes events (Laird et al. 2010b) met the Great Lakes 13°C threshold, with mean $\Delta T_{850}$ values for various event classes ranging from 16.0°–19.2°C. Steenburgh (2000) examined radiosonde observations at Salt Lake City for all 16 well-defined events and found no cases of a capping inversion or stable layer below 700 hPa (the pressure at lake level is typically near 860 hPa), although the majority of the environmental instability was

typically below 500 hPa. Niziol (1987) suggested that a capping inversion typically existed 1–2 km above the lake surface in Great Lakes events, with inversion heights above 3 km often yielding the strongest convection and thundersnow events.

Niziol (1987) suggested significant (>60°) directional shear in the steering layer could limit the development of lake effect on the Great Lakes, producing only scattered clouds and flurries when the thermodynamic environment was otherwise favorable. Of 29 radiosonde profiles associated with well-defined events in the Steenburgh et al. (2000) study, there was only one case of 800–600-hPa directional shear greater than 60°. In addition to weak directional shear, Kristovich and Laird (1998) suggest upstream moisture also affects the development and intensity of lake effect. On the GSL, Steenburgh et al. (2000) find a minimum 700-hPa relative humidity of 54% during well-defined events, although their radiosonde observations are from a site downstream of the Great Salt Lake and measurements of this airmass could reflect modification by the lake. It remains to be determined specifically which of the conditions identified by Steenburgh et al. (2000) are necessary for the development of GSLE and which are inherent attributes of the typical GSLE thermodynamic and kinematic environment in postfrontal northwest flow.

Passarelli and Braham (1981), and Niziol (1995) highlight the importance of land breeze circulations to the initiation and organization of lake-effect events on the Great Lakes. When the lake is much warmer than the adjacent land surface, a confluence zone and surface pressure trough may develop where offshore flow from one side of a lake opposes either the mean flow or offshore flow from the other side. When instability is sufficient, convective updrafts in this confluence zone strengthen the incoming land

breezes and effectively generate a "self-maintaining" system (Passarelli and Braham 1981). Steenburgh et al. (2000) identified overlake convergence as a characteristic of GSLE events, noting that radar echoes > 10 dBZ were most frequent and focused in a narrow area when the lake was much warmer than the surrounding land stations. Of the 16 well-defined events studied by Steenburgh et al. (2000), 13 initiated between 0000 and 1200 UTC (1700 and 0500 LST) and lake effect was less frequently observed in the afternoon than at other times of the day. Although these findings support a link between land-breeze circulations and diurnal modulation of lake effect, Kristovich and Spinar (2004) also point to a morning maximum in sensible heat fluxes and afternoon drying of the lower boundary layer as factors contributing to changes in lake effect intensity.

Lake effect structures associated with the Great Lakes are typically classified as one of three morphological types (Niziol et al. 1995; Laird et al. 2003): 1) widespread coverage of multiple wind-parallel bands, 2) solitary shoreline or midlake bands, and 3) mesoscale vortices. Widespread coverage events tend to be associated with shorter, cross-lake fetch distances, while shoreline and midlake bands extend along the long axis of oblique lakes such as Lakes Ontario and Erie (Niziol et al. 1995). Shoreline and midlake bands are essentially the same structures but their positions are affected by the locations of land-breeze convergence zones. Laird et al. (2003a; 2003b; 2004) used climatological and numerical techniques to determine environmental factors affecting lake effect morphology and through scale analysis identified the ratio of wind speed to fetch distance ($U/L$) as an important quantity. In idealized modeling experiments, the lowest values of $U/L$ (<~0.02 m $s^{-1}$ $km^{-1}$) produced mesoscale vortices, intermediate values (~0.04–0.08 m $s^{-1}$ $km^{-1}$) shoreline bands, and the highest values (>0.08 m $s^{-1}$ $km^{-1}$)

widespread coverage (Laird et al. 2003b), although these idealized results did not yield outstanding skill when used to produce hindcasts of lake-effect mode (Laird et al. 2004). Neither Carpenter (1993) nor Steenburgh et al. (2000) attempted to determine controls on the morphology of GSLE events, but Steenburgh et al. (2000) found a frequent occurrence of both solitary wind-parallel midlake bands and broad precipitation shields.

A unique of the environment around the GSL is the presence of large topographic features upstream, downstream and adjacent to the lake. The Raft River and Albion Mountains extend from west to east along the Utah-Idaho border, ~20–30 km upstream of the lake in the majority of GSLE events. These mountains present 1600 m of relief above both upstream areas of the Snake River Plain and downstream areas surrounding the lake. The Wasatch Mountains are roughly parallel to the eastern shore of the GSL, with a crest height of 2700 m near the Idaho border to 3450 m immediately east of the Salt Lake Valley. Although lower than the crest of the Wasatch Mountains, the Oquirrh Mountains separate the Tooele and Salt Lake Valleys south of the GSL and rise 1300 m in elevation within only 6 km of the shore. GSLE bands often directly impact the Wasatch and Oquirrh Mountains (Yeager et al. 2013) and have contributed to substantial mountain snowfall totals, notably on 23–26 Nov 2001, when two GSLE events yielded a total of 5.54 cm snow-water-equivalent at Alta, UT (Steenburgh et al. 2003). The complex topography around the GSL suggests the consideration of a variety of potential lake-effect-orographic interactions, including but not limited to:

1) drying of the upstream airmass in the lee of the Raft River mountains,

2) lee convergence along the north arm of the GSL,

3) enhancement or other modification of land breezes due to thermally-driven downslope and canyon flows,

4) blocking by the Wasatch Mountains,

5) enhancement of GSLE due to flow into an orographic concavity (e.g., the Salt Lake Valley), and,

6) forced orographic ascent over the Wasatch Mountains.

Although knowledge is limited regarding the effects these various processes have on lake effect, past work on mountain waves, thermally-driven flows and orographic convection provide valuable insights that will now be discussed.

The development and intensity of lake-effect precipitation is particularly sensitive to relative humidity in the upstream environment (Laird and Kristovich 2003; Alcott et al. 2012) and thus any loss of water vapor through precipitation during flow over upstream terrain (e.g., Varney 1920; Sinclair 1994; Smith et al. 2003; and Smith et al. 2005, who describe the "airmass transformation" that occurs with larger barriers such as the Sierra Nevada and Cascade ranges) is likely to diminish the intensity of GSLE events. Mass (1981), Mass and Dempsey (1985), and Chien and Mass (1997) describe the formation of a convergence zone in the lee of the Olympic Mountains, a scenario that is perhaps replicated on a small scale near the Raft River and Albion Mountains, northwest of the GSL. This convergence zone may help to initiate GSLE convection, analogous to leeside orographic precipitation bands simulated by Cosma et al. (2002).

In the limited work on orographic modification of lake effect, the focus has typically been on the enhancement of convective bands due to ascent over downstream barriers. Hill (1971) estimated a 25–50 cm increase in annual snowfall per 100 m

increase in elevation downstream of the Great Lakes (Niziol 1987), notably in the Tug Hill Plateau region of New York. Niziol (1995) suggests that orography may act to create and/or modify convergence zones over the lake, while orographic lift on the lee shore increases the inversion height and leads to more intense precipitation. Hjelmfelt (1992) ran numerical simulations at 8-km horizontal resolution and showed that even modest relief along the Michigan coast (~200 m) increased precipitation rates by a factor of 2 or more, although the role played by land breezes in the initiation and distribution of precipitation was much greater. Orographic influences on lake effect can be large when precipitation structures interact with higher and steeper barriers. Two-dimensional sensitivity experiments conducted on simulated ocean-effect snow bands over the mountainous regions of Japan show a significant increase in precipitation over land for a barrier of more 1000 m versus a barrier of less than 700 m (near cloud base), partly due to an increase in precipitation efficiency from 40% to 80% (Saito et al. 2004).

The role played by downstream orography may involve more than enhancement of precipitation through forced ascent over a barrier. Rotunno and Ferretti (2001) present a situation where a strong horizontal moisture gradient leads to one airmass that has a low static stability and flows over a mountain range, while an adjacent airmass, drier and more stable, is forced around the barrier. The region where these two airmasses intersect is an area of convergence that yields increased precipitation rates. A similar situation is hypothesized for GSLE events, where northwest flow originating over the lake has a near-moist-neutral profile and flows over the Wasatch Mountains, while drier air north and east of the lake is blocked by the mountains and forced southward, yielding confluence in the Salt Lake Valley where the two airstreams meet. A numerical

simulation of the 7 Dec 1998 GSLE event by Steenburgh and Onton (2001) lends some support to this hypothesis, with northwest flow over the GSL and a strip of northerly flow to the east of the lake, adjacent to (and presumably blocked by) the Wasatch Mountains.

Thermally driven flows further complicate the wind pattern in GSLE events. Nocturnal katabatic flows could strengthen a land breeze and affect the location and intensity of overlake convergence. On Lake Tekapo (New Zealand), McGowan et al. (1996) find that steep mountains adjacent to the shore develop downslope flows that gradually initiate nocturnal land breezes when synoptic-scale flows are weak. A similar, combined katabatic-land-breeze scenario may develop over the GSL, the diagnosis of which will require analysis of the extensive MesoWest observation network (Horel et al. 2002), along with high-resolution numerical simulations.

This work explores the unique combination of complex orography and lake-effect convection on the Great Salt Lake in three stages: 1) development of an updated and expanded radar-based event climatology, 2) analysis of environmental factors associated with GSLE, and 3) analysis of orographic influences in GSLE storms. The final stage will utilize both observational and numerical modeling approaches. Through this progression the aim is to establish a record of the occurrence and structure of Great Salt Lake-effect events, identify environmental conditions necessary for GSLE, and finally to determine the extent to which orography modifies the evolution of GSLE. This dissertation consists of two major sections, the first (**Chapter 2**) focused on the updated climatology and relevant environmental factors, and the second (**Chapter 3**) describing orographic influences in two GSLE events. Findings from both studies are summarized in **Chapter 4**.

# CHAPTER 2[1]

# GREAT SALT LAKE EFFECT PRECIPITATION: OBSERVED FREQUENCY, CHARACTERISTICS AND ASSOCIATED ENVIRONMENTAL FACTORS


## Abstract

This climatology examines the environmental factors controlling the frequency, occurrence, and morphology of Great Salt Lake-Effect (GSLE) precipitation events using cool season (16 Sep – 15 May) WSR-88D radar imagery, radiosonde soundings, and MesoWest surface observations from 1997/98 – 2009/10. During this period, the frequency of GSLE events features considerable interannual variability that is more strongly correlated to large-scale circulation changes than lake area variations. Events are most frequent in fall and spring, with a minimum in January when the climatological lake-surface temperature is lowest.

Although forecasters commonly use a 16°C lake–700-hPa temperature difference ($\Delta T$) as a threshold for GSLE occurrence, GSLE was found to occur in winter when $\Delta T$ was only 12.4°C. Conversely, GSLE is associated with much higher values of $\Delta T$ in the


[1] Chapter 2 is reprinted from Alcott et al. (2012). 

fall and spring. Therefore, a seasonally varying threshold based on a quadratic fit to the monthly minimum $\Delta T$ values during GSLE events is more appropriate than a single threshold value. A probabilistic forecast method based on the difference between $\Delta T$ and this seasonally varying threshold, 850–700-hPa relative humidity, and 700-hPa wind direction offers substantial improvement over existing methods, although forecast skill is diminished by temperature and moisture errors in operational models.

An important consideration for forecasting because of their higher precipitation rates, banded features—with a horizontal aspect ratio of 6:1 or greater—dominate only 20% of the time that GSLE is occurring, while widespread, nonbanded precipitation is much more common. Banded periods are associated with stronger low-level winds and a larger lake-land temperature difference.

## Introduction

Lake- and ocean-effect precipitation occurs across the globe on a wide range of spatial scales, from the Sea of Japan (e.g., Kusunoki et al. 2004), North Channel (e.g., Browning et al. 1985), and Laurentian Great Lakes (e.g., Braham and Dungey 1984; Niziol 1987; Niziol et al. 1995) to smaller water bodies like the Great Salt Lake (e.g., Carpenter 1993; Steenburgh et al. 2000), Lake Champlain (e.g., Payer et al. 2007; Laird et al. 2009a) and the Finger Lakes (e.g., Laird et al. 2009b, 2010). These precipitation events occur when the interaction of a cold continental or Arctic airmass with a relatively warm body of water initiates or enhances moist convection. Although smaller water bodies have received more attention in the past decade (e.g., Steenburgh et al. 2000; Steenburgh and Onton 2001; Onton and Steenburgh 2001; Payer et al. 2007; Laird et al. 2009a, 2009b, 2010), most lake-effect research has been concerned with the Laurentian

Great Lakes (hereafter, the Great Lakes). In comparison, the Great Salt Lake (GSL) presents a unique situation where lake-effect events are associated with a meso-β-scale hypersaline lake adjacent to steep topographic barriers and a densely populated urban corridor. Past investigations of the GSL-effect (GSLE) have been limited by lack of radar data (i.e., Carpenter 1993) or a short study period (i.e., Steenburgh et al. 2000). GSLE storms remain a challenge to predict, and forecasters continue to struggle to identify the primary factors that contribute to their initiation and varied evolution.

A terminal lake, the GSL is approximately 120 by 45 km, with a maximum depth of only 10 m, and an area ranging from 2500 to 8500 $km^2$ over the past half-century, approximately $1/30^{th}$ to $1/10^{th}$ the area of Lake Superior (Fig. 2.1; USGS 2012). Despite the relatively small size of the GSL, multiple lake-effect precipitation events occur annually. These events can reduce visibilities to ¼ mi (400 m) or less, and have produced snow accumulations of over 60 cm at both valley and mountain sites (e.g., Carpenter 1993; Steenburgh et al. 2000; Steenburgh 2003). The GSL is flanked on its east and south shores by Interstates 15 and 80, respectively, and the adjacent Wasatch Front urban corridor has a population of more than 1.5 million (U.S. Census Bureau 2011).

Several factors contribute to the development of lake-effect precipitation over the Great Lakes—including a stationary or slow moving 500-hPa low to the north, a strong flow of relatively cold air over the lakes, a long fetch, and a sufficient temperature differential between the low-level air mass and the lakes (Wiggin 1950; Niziol 1987; Niziol et al. 1995). Steenburgh et al. (2000) found analogous conditions in GSLE events, with precipitation accompanied by a lake–700-hPa temperature difference of at least

16°C (approximately equivalent to a dry adiabatic lapse rate), a lack of stable layers below 700-hPa, weak low-level directional shear (<60° in the 800–600 hPa layer, with the GSL at ~870 hPa), and a large lake–land temperature difference, the latter favoring land-breeze convergence over the GSL. Although Steenburgh et al. (2000) established a parameter space in which GSLE events can occur, they did not attempt to differentiate between the conditions associated with GSLE and non-GSLE periods.

Near the Great Lakes, lake-effect precipitation has been classified using the following morphological categories: 1) widespread coverage of wind-parallel horizontal roll convection (e.g., Kristovich and Laird 1998), 2) shoreline bands (e.g., Hjelmfelt and Braham 1983), 3) solitary midlake bands (e.g., Passarelli and Braham 1981), and 4) mesoscale vortices (e.g., Laird 1999). Laird et al. (2003a) group shoreline and midlake bands together since both morphologies tend to occur with similar environmental conditions. Using a series of idealized model simulations, Laird et al. (2003b) identified the parameter $U/L$, the ratio of wind speed to fetch, as a discriminator between lake-effect morphologies. However, an investigation of historical lake-effect events in the Great Lakes showed $U/L$ had somewhat limited value in discriminating observed events (Laird and Kristovich 2004). Steenburgh et al. (2000) found GSLE precipitation structures ranging from a broad area of precipitation southeast of the lake to a single narrow midlake band, with no cases of multiple wind parallel bands such as those observed over the Great Lakes. It remains to be determined whether environmental factors can be used to discriminate morphological lake-effect transition zones on smaller lakes such as the GSL.

Our research seeks to better understand the environmental factors that affect the frequency, morphology and coverage of GSLE precipitation, and differentiate between GSLE and non-GSLE periods, through the development and analysis of a 13-year cool-season radar-derived climatology. We will show that GSLE events occur primarily within specific ranges of instability, moisture and kinematic parameters, whereas considerable overlap exists between the conditions associated with different GSLE morphologies. Furthermore, we identify deficiencies in current forecast techniques, and present a new probabilistic approach using lake-air temperature difference, low-level relative humidity, and wind direction.

## Data and Methods

### Event Identification

GSLE events were identified visually using lowest-tilt (0.5°) radar reflectivity images from the Weather Surveillance Radar–1988 Doppler (WSR–88D) at Promontory Point, UT (Fig. 2.1; KMTX), for the cool seasons (16 Sep–15 May) of 1997/98–2009/10. Radar data were obtained from the National Climatic Data Center Hierarchical Data Storage System, where temporal coverage was poor during 1994–1996 and greatly improved by fall 1997. Hence we began our examination later than Steenburgh et al (2000), who used 1994/95–1997/98. Following Laird et al. (2009a), GSLE events were defined as periods $\geq$ 1 h where precipitation features were: (a) coherent and quasi-stationary with a distinct connection to the lake, (b) shallow and distinguishable from large, transitory "synoptic" features, and (c) exhibiting increasing depth and/or intensity in the downwind direction.

Although topography partially or completely blocks a large portion of the 0.5°

radar tilt east of the Wasatch Range, horizontal coverage over the Great Salt Lake, northern Wasatch Front and Salt Lake Valley is nearly uninhibited (Wood et al. 2003). Radar data is available in two forms, with base data in Level II files and base and derived products in Level III files (Crum et al. 1993). While Level II data are frequently missing (for 14.9% of the time during the study period), level III data are missing for less than 3% of the time. Out of 3162 total days, 26 days (0.8%) contained both missing Level II and Level III radar data for time periods longer than the average duration of a GSLE event (11.3 h).

## Surface and Upper Air Observations

Hourly surface observations were obtained from the MesoWest database at the University of Utah (Horel et al. 2002). Table 2.1 lists the basic and derived upper-air variables used in the analysis, all of which come from soundings launched by the National Weather Service Forecast Office at Salt Lake City International Airport (KSLC; see Fig. 2.1 for location). These data were obtained from the University of Wyoming archive and were interpolated to 10-hPa vertical intervals. A sounding is considered to be associated with GSLE if GSLE occurs within a 3-h window centered on the sounding time (e.g., at any point between 1030 and 1330 UTC for a 1200 UTC sounding). Of 5737 soundings analyzed, 140 were associated with GSLE (45 at 0000 UTC and 95 at 1200 UTC). The small size of this sample relative to the number of GSLE events reflects both the use of a narrow, 3-h window for verification, and the occurrence of some short-duration (< 6-h) GSLE events. In the majority of GSLE events, KSLC was downstream of the GSL and the observed atmospheric profiles likely represent air in the lower troposphere that experienced some modification over the GSL. However, the nearest

upstream upper-air observation sites (Boise, ID and Elko, NV) are 250–350 km from the GSL and are of limited value due to the existence of intervening mountain ranges.

For two-dimensional analyses of the large-scale patterns associated with GSLE, upper-air composites of the GSLE environment were produced using data from the North American Regional Reanalysis (NARR; Mesinger et al. 2006), obtained from the National Climatic Data Center.

## Event Classification

Through visual inspection of radar images, we classified both the *context* (i.e., the general character of GSLE events relative to other precipitation features), and the *morphology* (i.e., the convective mode) of GSLE every 3 h. Context was classified as follows: 1) isolated areas of lake-effect precipitation, with no other precipitation falling in the surrounding valleys (i.e., *pure* lake effect); 2) lake-effect precipitation concurrent with other primarily convective precipitation features; 3) lake-effect precipitation concurrent but not co-located with synoptic/transient stratiform precipitation; and (4) localized lake-enhancement of transient precipitation. Examples of these four categories are shown in Fig. 2.2. GSLE frequently coincides with orographic precipitation over the Wasatch and Oquirrh Mountains. No attempt was made to classify combined lake-orographic precipitation scenarios as a separate category, since nearby mountain ranges are often directly downstream of the GSL, and may be within a lake-effect precipitation structure.

GSLE morphology was classified as either (1) *nonbanded*, (2) *mixed mode* (i.e., primarily *nonbanded* with some banded features, or (3) *banded* (see examples in Fig. 2.3). Bands were defined as contiguous areas of reflectivity ≥ 10 dBZ with a horizontal aspect ratio of at least 6:1 (Weckwerth et al. 1997), which is approximately equal to the

aspect ratio of the main body of the GSL, aiding visual classification of the radar data. While the morphology was determined every 3 h during GSLE events, analysis of the environmental conditions affecting the morphology was performed only for 3-h periods surrounding upper-air sounding launches at KSLC (e.g., 1030–1330 UTC for a 1200 UTC sounding).

## Great Salt Lake Temperature

A consistent record of daily GSL temperature observations does not currently exist. Steenburgh et al. (2000) used data from bimonthly USGS bucket samples to construct a climatological curve for GSL temperature. Crosman and Horel (2010) later applied cloud and land masks to surface temperature data from the Moderate Resolution Imaging Spectroradiometer (MODIS) and obtained a representative GSL temperature by calculating the median temperature of all unmasked pixels. Although an improvement over the use of bucket samples, MODIS temperature data were not available on many days due to frequent obscuration of the lake by clouds. Crosman and Horel (2010) constructed a curve similar to that of Steenburgh et al. (2000) by fitting a cosine function to points representing the average temperature of all available images in each month.

For this study, a third climatology curve was calculated by applying a Fourier fit between the Julian day and MODIS-observed temperatures in the Crosman and Horel (2010) dataset, given by

$$T_{\text{LAKE-CLIMO}} = 13.8 - 11.9 * \cos(0.0172j) - 4.09 * \sin(0.017j) - 0.93 * \cos(0.0344j) + 0.677 * \sin(0.0344j) - 0.482 * \cos(0.0516j) - 0.600 * \sin(0.0516j), \quad (2.1)$$

where $T_{\text{LAKE-CLIMO}}$ is the climatological GSL temperature (°C) on Julian day $j$. This curve better captures the winter minimum and the rate of increase in spring (Fig. 2.4). The shallow waters of the GSL are prone to significant departures from climatology, as shown when MODIS-derived GSL temperatures (medians calculated as in Crosman and Horel 2010) are compared to the three curve fits. To address this issue we adapted the approach of Carpenter (1993) by calculating a linear relationship between the GSL temperature anomaly (relative to our Fourier-fit climatology curve) and the anomaly in 7-day mean temperature at KSLC. KSLC 7-day mean temperature anomalies were computed relative to a Fourier-fit estimation of the 1997–2010 KSLC temperature climatology, given by

$$T_{\text{KSLC-CLIMO}} = 11.3 - 13.4 * \cos(0.0167j) - 3.29 * \sin(0.0167j) + 0.472 * \cos(0.0334j) + 1.90 * \sin(0.0334j), \quad (2.2)$$

where $T_{\text{KSLC-CLIMO}}$ is the climatological 7-day mean temperature (°C) at KSLC ending on Julian day $j$. The relationship between GSL temperature and KSLC temperature,

$$T_{\text{LAKE}} = T_{\text{LAKE-CLIMO}} + 0.39 * ( T_{\text{KSLC}} - T_{\text{KSLC-CLIMO}} ), \quad (2.3)$$

where $T_{\text{LAKE}}$ is the estimated GSL temperature (°C), $T_{\text{LAKE-CLIMO}}$ is the climatological GSL temperature (°C), $T_{\text{KSLC}}$ is the 7-d mean temperature (°C) at KSLC, and $T_{\text{KSLC-CLIMO}}$ is the climatological 7-d mean temperature (°C) at KSLC, was calculated from a dependent set containing 80% of the 1700 MODIS images, and then tested on an independent set containing the remaining 20%. This methodology yields a substantial improvement in GSL temperature estimation over any previous climatology curve (Table 2.2) and has been applied to the entire 13-cool-season study period to produce a

continuous GSL-temperature record. Errors in temperature estimation were less than 2°C in 82% of the independent test cases and were largest in spring when Crosman and Horel (2010) found the largest diurnal ranges (Table 2.2). Most of the large regression errors in spring were daytime underestimates and nighttime overestimates.

## Results

### Frequency, Characteristics and Seasonality of GSLE Events

During the 13 cool seasons, 149 GSLE events were identified. The mean event duration was 11.3 h, although events lasted an average of 3.1 h longer in fall (16 Sep – 30 Nov) and winter (1 Dec – 28 Feb) than in spring (1 Mar – 15 May). There were 11 events with durations ≥ 24 h, up to a maximum of 48 h on 25–27 Nov 2001. GSLE context was distributed as follows: isolated areas of lake-effect precipitation, 1780 h (62% of the time GSLE was observed); lake effect concurrent with other primarily convective precipitation features, 356 h (20%); lake effect concurrent but not co-located with synoptic/transient stratiform precipitation, 178 h (10%); and localized lake-enhancement of transient precipitation, 142 h (8%).

There exists large interannual variability in event frequency, with the number of events per cool season averaging 13 but ranging from 3–20 (Fig. 2.5a). Cool seasons with fewer trough days (e.g., days when the 500-hPa relative vorticity exceeds $2 \times 10^{-5}$ $s^{-1}$ at Salt Lake City at 0000 and 1200 UTC) are generally marked by fewer GSLE events, (Fig. 2.5b [shown as standardized anomalies, i.e., departures from the study period mean expressed as number of the standard deviations]; correlation coefficient $R = 0.64$), as are cool seasons with a lower mean lake–700-hPa temperature difference ($R = 0.62$). Although the sample size is small, the null hypothesis of zero true correlation can be

rejected with at least 98% confidence ($P < 0.02$) for both of these factors. The GSL ranged in area between 3100–4500 km$^2$ over the study period (USGS 2012), but over this interval, the relationship between GSL area and GSLE frequency is weaker than for the aforementioned synoptic factors (Fig. 2.5b; $R = 0.34$, $P = 0.26$). These results suggest atmospheric factors have a larger impact on interannual variability in GSLE frequency than do fluctuations in the lake area. From 1861–2011, the area of the GSL varied between 2460 and 8550 km$^2$ (USGS 2012), a much larger range that could have had a more measureable effect on GSLE frequency, but an analogous event climatology does not exist for longer time periods.

The seasonal event distribution is bimodal, with the frequency highest from mid-Oct to mid-Dec and in early Apr (Fig. 2.6a). Our results differ from those of Steenburgh et al. (2000), who found a mid-winter peak in event frequency for 1994–1998. This discrepancy might reflect the smaller sample size (34 events versus 149 in the current study), differing techniques for event identification and/or missing radar data shortly after KMTX became operational in 1994.

## Factors Affecting the Occurrence of GSLE

### Lake–Atmosphere Temperature Difference

The mean lake–700-hPa temperature difference ($\Delta T$) for GSLE events is 20.7°C, but in 9 of the 143 GSLE soundings $\Delta T$ was less than 16°C, with these occurrences confined to 4 Dec – 12 Feb. This finding indicates that $\Delta T$ corresponding to a dry-adiabatic lapse rate (e.g., Holroyd 1971; Niziol 1987; Carpenter 1993; Niziol et al. 1995; Steenburgh et al. 2000) is not an absolute minimum for the occurrence of GSLE, which calls into question the use of this threshold in operational forecasting. On 5 Jan 2007,

GSLE produced snowfall totals of 10-20 cm in the Salt Lake and Tooele Valleys with a $\Delta T$ of only 14.1°C. The lowest $\Delta T$ associated with GSLE in this study was 12.4°C at 1200 UTC 2 Jan 2000, when the sounding exhibited a moist-adiabatic lapse rate and near-saturated conditions up to the tropopause (Fig. 2.7). High values of $\Delta T$ were reached much less often during winter due to a lake temperature remaining near 0°C, a result that may partially explain the winter minimum in event frequency.

Although low-$\Delta T$ (<16°C) values could arise from errors in the regression estimation of lake temperature, the mean absolute error in lake temperature estimation during Dec–Feb was only 0.9°C, so this contribution is expected to be small. Alternatively, events featuring low-$\Delta T$ values could be due to erroneous attribution of precipitation features to lake-effect processes. A re-examination of the radar data for these events suggests that this source of error is unlikely. Parcel theory suggests that when the boundary layer profile is saturated and moist adiabatic, any $\Delta T$ greater than a *moist*-adiabatic lapse rate could be sufficient for overlake flow to yield a buoyant surface parcel. For 700-hPa temperatures of –20° and 0°C, this lapse rate would be achieved at a $\Delta T$ of 13° and 10°C, respectively.

The monthly minimum $\Delta T$ associated with GSLE (hereafter $\Delta T_{\text{min}}$) exhibits a marked seasonal variation, decreasing from 21°C in Sep to 12°C in Jan, and increasing again to 22°C in May (Fig. 2.6b). While occasionally observed in winter when $\Delta T$ was from 12–18°C, GSLE only occurred in Apr–May when $\Delta T$ exceeded 19°C. Long nights and widespread snow cover in winter may be more favorable for persistent land-breeze circulations and overlake convergence, which could contribute to the development of GSLE with relatively low values of $\Delta T$. However, the mean lake–land temperature

difference is in fact smaller during winter GSLE events, and the seasonal dependence of $\Delta T_{\min}$ more likely reflects the climatological relationship between $\Delta T$ and the synoptic environment.

In winter $\Delta T$ rarely reaches as high as the 16°–19°C range, but the composite NARR analysis for all winter soundings (with or without GSLE) when $16° \leq \Delta T \leq 19°C$ shows a 500-hPa trough, 700-hPa flow from the northwest, and high low-level relative humidity in the GSL region—all conditions that Steenburgh et al. (2000) indicate are favorable for GSLE (Fig. 2.8a-b). During Apr–May, $\Delta T$ exceeds 16°C in 41% of all soundings, but the composite analysis for all soundings with $16° \leq \Delta T \leq 19°C$ in Apr–May shows near zonal flow at 500 and 700 hPa, and drier air at low-levels (Fig. 2.8c-d). Thus while values of $\Delta T$ considered marginally sufficient for GSLE occurs very frequently in the warmer months, these values were often accompanied by high environmental stability, unfavorable flow and inadequate low-level moisture.

Fitting a quadratic curve to the monthly minimum $\Delta T$ points ($\Delta T_{\min}$) is a simple approach to developing a seasonally varying threshold as an alternative to a single value (e.g., 16°C). The equation for this best fit curve (plotted in Fig. 2.6b) is:

$$\Delta T_{\min} = 0.0006425d^2 - 0.152d + 21.35 \text{ (°C)}, \qquad (2.4)$$

where $d$ is the number of days since 15 Sep. The remainder of the manuscript will refer to $\Delta T - \Delta T_{\min}$ as the excess of $\Delta T$ (hereafter $\Delta T_{\text{excess}}$) in a given sounding above this seasonally varying threshold. By this method $\Delta T_{\text{excess}} \geq 0°C$ is considered the minimum "requirement" for GSLE, although some values associated with GSLE are slightly less than zero due to an imperfect $\Delta T_{\min}$ curve fit.

Figure 2.9 shows $\Delta T_{\text{excess}}$ values for four types of soundings: a) soundings with no lake effect; b) soundings with lake effect; c) soundings with *pure* lake effect (i.e., when no transient or non-lake-effect precipitation is present) and a *low coverage* of radar echoes ≥10 dBZ (< 80 km$^2$, the lowest tertile of this parameter); and d) soundings with pure lake effect and a *high coverage* of radar echoes ≥10 dBZ (> 600 km$^2$, the highest tertile). The median value of $\Delta T_{\text{excess}}$ for all soundings with GSLE was 4.0°C, with a maximum of 11.4°C. Large values of $\Delta T_{\text{excess}}$ do not indicate an increased likelihood of high-coverage events, and in fact the median $\Delta T_{\text{excess}}$ for high-coverage events (3.4°C) is significantly lower than for low-coverage events (5.5°C).

When considering only $\Delta T_{\text{excess}}$, there remains a large portion of soundings where the seasonally varying threshold is exceeded but no lake effect occurs. In fact, no GSLE was observed within 12 h for 77% of soundings with $\Delta T_{\text{excess}} \geq 0$°C, a result that necessitates the examination of additional environmental variables.

Environmental Moisture

The presence of low-level moisture is crucial for GSLE events, and low relative humidity values may preclude the development of lake-effect precipitation even when $\Delta T_{\text{excess}}$ is large. Among moisture variables, the largest difference in the medians for GSLE and non-GSLE soundings, given $\Delta T_{\text{excess}} \geq 0$°C, was found for 850–700-hPa layer-mean relative humidity ($RH_{850–700}$), and the median $RH_{850–700}$ for GSLE soundings (81%) was considerably higher than for non-GSLE soundings (67%) (Fig. 2.10a). High-coverage GSLE soundings exhibited a slightly higher median $RH_{850–700}$ than low-coverage soundings (83% versus 77%, respectively; significant at the 90% level). There were no GSLE soundings with a $RH_{850–700} < 53\%$ and no high-coverage GSLE soundings

with a $RH_{850–700} < 60\%$. Only 27% of soundings with a $\Delta T_{excess} \geq 8°C$ and a $RH_{850–700} < 60\%$ were associated with GSLE, versus 72% for a $\Delta T_{excess} \geq 8°C$ and a $RH_{850–700} \geq 60\%$ (not shown), indicating that a large value of $\Delta T_{excess}$ was often insufficient for GSLE when dry air was present at low levels.

The median values of mid-level (700–500-hPa) layer-mean relative humidity ($RH_{700–500}$; Fig. 2.10b) were also significantly higher for GSLE (71%) than for non-GSLE soundings (56%). However, several GSLE soundings had $RH_{700–500}$ less than 30%, perhaps reflecting the existence of GSLE convection primarily in the lowest 1–3 km above ground. Soundings with high-coverage GSLE showed very high median $RH_{700–500}$ relative to low-coverage soundings, with a median of 76% and no values less than 55%. Occurrences of high-coverage GSLE therefore tend to depend on the presence of both low- and mid-level moisture.

The importance of moisture for lake-effect precipitation is underscored by past research. Steenburgh et al. (2000) found no GSLE events with a 700-hPa relative humidity less than 54%, and Kristovich and Laird (1998) highlight the dependence of lake-effect cloud formation on upstream moisture conditions, suggesting that moisture might play a key role in determining whether GSLE convection develops. Around the Great Lakes, where upstream moisture is perhaps less important due to longer overlake fetch, neither Niziol (1987) nor Niziol et al. (1995) include relative humidity when describing significant parameters in the operational forecast process for lake-effect snow.

Stability and Wind Shear

The median 700–500-hPa lapse late for GSLE was 6.7 K $km^{-1}$, significantly greater than that of non-GSLE soundings (5.7 K $km^{-1}$; Fig. 2.10c), suggesting that mid-

level environmental stability was also important for the *occurrence* of GSLE, given the presence of sufficient $\Delta T_{\text{excess}}$. The median 700–500-hPa lapse late for high-coverage events (7.3 K km$^{-1}$) greatly exceeded the median for low-coverage events (5.3 K km$^{-1}$), indicating a tendency for more widespread precipitation to occur when conditional instability was present at mid-levels.

Soundings with GSLE were associated with lower median values of 800–600-hPa[2] directional shear than were non-GSLE soundings (25° versus 37°, respectively; Fig. 2.10d). The median value for high-coverage events (21°) was also significantly lower than for low-coverage events (31°). However, high values of directional shear (>60°) alone did not decrease the likelihood of GSLE, given that modest lake-induced instability and low-level moisture were present. For $\Delta T_{\text{excess}} \geq 4$°C and $\text{RH}_{850–700} \geq 60\%$, GSLE was associated with 32% of soundings with 800–600-hPa directional shear ≤ 60°, and 30% of soundings with directional shear > 60° (not shown). In fact there were eight soundings where GSLE was associated with directional shear ≥ 90° and 700-hPa wind speeds > 5 m s$^{-1}$, including one high-coverage event. These results conflict with findings in previous studies. Niziol (1987) found from discussions with forecasters that low-level (surface–700-hPa) wind shear greater than 60° tended to prevent lake-effect convection on the Great Lakes. Steenburgh et al. (2000), who studied a much smaller sample of GSLE events, found only one radiosonde observation during a GSLE event where 800–600-hPa directional shear exceeded 60°.

[2] This layer was chosen following Steenburgh et al. (2000) who describe it as the "steering layer".

Wind Direction

The median wind direction in GSLE soundings was 315° at 700-hPa, and 325° at 800-hPa, with the latter value corresponding to the direction of maximum fetch over the GSL. The GSL has a large horizontal aspect ratio, and fetch is dramatically reduced for wind directions approaching southwest or northeast, from a peak of ~125 km at 325° and 145° down to ~40 km at 235° and 55°. Accordingly, for $\Delta T_{\text{excess}} \geq 0$ and $\text{RH}_{850\text{–}700} \geq 55\%$, 22% of soundings with 700-hPa wind directions between 292° and 7° were associated with GSLE, versus only 9% with winds outside this range (Fig. 2.11). In all of the soundings examined by Steenburgh et al. (2000), the 700-hPa wind direction was between 285° and 5°, but our analysis of a larger sample of radar data found that the 700-hPa wind direction was outside of this range in 16% of soundings associated with GSLE. While at some of these sounding times weak GSLE convection was present in unusual areas [e.g., the far northern Wasatch Front, Skull Valley and the West Desert region (see Fig. 2.1 for locations)], wind speeds were otherwise very light ($< 3$ m s$^{-1}$) and lower-level flow (i.e., at 800 hPa) was still from the west, northwest or north.

Lake–Land Temperature Difference

The timing of GSLE events suggests the importance of land breeze convergence for convective initiation. There was a strong tendency for GSLE to initiate in the overnight hours and end during the day, a characteristic shared by 73% of events. The median start time for events was 3.1 h after sunset (Fig. 2.12a), and the median end time was 2.7 h after sunrise (Fig. 2.12b). Only 12 events (8%) initiated between noon and sunset. GSLE was most likely to be present between 1100 and 1500 UTC (0400–0800 LST), and least likely between 2100 and 0100 UTC (1400–1800 LST; Fig. 2.12c), times

that correspond, respectively, to the maximum and minimum values of lake-land temperature difference[3] ($\Delta T_{\text{LAKE–LAND}}$).

On days with GSLE, the median values of $\Delta T_{\text{LAKE–LAND}}$ were 7.8°, 4.5°, and 6.1°C at mid-afternoon, and 12.2°, 8.3°, and 11.7°C in the early morning, during the fall, winter, and spring, respectively (Fig. 2.12d). The maxima in $\Delta T_{\text{LAKE–LAND}}$ clearly correspond with the times of peak GSLE frequency (i.e., Fig. 2.12c). There were no times over the entire period of record where GSLE occurred with a lake temperature colder than the mean temperature at adjacent land stations (i.e., $\Delta T_{\text{LAKE–LAND}} < 0$). On a lake that is warmer than the adjacent land surface, a confluence zone and surface pressure trough may develop where offshore flow from one side of a lake opposes either the mean flow or offshore flow from the other side (e.g., Hjelmfelt 1990). When instability is sufficient, convective updrafts in this confluence zone strengthen the incoming land breezes and effectively generate a "self-maintaining" system (Passarelli and Braham 1981). The concept of land breezes driving convective initiation brings forth difficulty in the determination of cause and effect, in that convective structures may induce their own local wind field. However, the large magnitude of $\Delta T_{\text{LAKE–LAND}}$ on days with GSLE, and the timing of events suggest that mesoscale thermally driven flows are likely to play a significant role in initiating and maintaining GSLE.

The diurnal modulation of GSLE exhibits marked seasonal differences that appear counterintuitive in the context of thermally-driven circulations. Several GSLE events persist throughout the day in fall, and the frequency of GSLE in winter has almost no

[3] The lake–land temperature difference ($\Delta T_{\text{LAKE–LAND}}$) is computed as the difference between the GSL temperature and the mean 2-m temperature at 11 mesonet sites surrounding the GSL (see Fig. 2.1 for locations). Positive values of $\Delta T_{\text{LAKE–LAND}}$ indicate that the GSL is warmer than land stations.

dependence on time of day. However, GSLE is very rare in spring between 1900 and 0200 UTC (1200–1900 LST), despite median $\Delta T_{\mathrm{LAKE–LAND}}$ values that are comparable to or greater than those in the fall. Analysis of radar imagery reveals a tendency for events in spring to transition to disorganized land-based convection during the afternoon, despite atmospheric profiles favorable for GSLE. Conversely, winter events often retain organized lake-effect convection through the afternoon hours with much lower values of $\Delta T_{\mathrm{LAKE–LAND}}$. We attribute this seasonal contrast to the presence of more intense daytime surface heating in spring, when the solar zenith angle is smaller, which yields deeper mixing and drier air at low levels by mid-afternoon. On days with GSLE, 1200 UTC (0500 LST) profiles of median relative humidity were similar in fall, winter and spring (Fig. 2.13). At 0000 UTC (1700 LST), however, the median relative humidity in the lowest levels (i.e., 850-800-hPa) dropped to 40-50% in spring, versus 60% in fall and winter. Several studies point to decreasing upstream low-level relative humidity due to afternoon turbulent mixing as a mechanism for the diurnal modulation of lake-effect precipitation (e.g., Lavoie 1972; Hjelmfelt 1990; Kristovich and Spinar 2005). Although the KSLC sounding site is generally downstream of the GSL in the majority of GSLE events, the observed daytime drying at low levels is likely to be occurring throughout the surrounding region, thus removing the crucial moisture ingredient necessary for lake-effect precipitation.

## GSLE Morphology

GSLE precipitation covers a wide range of convective modes, from widespread areas of nonbanded structures to narrow, solitary bands. We found nonbanded precipitation was the most frequently observed mode, comprising 54% of the 605

analyzed 3-h GSLE periods. The remaining periods were characterized as either mixed mode (25%; primarily nonbanded with some embedded linear features), or banded (20%). Banded periods were less common in the winter months (Dec-Feb), comprising only 10% of GSLE periods, than in fall (27%) or spring (25%). Steenburgh et al. (2000) suggested a link between midlake banded structures and the existence of thermally driven convergence, and accordingly we found a significant increase in frequency of banded GSLE when $\Delta T_{\mathrm{LAKE-LAND}}$ was large. For $\Delta T_{\mathrm{LAKE-LAND}} < 4$°C, only 13% of GSLE periods were banded, versus 30% for $\Delta T_{\mathrm{LAKE-LAND}} > 14$°C.

The morphology differentiation factor $U/L$ (wind speed divided by fetch) proposed by Laird and Kristovich (2003b) in the Great Lakes shows some utility for GSLE, although the classification scheme in the current study differs considerably from the one used in the Great Lakes. Values of $U/L$ were calculated using the 800-hPa wind speed, the level at which the relationship between $U/L$ and GSLE mode was found to be strongest. High values of $U/L$ (i.e., > 0.08 m $s^{-1}$ $km^{-1}$) are associated with banded GSLE (Fig. 2.14a), features that are similar in structure to midlake and shoreline bands observed over the Great Lakes. High values of $U/L$ in the Great Lakes instead tend to favor widespread coverage events. Low values of $U/L$ in the Great Lakes (< 0.05 m $s^{-1}$ $km^{-1}$) are typical of mesoscale vortex events, but only one GSLE period showed any signs of an organized circulation (not shown). There exists, however, substantial overlap in the conditions associated with nonbanded and banded periods, indicating that the relationship between $U/L$ and GSLE mode is weak.

Banded convection in the boundary layer is generally associated with stronger low-level winds and speed shear than nonlinear or cellular convection (Kristovich 1993;

Kristovich et al. 1999; Weckwerth et al. 1997). Model sensitivity studies of a Great Lakes lake-effect event by Cooper et al. (2000) showed a shift from horizontal rolls to cellular convection when boundary layer wind speeds were reduced below 5 m $s^{-1}$, while variations in the thermodynamic profile had little impact on convective mode. Similarly, banded periods in this study occurred with significantly stronger 750-hPa wind speeds than did nonbanded structures (Fig. 2.14b; the level at which this relationship was strongest). The median speed shear in the lowest 100 hPa was also slightly higher for banded GSLE, but the difference was not significant at the 90% level. The relationship between GSLE morphology and lake-induced or environmental instability was weak, but banded GSLE tended to occur with slightly greater values of $\Delta T$ and low-level lapse rate (not shown). Overall the environmental conditions associated with nonbanded versus banded GSLE convection exhibit only minor differences, but there is some tendency for banded GSLE to dominate when $U/L$ is high, low level wind speeds are strong, and $\Delta T_{\mathrm{LAKE-LAND}}$ is large.

## Implications for Operational Weather Forecasting

Operational forecasting of GSLE currently involves identifying periods of west–north flow at 700 hPa and lake–700-hPa temperature difference ($\Delta T$) exceeding 16°C, with minimal consideration of low-level moisture (Larry Dunn, National Weather Service, personal communication). This existing forecasting methodology rarely results in a missed event (i.e., a high probability of detection), but yields a high false alarm rate. Table 2.3 illustrates the utility of various forecast parameters, where $N_{\mathrm{soundings}}$ is the total number of soundings that meet the given criteria, $N_{\mathrm{GSLE}}$ is the number of soundings that meet the criteria and are associated with GSLE, FO is the frequency of occurrence of

GSLE, FAR is the false-alarm rate, and POD is the probability of detection. Of 881 soundings with $\Delta T \geq 16$°C and a 700-hPa wind direction between 270° and 360°, only 200 (22%) were associated with GSLE within 12 h, a fairly generous verification window. Although much more likely at high values of $\Delta T$ (i.e., $\geq 22$°C), GSLE was still only associated with only 38% of soundings satisfying this condition. Consideration of other parameters (e.g., weak 800–600-hPa directional shear and the absence of stable layers or temperature inversions in the lowest 150 hPa) suggested by Steenburgh et al. (2000) leads to some improvement, but the false alarm rate remains high (Table 2.3).

Based on our revised climatology, the use of a seasonally varying $\Delta T$ threshold reduces the number of these false alarms due to a higher threshold in the early fall and spring. Further improvement results from including a $RH_{850–700}$ threshold of 55%. Nonetheless, forecasting of GSLE or other relatively rare events (such as tornadic thunderstorms) is often limited by the use of exclusively deterministic techniques such as the exceedance of specific thresholds (e.g., Murphy 1991).

We propose a probabilistic forecast methodology for GSLE that considers $\Delta T_{excess}$, $RH_{850–700}$, and 700-hPa wind direction. Figure 2.15a shows the fraction of soundings associated with GSLE for ranges of both $\Delta T_{excess}$ and $RH_{850–700}$, regardless of 700-hPa wind direction, calculated over intervals of 1°C and 8%, respectively. Given a good forecast of environmental conditions, and a lake temperature calculated using the approach described in section 2, Fig. 2.15a translates to the probability of GSLE. Thus, the probability of GSLE increases with increasing $\Delta T_{excess}$ and $RH_{850–700}$, and exceeds 80% for $\Delta T_{excess} \geq 8$°C and $RH_{850–700} \geq$ 90%. Plots for 290°–360° and 1°–289° 700-hPa wind directions are shown in Figs. 2.15b and c, respectively, indicating higher

probabilities of GSLE in 290°–360° flow than for other wind directions, regardless of the magnitudes of $\Delta T_{excess}$ and $RH_{850–700}$.

One difficulty in forecasting the occurrence of GSLE by the aforementioned probabilistic method stems from uncertainty in operational model forecasts of low-level relative humidity and 700-hPa temperature. North American Mesoscale (NAM) model forecasts for KSLC on days when GSLE was possible ($\Delta T_{excess} \geq 0$ at 0000 or 1200 UTC) were skewed to higher values of $RH_{850-700}$ (Fig. 2.16), and slightly warmer values of 700-hPa temperature (not shown) relative to observed RAOB soundings. The mean bias in these 24-h forecasts of $RH_{850-700}$ and 700-hPa temperature were 10% and 0.7°C, respectively. Absolute errors in $RH_{850-700}$ averaged 12% and exceeded 25% in several cases. Absolute errors in 700-hPa temperature were small however, and averaged only 1.1°C. Assuming NAM biases have not changed, these results suggest that direct application of Fig. 2.15 (utilizing NAM output) in operations could overestimate the probability of GSLE.

Another forecast concern is the GSL temperature estimate. In general, the GSL temperature can be reliably estimated from recent MODIS data, but long periods of mostly cloudy to overcast conditions preclude the retrieval of recent temperature data and provide an additional source of error in calculating $\Delta T_{excess}$. When MODIS data are unavailable or unreliable, forecasters can employ the technique for estimating GSL temperature described in section 2 of this paper, acknowledging that errors can occasionally exceed 2°C.

The relationship between $\Delta T$ and the coverage of GSLE was weak, and our results alternatively suggest considering 700–500-hPa lapse rate and $RH_{700–500}$. Although low-

coverage (< 80 $km^2$) GSLE can occur even at high values of both variables, major GSLE (> 640 $km^2$) occurred almost exclusively with a 700–500-hPa lapse rate ≥ 5.5 K $km^{-1}$ and $RH_{700–500} \geq 60\%$ (Fig. 2.17). Given that GSLE is expected, values outside of this phase space can indicate to forecasters that the areal coverage of precipitation is likely to be low.

## Summary

Radar data was examined over a 13-year period to identify 149 GSLE events affecting northern Utah. Large interannual variability exists in event frequency, and is more strongly correlated with atmospheric factors than the area of the GSL. GSLE events exhibited fall and spring peaks in frequency, and were less common in mid-winter when the lake temperature fell to near freezing. In the coldest months, GSLE occurred at values of lake–700-hPa temperature difference ($\Delta T$) less than the 16°C (Steenburgh et al. 2000) or 17°C (Carpenter 1993) thresholds often used in operational forecasting. In fall and spring, however, GSLE occurs only at much higher values of $\Delta T$. A seasonally varying threshold ($\Delta T_{min}$), calculated from a quadratic curve fit to the monthly minimum $\Delta T$ values for GSLE soundings, is considered more appropriate for use in forecast applications than a single threshold value. The minimum requirement for GSLE is thus a positive value of $\Delta T_{excess}$, equal to $\Delta T - \Delta T_{min}$.

A large positive $\Delta T_{excess}$ does not guarantee that GSLE convection will initiate, and our results suggest that low-level moisture is a crucial secondary ingredient. Higher relative humidity and steeper lapse rates at mid levels, while not crucial for GSLE development, are associated with high-coverage events. Alignment of the 700-hPa flow along the long axis of the GSL (i.e., near 325°) also substantially increases the likelihood

of lake effect above that observed with westerly or northeasterly flow. GSLE only occurred when the lake temperature was greater than the average temperature at adjacent land stations, suggesting the importance of thermally driven land breezes in the initiation and maintenance of convection. Lastly, large values of low-level directional shear were not found to inhibit GSLE formation when thermodynamic profiles were otherwise favorable.

Banded GSLE, which tends to be associated with higher snowfall rates and thus greater transportation impacts, was more common than widespread, nonbanded convection when low-level (750-hPa) winds were strong (> 7 m $s^{-1}$) and when the lake temperature was much warmer than adjacent land stations. However, it remains an issue that there is substantial overlap in the conditions associated with these GSLE modes. Sensitivity to low-level moisture and wind direction, and vague distinctions between morphological parameter spaces perpetuate the difficulties of forecasting the occurrence and mode of these storms.

Based on these results, we propose a probabilistic approach to forecasting the occurrence of GSLE that considers $\Delta T_{excess}$, 850–700-hPa relative humidity, and 700-hPa wind direction (see Fig. 2.15). Although not a perfect indicator, the 700–500-hPa lapse rate and 700–500-hPa relative humidity can be used to anticipate the areal coverage of GSLE precipitation. This methodology has the potential to reduce false alarms encountered with the existing techniques, particularly through consideration of low-level moisture and a seasonally varying threshold for $\Delta T$. The National Weather Service in Salt Lake City has recently incorporated findings from this study into their operations. Forecast errors in current 12-km operational NAM (and other) model guidance provide

an additional source of uncertainty, and could lead forecasters to overestimate (in the case of the NAM) the probability of GSLE. Nonetheless, implementation of the new probabilistic method offers the potential for improved prediction of events that can have significant transportation impacts along the Wasatch Front urban corridor.

Table 2.1

Sounding and surface variables used in the analysis.

| Variable | Levels |
|---|---|
| temperature, geopotential height, relative humidity, zonal and meridional wind components, wind speed, wind direction, fetch, potential temperature, equivalent potential temperature, lake-air temperature difference | surface, 850-100 hPa in 10 hPa intervals |
| mean relative humidity, mean wind speed, lapse Rate, vertical gradient in potential temperature, vector wind shear magnitude, speed shear, directional shear | all 50-550-hPa intervals between 850 and 300 hPa |
| Locomotive Springs relative humidity | 2 m |
| lake-land temperature difference (mean of 11 sites surrounding the GSL) | 2 m |

Table 2.2

Performance of four methods for estimating GSL temperature, evaluated for an independent set of 240 MODIS overpasses.

| $T_{Lake}$ Method | $R^2$ | RMSE (°C) | Bias (°C) |
|---|---|---|---|
| Steenburgh et al. (2000) | 0.88 | 7.06 | -1.39 |
| Crosman and Horel (2010) | 0.90 | 4.35 | -0.30 |
| Fourier Fit | 0.92 | 3.51 | -0.10 |
| KSLC Anomaly Regression | 0.95 | 2.31 | -0.11 |

Table 2.3

Utility of various forecast parameters

| Condition | $N_{soundings}$ | $N_{GSLE}$ | FO | FAR | POD |
|---|---|---|---|---|---|
| $\Delta T \geq 16°C$ | 1432 | 275 | 19% | 81% | 91% |
| $\Delta T \geq 22°C$ | 365 | 120 | 33% | 67% | 47% |
| $\Delta T \geq 25°C$ | 38 | 19 | 50% | 50% | 12% |
| $\Delta T \geq 16°C$ & Shear < 60° | 936 | 194 | 21% | 79% | 72% |
| $\Delta T \geq 16°C$ & Shear < 60° & No stable layers | 619 | 145 | 23% | 77% | 55% |
| $\Delta T_{excess} \geq 0$ | 1134 | 264 | 23% | 77% | 96% |
| $\Delta T_{excess} \geq 2$ | 673 | 203 | 30% | 70% | 79% |
| $\Delta T_{excess} \geq 0$ & $RH_{850\text{-}700} > 55\%$ | 884 | 236 | 27% | 73% | 94% |
| $\Delta T_{excess} \geq 2$ & $RH_{850\text{-}700} > 55\%$ | 529 | 189 | 36% | 64% | 79% |

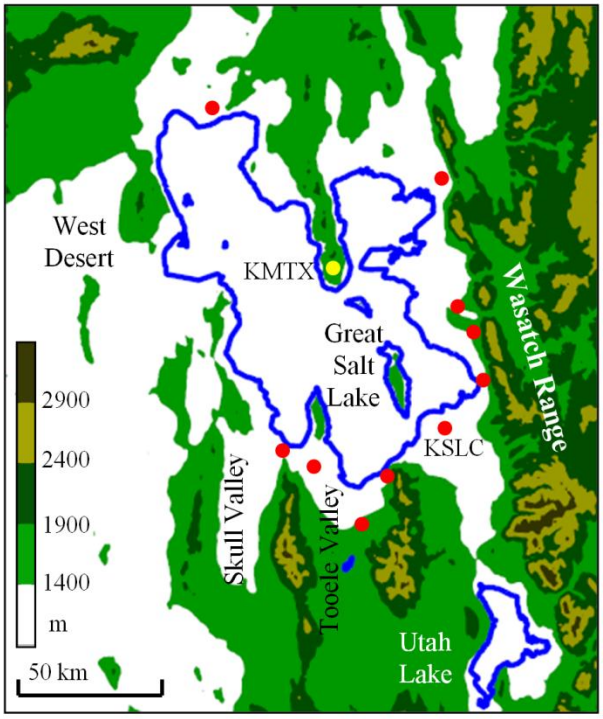


Fig. 2.1. Topography and landmarks of the study region; red dots mark the locations of mesonet stations used in the calculation of $\Delta T_{\mathrm{LAKE-LAND}}$.

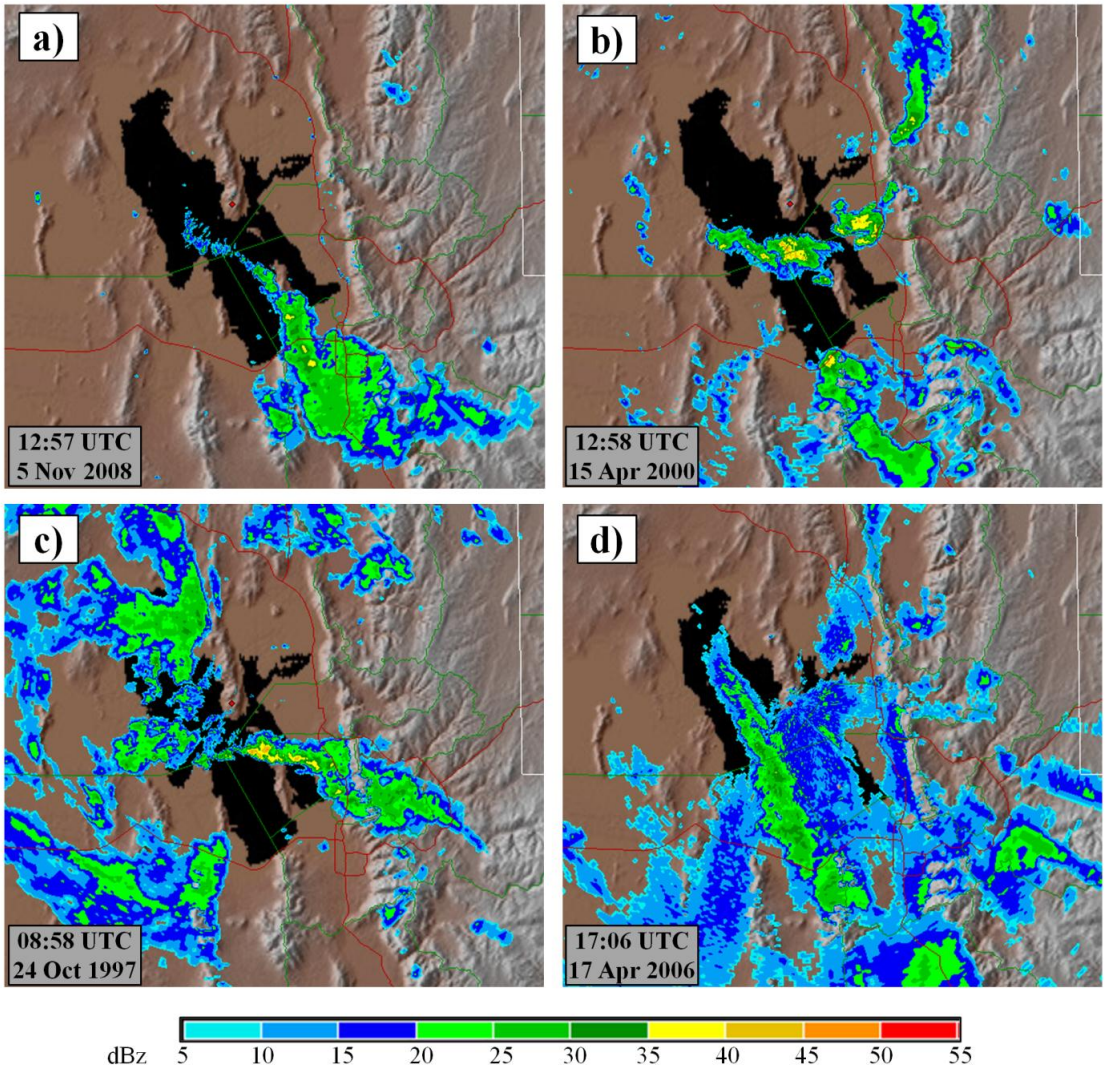


Fig. 2.2. Examples of Great Salt Lake-effect precipitation context: (a) isolated areas of lake-effect precipitation, with no other precipitation falling in the surrounding valleys; (b) lake-effect precipitation concurrent with other primarily convective precipitation features; (c) lake-effect precipitation concurrent but not co-located with synoptic/transient stratiform precipitation, and (d) localized lake-enhancement of transient precipitation.

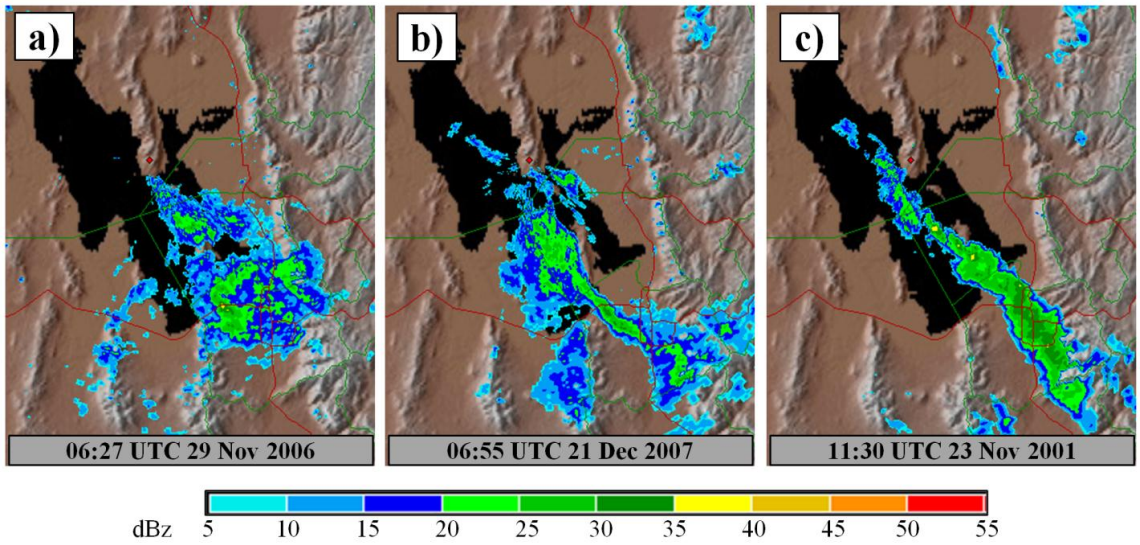


Fig. 2.3. Examples of GSLE morphology categories: (a) nonbanded; (b) mixed-mode; (c) banded.

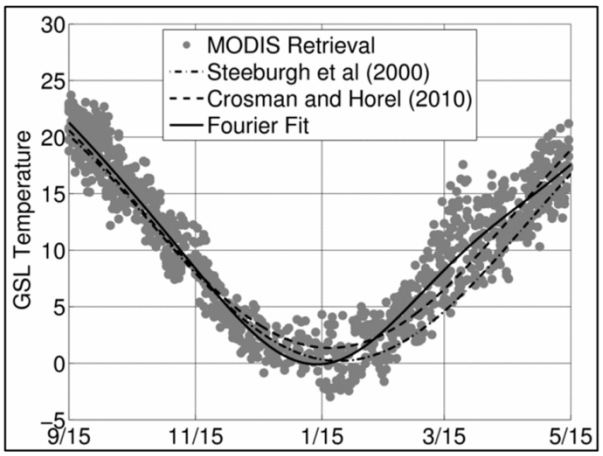


Fig. 2.4. MODIS GSL temperature versus three climatological curve fits.

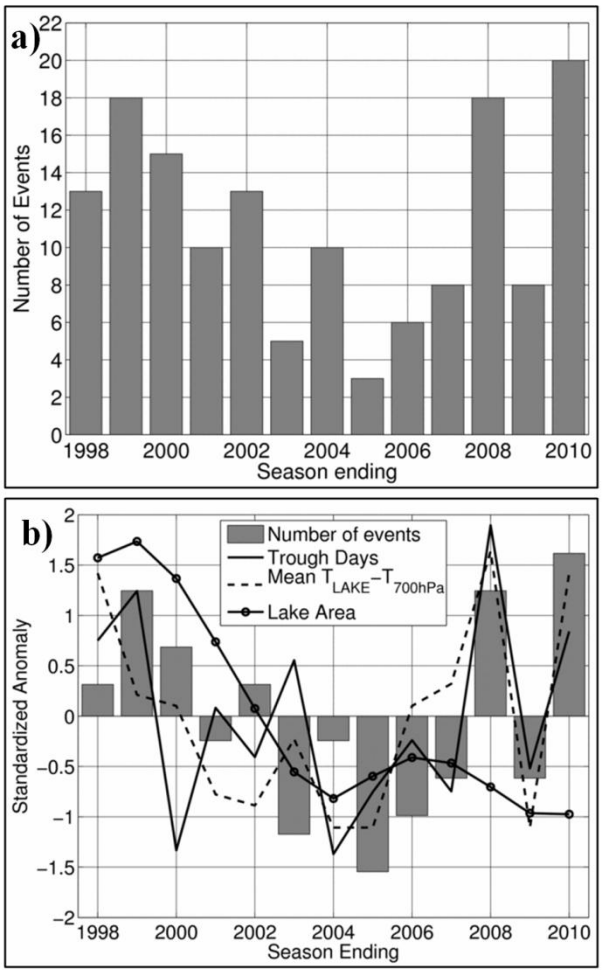


Fig. 2.5. Occurrence of GSLE. (a) Annual frequency of GSLE events. (b) Standardized anomalies of event frequency, lake area and synoptic factors.

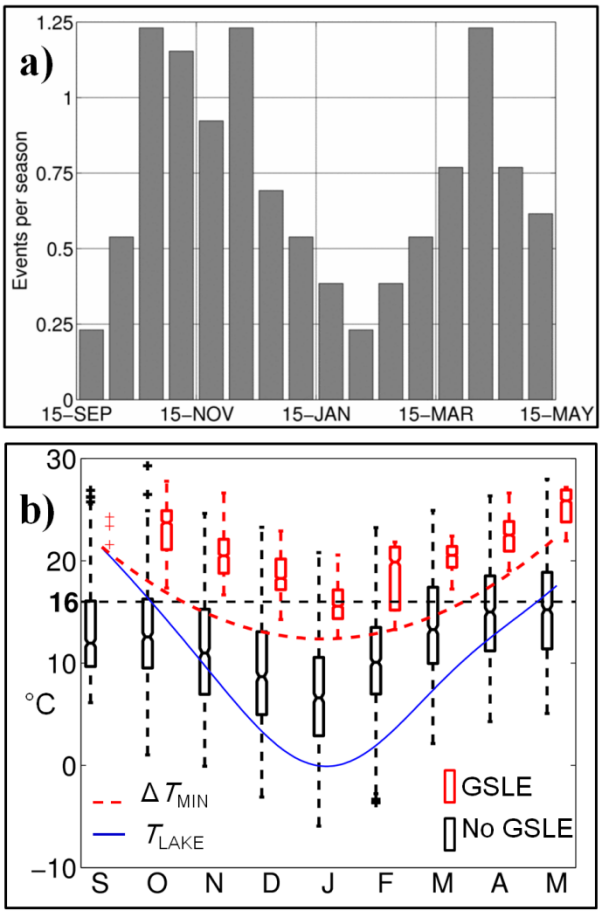


Fig. 2.6. Seasonal variability in GSLE frequency. (a) Number of events by half-month. (b) Standard box-and-whisker plot of lake-700-hPa temperature difference ($\Delta T$) by month, for non-GSLE soundings (black) and GSLE soundings (red). Black dashed line indicates 16°C operational forecast threshold, and red dashed line the quadratic curve fit for a seasonally varying threshold ($\Delta T_{min}$). Blue line denotes climatological lake temperature.

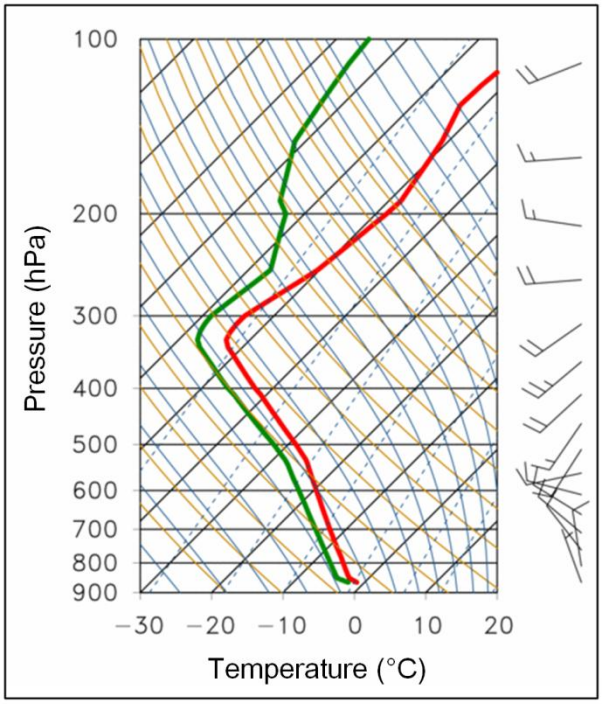


Fig. 2.7. Skew *T*-log*p* [temperature, dewpoint, and wind barbs (full and half barbs denote 5 and 2.5 m $s^{-1}$, respectively)] diagram for KSLC at 1200 UTC 2 Jan 2000.

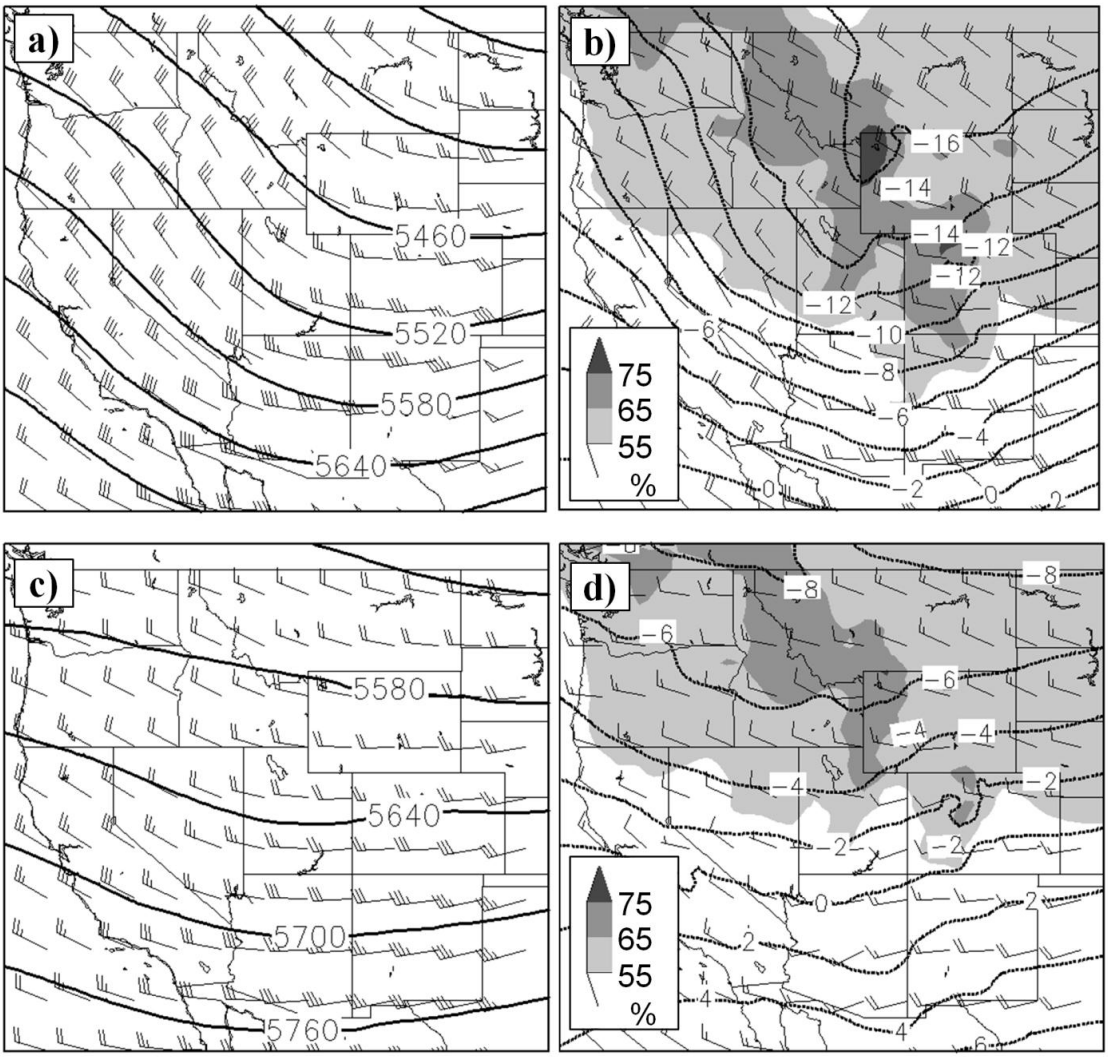


Fig. 2.8. NARR composite maps. (a) 500-hPa geopotential height (solid contours), and 500-hPa wind (full and half barbs denote 5 and 2.5 m $s^{-1}$, respectively); (b) 700-hPa temperature (dashed contours, °C), 700-hPa wind, and 850-700-hPa mean layer relative humidity (%, shaded according to scale at left), for winter (Dec-Feb) soundings with 16° < $\Delta T$ < 19°C. (c) and (d) same as (a) and (b) except for fall and spring (Sep-Nov, Mar-May) soundings.

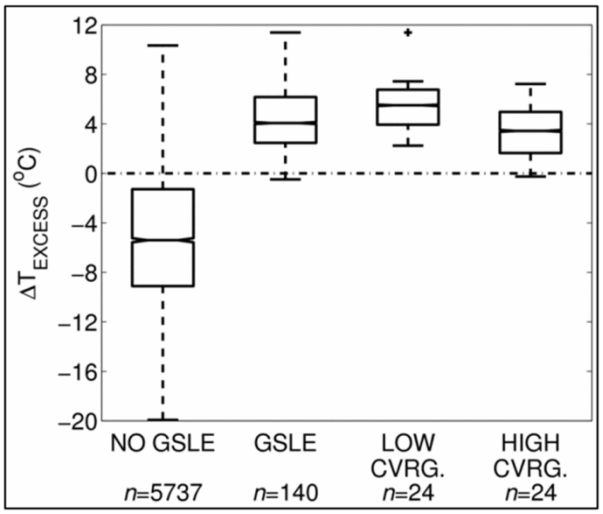


Fig. 2.9. Comparison of $\Delta T_{excess}$ for four categories of soundings: soundings with GSLE; without GSLE; with pure lake effect and low coverage (< 80 $km^2$ of 10 dBZ radar echoes, the lowest tertile); and with pure lake effect and high coverage (> 640 $km^2$ of 10 dBZ radar echoes, the highest tertile). Box top and bottom are the $25^{th}$ and $75^{th}$ percentiles, the median is denoted by a horizontal line in the box (medians of two distributions differ at the 90% level when the notches around their respective median lines do not overlap), whiskers extend to 1.5 times the interquartile range, and outliers beyond 1.5 times the interquartile range are denoted by '+'.

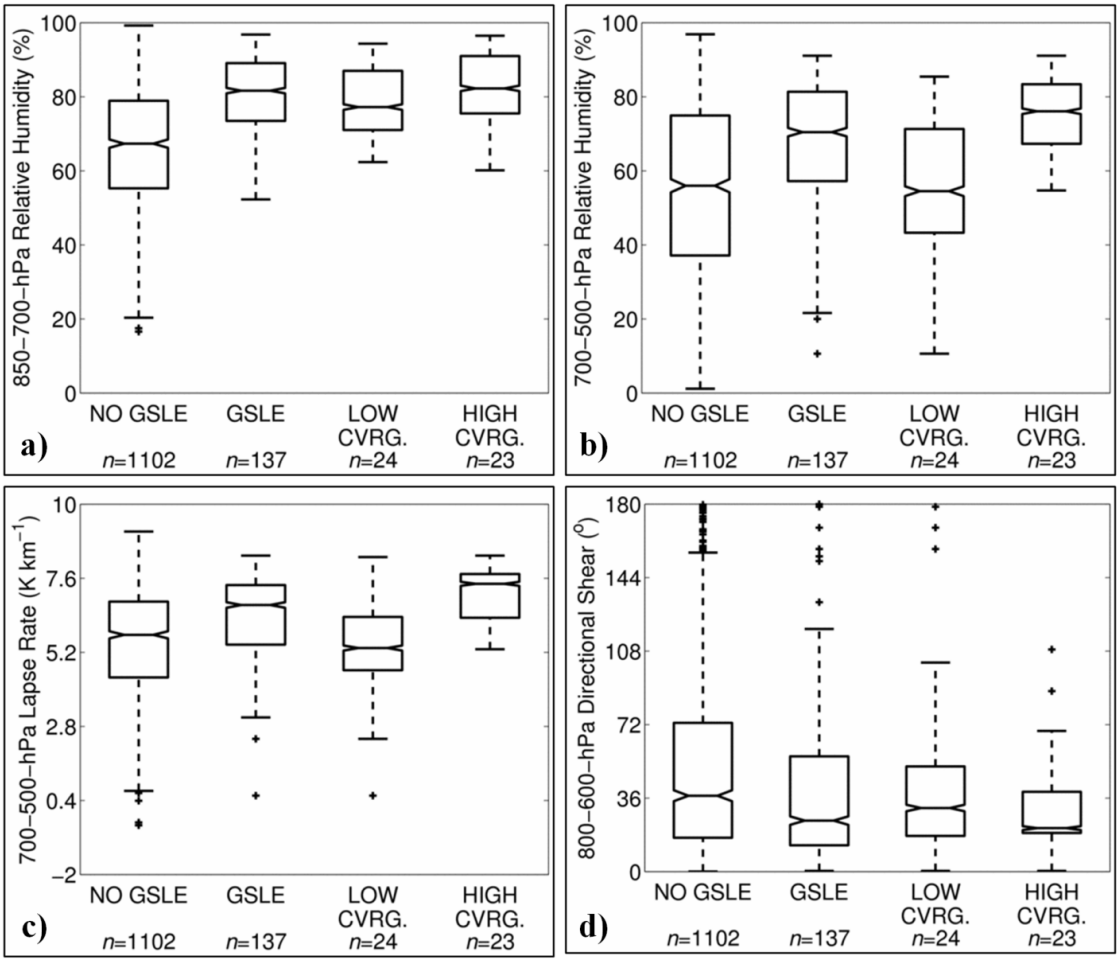


Fig. 2.10. Comparison of variables in the same categories of soundings as Fig. 9, but for $\Delta T_{\text{excess}} \geq 0$: (a) 850–700-hPa mean layer relative humidity (%); (b) 700–500-hPa mean layer relative humidity (%); (c) 700–500-hPa lapse rate (K km$^{-1}$); (d) 800–600-hPa directional shear (°). Box-and-whisker plotting convention as in Fig. 2.9.

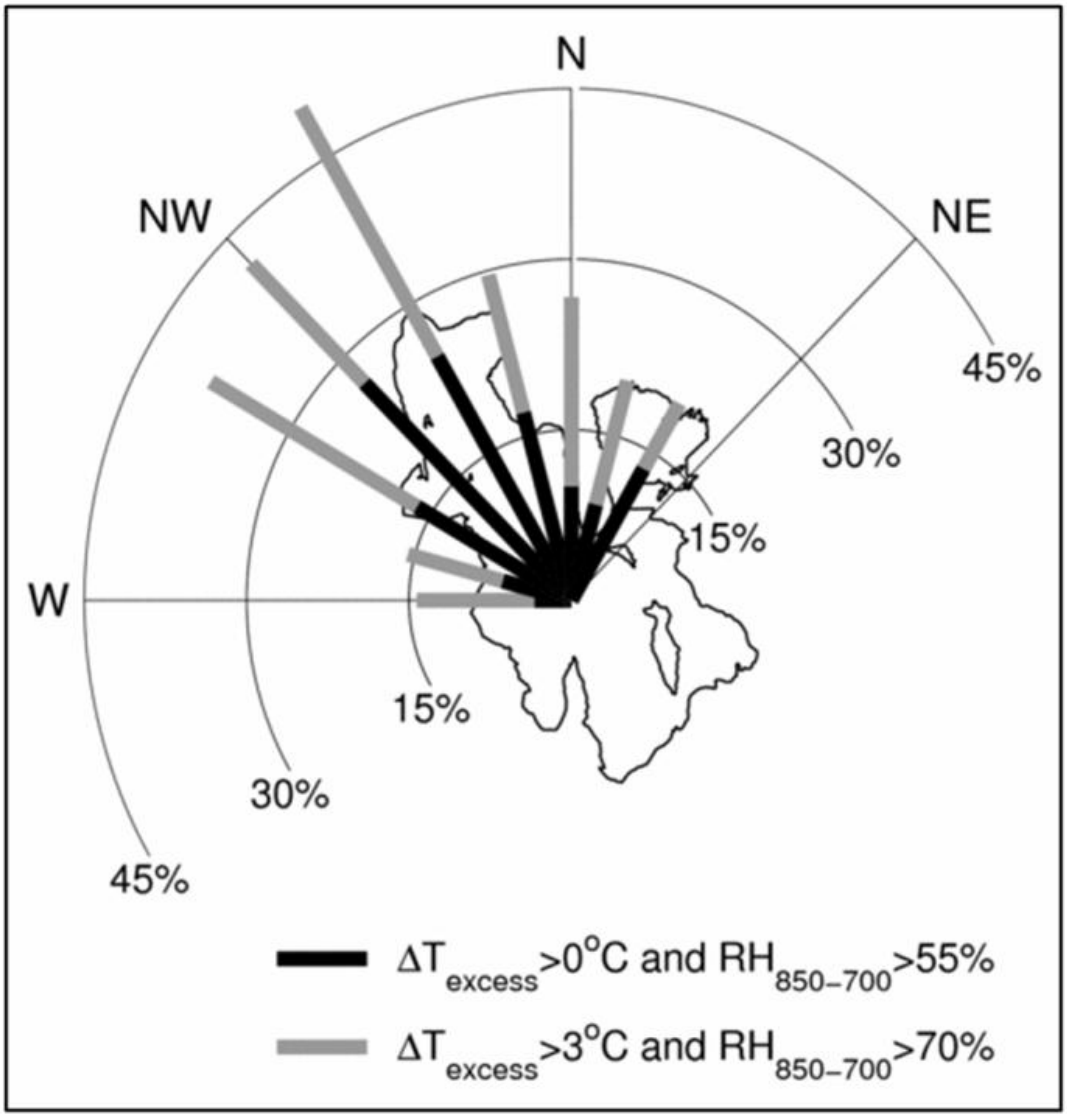


Fig. 2.11. Fraction of soundings (%) with GSLE versus 700-hPa wind direction, overlaid on GSL shoreline map, given $\Delta T_{excess} \geq 0$ and $RH_{850\text{-}700} \geq 55\%$ (black bars) or $\Delta T_{excess} \geq 3$ and $RH_{850\text{-}700} \geq 70\%$ (gray bars).

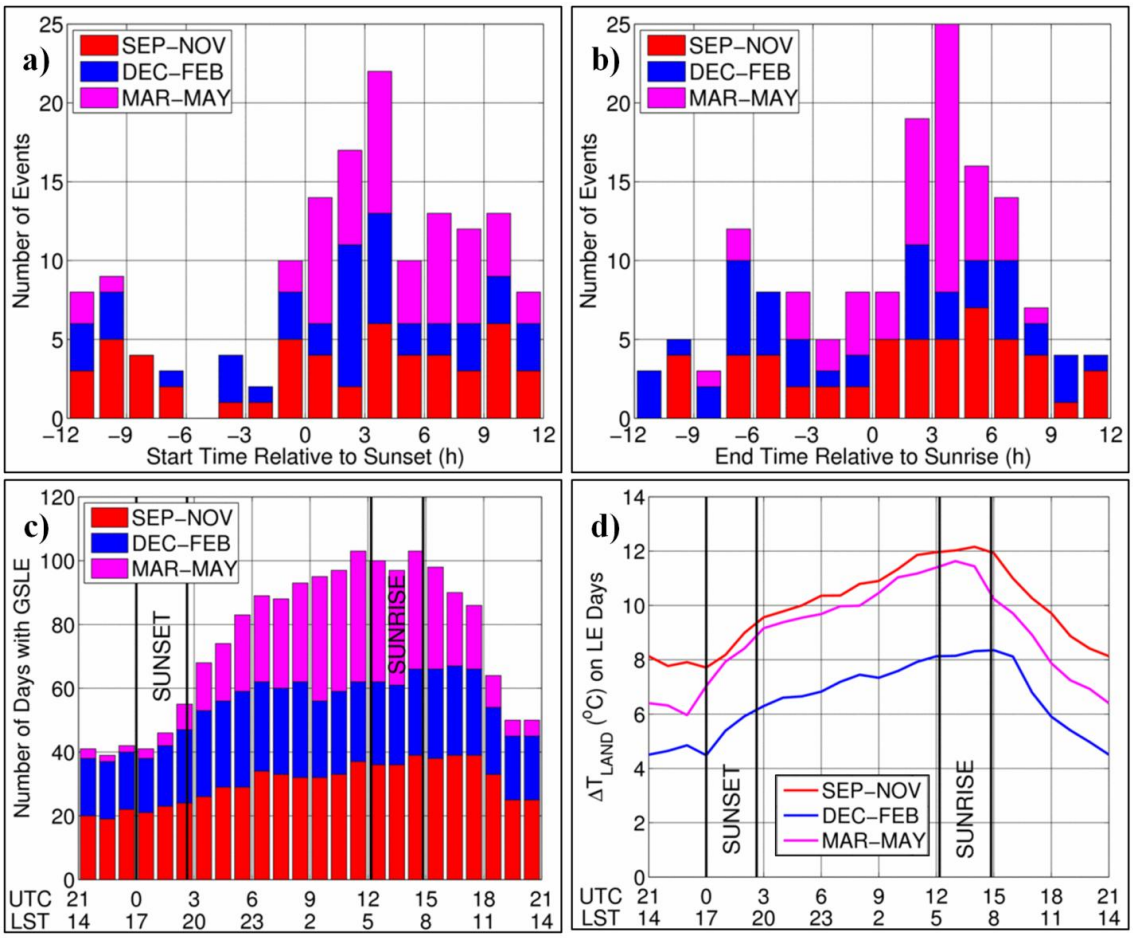


Fig. 2.12. Timing of GSLE events: a) event start time relative to sunset (h); b) event end time relative to sunrise (h); c) number of days with GSLE at a given time of day (h, UTC and LST), where vertical bars indicate the ranges of sunrise and sunset times (16 Sep – 15 May); d) hourly median $\Delta T_{\mathrm{LAKE-LAND}}$ on days with GSLE.

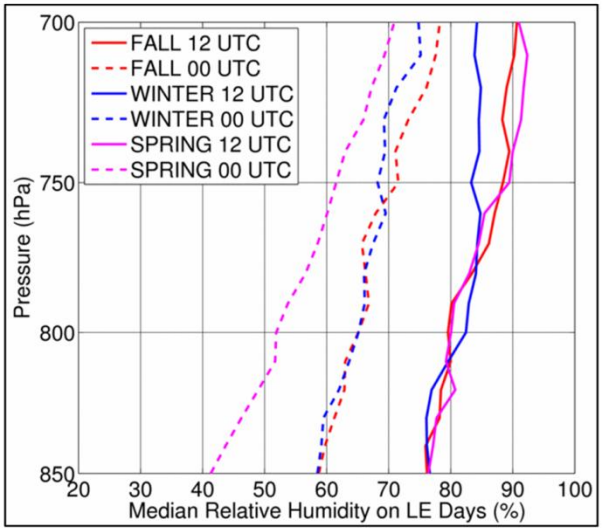


Fig. 2.13. Profiles of median relative humidity (%) on days with GSLE.

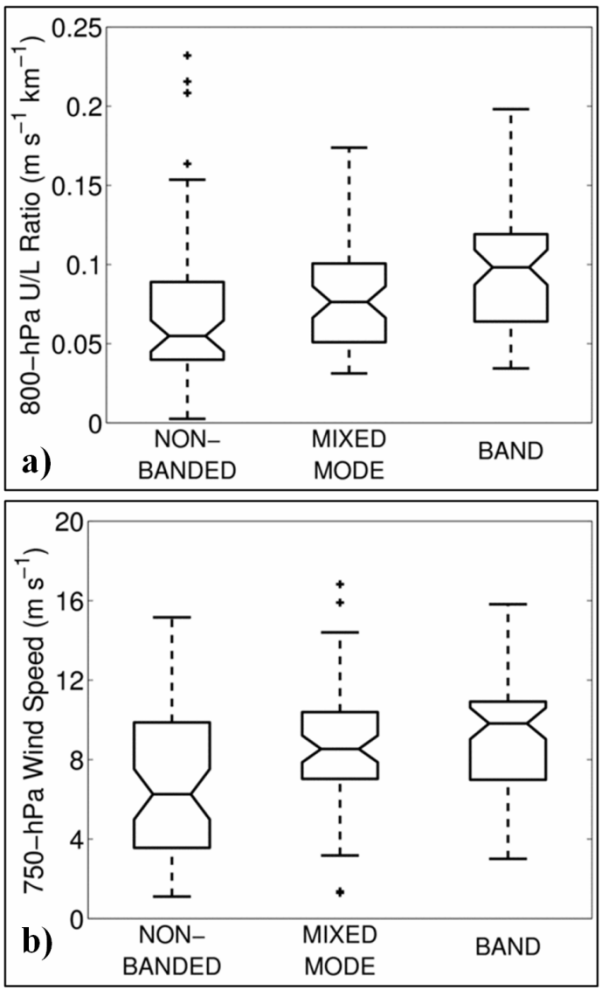


Fig. 2.14. GSLE mode versus (a) 800-hPa wind speed–fetch ratio ($U/L$; m s$^{-1}$ km$^{-1}$), and (b) 750-hPa wind speed (m s$^{-1}$). Box-and-whisker plotting convention as in Fig. 2.9.

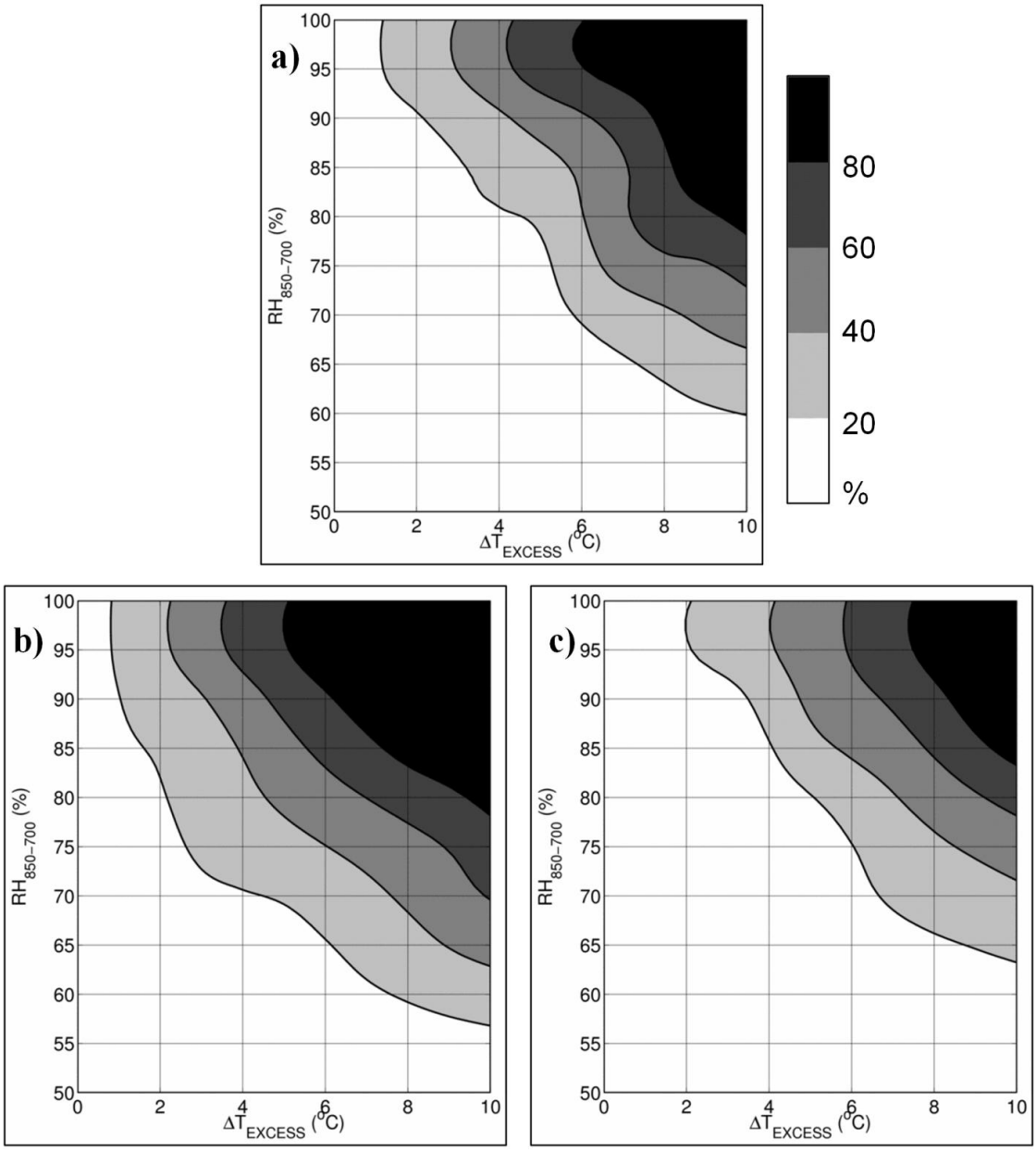


Fig. 2.15. Frequency of occurrence of GSLE. (a) Fraction of soundings with GSLE (%, shaded according to scale at right) as a function of $\Delta T_{excess}$ (°C) and $RH_{850–700}$ (%). (b) Same as (a) except for 700-hPa wind directions 290°–360°. (c) Same as (a) except for 700-hPa wind directions 1°–289°.

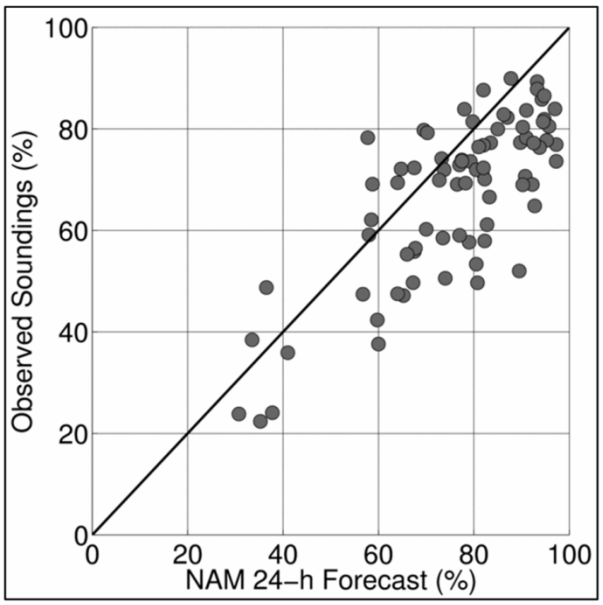


Fig. 2.16. Observed 850–700-hPa relative humidity (%) from KSLC soundings versus 24-h NAM forecasts, from the 2008/09 and 2009/10 cool seasons. Diagonal line indicates a perfect forecast.

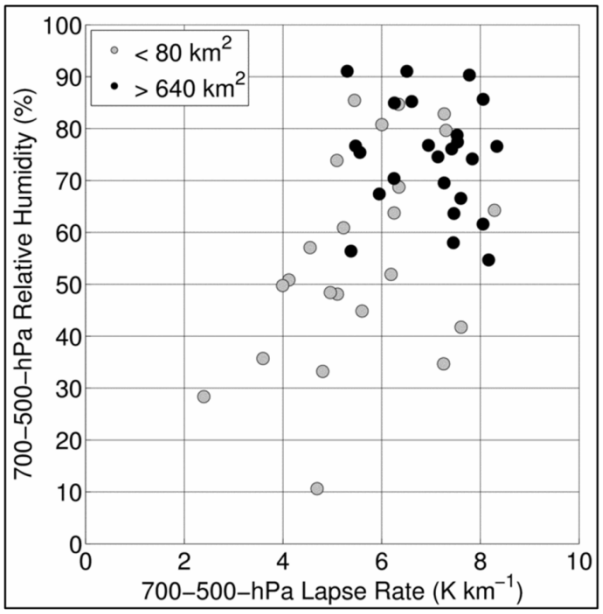


Fig. 2.17. GSLE coverage (area extent of radar echoes ≥ 10 dBZ; $km^2$) versus 700–500-hPa lapse rate and relative humidity.

# CHAPTER 3

# OROGRAPHIC INFLUENCES IN GREAT SALT LAKE-EFFECT SNOWSTORMS


## Abstract

The Great Salt Lake (GSL) in northern Utah is surrounded by several mountain ranges and is associated with multiple GSL-effect (GSLE) storms each year. Past research has emphasized the importance of orography in the evolution of GSLE events, but the relevant physical processes have not been identified.

This study examines the influence of orography on one lake-effect event (27 Oct 2010) and one lake-enhanced event (5 Nov 2011) associated with the GSL, through analysis of observations and numerical-model sensitivity studies. Both events involve synergistic interactions between lake-effect and orographic processes, and show a dramatic decrease in simulated precipitation intensity and coverage when either the lake or terrain forcings are removed.

A foehn-like flow over upstream orography reduces the relative humidity of the incipient low-level airmass and limits the intensity of both events. A convergence zone in the lee of isolated upstream topography is positioned over the north arm of the GSL, and may play a role in organizing the 27 Oct 2010 lake-effect band. Downstream orographic influences are large in both events, and include (1) overlake convergence due to flow stagnation along and/or or blocking by the Wasatch Mountains, (2) flow

deflection around the Oquirrh Mountains into an orographic concavity, and (3) hydrometeor transport into high terrain. These influences are not unique to the GSL region, and our results suggest applicability to other areas where lake-effect occurs in proximity to mountain barriers, particularly in the case of small water bodies.

## Introduction

The Great Salt Lake (GSL) Basin of northern Utah is one of several regions where topography affects lake-, sea- and ocean-effect precipitation (hereafter referred to collectively as lake effect). Covering an area less than $1/10^{th}$ the size of Lake Superior, the GSL is surrounded by mountain ranges that are much larger than the modest topography around the Laurentian Great Lakes, which are the subject of the majority of lake-effect literature. With a few exceptions (e.g., Hjelmfelt 1992; Onton and Steenburgh 2001), studies examining the role of orography in the evolution of lake-effect precipitation are nearly absent from peer-reviewed literature. This work examines the unique lake–orographic environment of the GSL region, utilizing observations and numerical simulations to improve understanding of how orography affects the initiation, morphology and intensity of Great Salt Lake-effect (GSLE) events.

GSLE events occur several times per year and impact transportation along a densely populated urban corridor (Carpenter 1993; Steenburgh et al. 2000; Steenburgh 2003; Alcott et al. 2012; Yeager et al. 2013). They develop when a cold airmass is advected over the relatively warm waters of the GSL, initiating or enhancing moist convection. On average, periods with GSLE (which is sometimes concurrent with precipitation generated by non-lake-effect processes) account for up to 8.4% of the total cool-season (16 Sep – 15 May) precipitation (snow-water equivalent) in areas south and

east of the GSL (Yeager et al. 2013). Intense and long-duration events occasionally occur, such as two mid-lake band periods during the 22–27 Nov 2001 "Hundred-Inch Storm" that produced a total of 55.4 mm of snow-water equivalent at the Alta-Collins snow study plot in the Wasatch Mountains, and 14.5 mm at the Salt Lake City International Airport (Steenburgh 2003).

The complex orography around the GSL creates the potential for a variety of lake–mountain interactions during GSLE events (Fig. 3.1). The GSL is bordered to the northwest by the Raft River and Albion Mountains, to the east by the Wasatch Mountains, and to the south by the Cedar, Stansbury and Oquirrh Mountains, all of which rise 1–2 km above lake level. The Promontory Mountains extend as a peninsula into the northern portion of the GSL, and a series of smaller barriers, including the Hogup and Lakeside Mountains, rise above the western shore.

Although unusual due to the close proximity of steep and high terrain, northern Utah is one of many regions where lake effect occurs near orographic barriers. Around the Laurentian Great Lakes, the modest rise in elevation from Lake Michigan to the hills of central Michigan has a minor, localized influence on lake-effect intensity (e.g., Hjelmfelt 1992). Hill (1971) found a 25–50 cm increase in mean annual snowfall for every 100 m increase in elevation above Lakes Erie and Ontario, including the Tug Hill plateau region of western New York. Laird et al. (2009a) suggested that topography to the east and west of narrow Lake Champlain channels low-level flow and enhances overlake convergence during lake-effect events.

Beyond North America, lake-effect snows frequently affect Japan during the winter monsoon when cold, continental air masses from mainland Asia move over the

relatively warm waters of the Sea of Japan (Hozumi and Magono 1984). These events impact regions where high terrain lies close to the shoreline and contribute to winter season snow-water equivalent accumulations of up to 1620 mm in the mountains of the Hokuriku district (Matsuura et al. 2005). Sea of Japan snowstorms have been investigated through a variety of observational and numerical modeling approaches (e.g., Magono et al. 1966; Hozumi and Magano 1984; Saito et al. 1996; Kusunoki et al. 2004), with studies of orographic effects focused primarily on microphysical processes. Lake-effect snows also occur east and south of the Black Sea, where significant orographic barriers lie downstream in Georgia and Turkey (Kindap 2010; Markowski and Richardson 2010).

The situation around the Great Salt Lake is complicated by the presence of large orographic barriers surrounding the lake. Hence we consider independently the effects of *upstream* and *downstream* barriers, located to the northwest and southeast of the GSL, respectively (based on the tendency for GSLE events to occur with 700-hPa flow from the northwest; Alcott et al. 2012). Although the role played by orography in GSLE events is not well understood, there is a wealth of peer-reviewed literature concerning orographic influences in northern Utah and other regions that provides valuable insight. Relevant concepts include: 1) airmass transformation and leeward drying (the latter due to net subsidence) (e.g., Varney 1920; Sinclair 1994; Smith et al. 2003; Smith et al. 2005), 2) windward blocking and flow deflection (e.g., Mayr and McKee 1995; Colle et al. 2005; Cox et al. 2005), 3) terrain-induced convergence (e.g., Mass 1981; Mass and Dempsey 1985; Chien and Mass 1997; Andretta and Hazen 1998), 4) orographic convection (Kirshbaum and Durran 2004; Kirshbaum and Durran 2005a,b; Fuhrer and

Schär 2005, 2007), and 5) thermally driven lake-mountain wind systems (e.g., McGowan et al. 1995; Stewart et al. 2002).

This work explores the influence of upstream and downstream orographic features on lake-effect (27 Oct 2010) and lake-enhanced (5 Nov 2011) snowstorms in the GSL region using radar, surface and upper-air observations, gridded analyses, and numerical model simulations. Our results show that events a synergy between lake and orographic processes is important in some GSLE events. In both events, fluxes from the lake and convergence near downstream terrain combined to produce much heavier precipitation than would result in hypothetical scenarios without the lake or terrain, while low-level drying by upstream terrain reduces lake-effect intensity. The effects of upstream and downstream terrain in these events suggest a broader applicability of the synergistic concept to other lake-mountain systems spanning a range of spatial scales across the globe.

## Data and Methods

### Surface and Upper-Air Data and Analyses

Observational analyses use surface observations, conventional and supplemental upper-air observations, radar data and gridded atmospheric analyses. Surface observations were obtained from the MesoWest cooperative network (Horel et al. 2002). These data were first evaluated through an examination of MesoWest data quality ratings (Splitt and Horel 1998), calculated by comparing observed station values to an objective analysis produced using multivariate linear regression. Observations that were deemed questionable through the objective technique, or failed subjective checks of temporal and spatial consistency, were not included in our event analyses. Upper-air profiles include

soundings launched by the National Weather Service at Salt Lake City International Airport (KSLC; see Fig. 3.1 for location) and obtained from an archive at the University of Wyoming Department of Atmospheric Science. Our analysis of the 5 Nov 2011 event is supplemented with data from the Sounding Observations of Lake-effect Precipitation Experiment (SOLPEX) intensive observation period 6 (hereafter IOP6). During the 20 Oct 2010 to 1 Dec 2011 SOLPEX field campaign, University of Utah Atmospheric Sciences students launched GRAW mobile soundings at Kelton (KEL1) and Syracuse (QSY) during lake-effect periods, and additional surface mesonet stations were operated in the lee of the Raft River Mountains (KEL1 and KEL2; see Fig. 3.1 for locations). SOLPEX upper-air observations were not available for the 27 Oct 2010 event due to exhaustion of resources during a deployment for what turned out to be a weaker event on the previous day.

North American Mesoscale (NAM) model analyses were used to examine large-scale conditions for the two cases in this study, and to provide initial, lateral and surface boundary conditions for numerical model simulations. These analyses were obtained from the National Climatic Data Center (NCDC) at 12-km and 25-hPa horizontal and vertical resolutions, respectively.

## Numerical Model Simulations

Numerical simulations were performed with the Weather Research and Forecasting model version 3.3.1 (hereafter WRF), which uses a nonhydrostatic, pressure-based, terrain-following $\eta$ coordinate. All simulations use the Advanced Research WRF core and feature 3 one-way-nested domains with 35 vertical levels and horizontal resolutions of 12, 4 and 1.33 km (Fig. 3.2). Only output from the 1.33-km domain is

presented. Physics packages include the Thompson et al. (2008) microphysics scheme, the Yonsei University planetary boundary layer scheme (Hong et al. 2006), the Rapid Radiative Transfer Model longwave and shortwave radiation schemes (Iacono et al. 2008), the Noah land surface model (Chen and Dudhia 2001), and the Kain–Fritsch 2 cumulus parameterization (Kain 2004). The convective parameterization is utilized only for the 12- and 4-km domains, while the other physics packages are applied to all three domains.

NAM analyses provide the initial cold-start atmospheric and land-surface conditions, and lateral boundary conditions at 6-h intervals throughout the 24-h WRF simulations. Some modifications of the NAM analyses were necessary in order to create a more realistic initial land- and lake-surface analysis. For both GSLE events, inspection of visible satellite imagery, SNOwfall TELemetry (SNOTEL) data, and snow analyses from the National Operational Hydrologic Remote Sensing Center (NOHRSC) showed that the NAM land-surface analyses underestimated snow-cover extent and snow depth over northern Utah. Based on NOHRSC and SNOTEL data, an approximate relationship between elevation and snow-water equivalent on the ground was used to more accurately specify the initial snow cover and snow depth across the 1.33-km domain. Nonetheless, sensitivity to snow cover and snow depth is low, and simulations with no snow cover produced a precipitation distribution nearly identical to the control simulations. For the 4-km and 12-km domains, snow data from the NAM analyses were deemed adequate. Based on satellite-derived skin temperature data from the Advanced Very High Resolution Radiometer (AVHRR), the NAM lake-surface temperatures were too cold in both GSLE events. Therefore, we used the most recent, median, cloud-masked AVHRR

skin temperature over the GSL (13.3°C and 10.2°C, for 27 Oct 2010 and 5 Nov 2011, respectively) to more accurately initialize GSL temperatures in all 3 WRF domains. The AVHRR values used for both of our events were within 0.5°C of the 0.4-m and 1.4-m water temperatures observed at a USGS buoy in the center of the lake. Following Steenburgh and Onton (2001), the surface layer parameterization was modified to reduce saturation vapor pressure by 30% and 6% over the north and south arms of the GSL, respectively, to account for the effects of high salinity on latent heat fluxes.

In each event, our analysis uses a control simulation followed by a series of sensitivity experiments involving modification of the terrain surrounding the GSL. The control simulation (CTL) was performed with topography generated by the WRF preprocessing system from the standard WRF 30-s terrain dataset. Terrain features were removed from the flat-no-lake (FLAT-NL), flat (FLAT), Wasatch Mountains (WAS), and downstream terrain (DT) simulations as shown in Fig. 3.3. The "removal" of terrain involved limiting the elevation of a specified area to 1280 m, the approximate level of the GSL. Where terrain modification was performed in the 1.33-km domain, elevations in the parent 4-km domain were also reduced to 1280 m outward for an additional 5 grid points (20 km). Terrain was not modified in the outermost, 12-km domain. Transition zones between real and modified terrain in both the 1.33- and 4-km domains were smoothed over a distance of 10 grid points to remove steep slopes.

Where terrain is reduced in elevation, land-surface characteristics such as land use, soil type, vegetation type, and vegetated fraction are retained. However, soil temperatures, soil moisture, and land surface temperature are adjusted by the WRF preprocessing system using implicit relationships between these variables and elevation.

Where the elevation of terrain is reduced to below the snow line, snow cover is automatically removed. The sensitivity to snow cover and land use is very low in both events and we find it reasonable to attribute differences between CTL and the WAS, DT and FLAT simulations to changes in topography. The atmosphere in the volume previously occupied by topography is derived from NAM initial analyses, or uses a moist-adiabatic lapse rate at levels below the NAM model surface. Given the small upstream topographic volume removed, and the 6–9-h integration time prior to lake-effect precipitation, our results are likely insensitive to these prescribed initial conditions.

In the FLAT-NL and no-lake (NL) simulations, points over the GSL are converted from water to barren, sparsely-vegetated land. Land surface characteristics, including soil moisture, soil temperature, albedo, and skin temperature, are interpolated across the GSL area from adjacent land points.

## Results

### Orographic Influences in a Lake-Effect Event

#### Observed Evolution

On 27 Oct 2010 GSLE developed in the wake of a baroclinic trough that passed the Salt Lake City International Airport (KSLC) shortly after 0000 UTC. During the event (0600 UTC), a 500-hPa shortwave trough axis was located over western Utah (Fig. 3.4a). At 700-hPa, a cold pool extended southward from Canada into Nevada, Utah and Wyoming, with northwest flow over the GSL (Fig. 3.4b). The mean 850–700-hPa relative humidity was above 70% over much of northern Utah and southern Idaho, indicating sufficient low-level moisture for GSLE (Alcott et al. 2012). The 0000 UTC radiosonde observation from KSLC (Fig. 3.4c), launched downstream of the GSL prior to

the passage of the baroclinic trough, featured a deep, dry convective boundary layer. Temperatures dropped and lake-effect precipitation developed following the trough passage, and based on visual inspection of KMTX Level III radar reflectivity, lake-effect precipitation began at ~0228 UTC. The 1200 UTC sounding at KSLC, launched late in the event, shows near-saturated, moist-adiabatic conditions from the surface through 670-hPa, with dry air at mid and upper levels (Fig. 3.4d). Light southerly and southwesterly winds were observed near the surface, while winds above 800-hPa were northerly and northwesterly. Based on satellite-derived skin temperature data collected prior to the event on 25 Oct, the median GSL water temperature was 13.3°C, which signifies lake–700-hPa temperature differences of 21.8° and 25.0°C given the observed 700-hPa temperatures of –8.5° and –11.7°C at 0000 and 1200 UTC, respectively.

Figure 3.5 shows the Level III 0.5° reflectivity and observed mesonet surface winds at 0400, 0600, 0900 and 1100 UTC. At 0400 UTC, a wide band of radar echoes extended from the Promontory Mountains over the southeast shore of the GSL and into the Wasatch Mountains (Fig. 3.5a). Winds were moderate (7.5–10 m $s^{-1}$) and out of the west–northwest over the Bonneville Salt Flats and along the western shore of the GSL, but light and variable along the northern Wasatch Front and in the Salt Lake Valley. The band narrowed after 0400 UTC and occasionally produced radar echoes ≥35 dBZ (Fig. 3.5b, c). By 1100 UTC the band began moving westward through the Salt Lake Valley toward the Oquirrh Mountains (Fig. 3.5d). The precipitation diminished after 1200 UTC (not shown), and by 1659 UTC, radar echoes were no longer observed in association with the GSL. Based on radar data, we define the 27 Oct 2010 event from 0228 to 1659 UTC.

During the 27 Oct 2010 event, 30 cm of snow fell (based on snow depth change)

at the Alta-Collins snow study plot in the central Wasatch Mountains (CLN, see Fig. 3.1 for location), with a total of 23 mm of snow-water equivalent (Fig. 3.6a). KSLC received 7 mm of snow-water equivalent, with visibilities reduced to 0.5 mi (800 m) near 0500 UTC (Fig. 3.6b). Event precipitation totals were estimated at 6-10 mm for much of the Salt Lake Valley using level III reflectivity and the reflectivity–snow-water-equivalent (Z-S) relationship given by Vasiloff (2001):

$$Z = 75S^2, \tag{3.1}$$

where $Z$ is the radar reflectivity and $S$ is the accumulation rate of snow-water equivalent in mm $h^{-1}$ (Fig. 3.7). However, this methodology underestimated precipitation amounts in the Wasatch Mountains.

Simulated Evolution

The control WRF model simulation produces a lake-effect band similar to the observed evolution, although with some differences after 0600 UTC. For comparison with observed radar reflectivity, Fig. 3.8 shows model simulated radar reflectivity calculated using the read-interpolate-plot (RIP) graphic software, developed by M. Stoelinga from the University of Washington, (a description is available online at: http://www.atmos.washington.edu/~stoeling/RIP_sim_ref.pdf). At approximately 0400 UTC, precipitation has developed in an area of confluence extending from the southern end of the Promontory Mountains to the northern Salt Lake Valley (Fig. 3.8a). Model diagnostics (not shown) indicate that winds in this zone are convergent, and hereafter we refer to it as a convergence zone. At 0600 UTC, the convergence zone extends along the entire long axis of the GSL, with northwesterly and westerly flow from the Bonneville

Salt Flats meeting northerly flow along the Promontory and Wasatch Mountains (Fig. 3.8b). Winds are light and variable along the northern Wasatch Front and in the Salt Lake Valley. Precipitation has intensified and forms a band along the southeast portion of the convergence zone that extends and broadens downstream over the Wasatch Mountains. As in the observed event, the simulated band peaks in intensity around 0600 to 0700 UTC.

By 0900 UTC, the axis of the simulated precipitation band remains well organized but has shifted considerably farther southwest than observed (cf. Figs. 3.5c, 3.8c). This difference is perhaps due to a more northerly 10-m wind component than observed over western portions of the GSL. The simulated winds along the southwestern shore remain northwesterly throughout the event, while observed winds in this region were consistently from the west-southwest. Steenburgh and Onton (2001) encountered similar issues in simulations of the 7 Dec 1998 event, with a convergence zone placed too far to the west. Although the position of the simulated band differs slightly from that of the observed band, the general structure and horizontal extent are well represented by the WRF through 1100 UTC. The simulated band begins to dissipate by 1100 UTC, with only light precipitation over and downstream of the Oquirrh Mountains (Fig. 3.8d). Simulated precipitation ends by 1300 UTC, approximately 4 h prior to the observed end of the event, although observed precipitation was very light after 1300 UTC.

Simulated 0230–1700 UTC precipitation totals of 12–20 mm in the central Wasatch Mountains (Fig. 3.9a) are in good agreement with gauge observations (cf. Fig. 3.7; e.g., 23 mm at CLN, and 15–20 mm at nearby sites). Despite the shorter duration and southwestward shift of the simulated band, total WRF precipitation in the Salt Lake

Valley is 2–8 mm more than suggested by radar-derived estimates and the observed total at KSLC. There is an analogous banded precipitation maximum in the CTL simulation and the radar-derived estimate extending southeastward from Antelope Island, but the simulated maximum (26.8 mm) is much larger than the radar estimate (14 mm). The simulated precipitation maximum is also displaced 5–10 km to the southeast of the radar-derived maximum. Over the lake-effect region (the domain shown in Figs. 3.9a–f), the mean precipitation in CTL is 1.08 mm, with a maximum of 26.8 mm, and an area of 730 $km^2$ receiving more than 10 mm (Table 3.1).

Sensitivity to Orography

The 27 Oct 2010 GSLE event is produced from lake-effect and orographic processes working in concert. Overall the sensitivity studies show that both GSL and the topography downstream are crucial to the development of a significant precipitation event. A brief summary of the sensitivity study results here will be followed by a more detailed examination of the relevant physical processes in the next section. Amounts presented in Table 3.1 refer to the precipitation occurring over the lake-effect region, defined by the domain displayed in Fig. 3.9.

In a simulation with no terrain and no GSL (FLAT-NL), no precipitation develops from 0230–1700 UTC (Fig. 3.9b; Table 3.1). In FLAT, the mean simulated precipitation is only 0.05 mm, 99% less than CTL, and the maximum is 3.2 mm (Fig. 3.9c; Table 3.1). The simulated precipitation in FLAT briefly organizes into a band but then shifts southwestward, which limits the maximum precipitation amount. The effect of removing all terrain is much more substantial for 27 Oct 2010 than for the 7 Dec 1998 case

simulated by Onton and Steenburgh (2001; cf. their Figs. 17a and 21). Their "FLAT" simulation resulted in more widely distributed precipitation than their control case, with a reduction in maximum precipitation from 19.3 to 11.1 mm.

Including only the Wasatch Mountains (WAS) yields a mean precipitation of 0.80 mm, 27% less that CTL, and a maximum of 21.6 mm, with an area of 214 $km^2$ receiving more than 10 mm (Fig. 3.9d; Table 3.1). When the remaining downstream terrain is added (DT), the mean precipitation is 1.77 mm, 61% more than CTL, and the maximum is 41.9 mm, with an area of 2017 $km^2$ receiving more than 10 mm (Fig. 3.9e; Table 3.1). The lack of upstream terrain in DT allows cold, moist air from the Snake River Plain to advect directly over the GSL without orographic modification, as discussed in the next section. The largest increase in precipitation from CTL to DT occurs in the center of the Salt Lake Valley and immediately downstream in the Wasatch Mountains near CLN. Contributing to these differences, the precipitation band in DT is more intense than CTL, remains focused on the Salt Lake Valley and adjacent terrain after 0600 UTC, and does not begin to dissipate until after 1500 UTC (not shown). In NL, removing the GSL reduces the mean precipitation to 0.11, 90% less than CTL, and the maximum to 2.5 mm (Fig. 3.9f; Table 3.1). Precipitation in NL is almost entirely confined to high elevations. These results emphasize that the 27 Oct 2010 event is generated by the synergistic interaction between lake and orographic effects; with the terrain and no GSL, precipitation is limited to light orographic precipitation over the Wasatch and Oquirrh Mountains, while with the GSL and no terrain, almost no precipitation is produced.

Upstream Orographic Influences

The terrain north and northwest of the GSL greatly modifies the thermodynamic and kinematic structure of the 27 Oct 2010 GSLE event. Flow over upstream barriers can lead to significant drying and warming of the low-level airmass, while semi-isolated terrain features produce lee convergence zones that may serve as foci for GSLE initiation and organization.

Terrain upstream of the GSL has a significant effect on the low-level thermal and moisture profile of the airmass that reaches northern portions of the lake. The relative humidity at the lowest sigma level in CTL is considerably lower immediately downstream of the Raft River range compared to upstream over the southern Snake River Plain (Fig. 3.10a). The drying extends from the surface to well above the crest level of the Raft River Mountains, as evidenced by a cross-section from the Snake River Plain to the north arm of the GSL (Fig. 3.10b). The control simulation indicates less than 0.2 mm precipitation fell over upstream topography during the entire event, and thus the leeside water vapor mixing ratio is unlikely to have been significantly reduced by hydrometeor fallout. This scenario instead resembles the structure of a typical foehn flow (e.g., Drechsel and Mayr 2008), where air near crest level on the upstream side flows over a blocked layer, and experiences adiabatic warming during descent on the downstream side. Therefore, based on trajectory paths and this conceptual model, we focus on dry-adiabatic descent (i.e., where surface parcels over the GSL originated at higher elevations over the Snake River Plain), rather than airmass transformation (i.e., warming and reduction in water vapor mixing ratio due to the generation of orographic precipitation) as the source of drying in the lee of the Raft River Mountains and adjacent topography.

In Fig. 3.11, selected paths are highlighted in red, orange, light green and dark green in (a), while model fields along these paths are plotted in (b), corresponding to colors in (a). Several backward trajectories from the GSLE band to the Snake River Plain show nearly 1 km of descent and a 20-40% reduction in relative humidity during their 6 h path (e.g., red, orange and dark green).

Due to the presence of low passes and high, isolated mountain ranges, terrain upstream of the GSL produces a combination of flow-over and flow-around scenarios. Although the majority of air parcels ending at the lowest sigma level over the GSL (~1340 m) originated at altitudes near or above 2 km, there is some evidence of "airmass scrambling" as trajectories originating at low elevations over the Snake River Plain cross paths with others that originate at higher elevations (e.g., light green in Fig. 3.11a–b; Smith et al. 2003). While other parcels ascend to 2500–2800 m and experience a 15–35% decrease in relative humidity, the light green parcel passes through Moburg Canyon, the lowest gap in the series of upstream ranges, and sees little change in relative humidity. This gap effectively forms a conduit through which some of the moist, low level air in the Snake River Plain is able to penetrate into the GSL basin.

Isolated obstacles within the three-dimensional upstream terrain also lead to the development of a convergence zone over the north arm of the GSL. At 0700 UTC, when the lake-effect band is near its peak intensity, low-level flow in CTL is blocked by the Albion Mountains and adjacent foothills and channeled along the Snake River Plain (Fig. 3.12a). Steenburgh and Blazek (2001) observed a similar channeling effect in this region behind a cold front on 3 Dec 1998. There is a pronounced wake in the lee of the Raft River Mountains with a complete wind reversal, supported by observations of light and

variable winds from 0600 to 1200 UTC (Figs. 3.4b–d). An additional, smaller wake forms in the lee of the foothills south of the Raft River Mountains. These isolated high obstacles within the upstream terrain are ideally located for creating convergence over the north arm of the GSL, and at 0700 UTC a convergence zone extends from the Raft River wake southeastward along the center of the north arm. Similar scenarios occur near larger isolated obstacles such as the Olympic Mountains, where precipitation rates are greatly enhanced in a lee convergence zone (Mass 1981; Mass and Dempsey 1985). Flow is also blocked and deflected to the south along the Promontory Mountains, which further contributes to convergence over the north arm.

The convergence zone that develops in the lee of the Raft River Mountains may act to better organize convection, since the band in CTL is slightly narrower and longer than in DT, and forms in the middle of the lake rather than on the southeast shore, despite drying of the upstream flow in CTL. Although model errors and the small scale of these bands preclude a definitive assessment, other studies support the relationship between the shape of upstream terrain features and lake-effect morphology. Tripoli (2005) suggests that the development of convective rolls in lake-effect associated with the Great Lakes may depend on the production of vorticity by variations in shape of the upstream shoreline. On a larger scale, Andersson and Gustafsson (1994) show that concave features in upstream terrain can act as foci for the formation of convective bands in the Baltic Sea.

Removal of upstream terrain in DT yields a near-uniform northwest flow pattern over the north arm of the GSL at 0700 UTC (Fig. 3.12b). Convergence produced in the lee of the Raft River Mountains and adjacent ranges appears insufficient to compensate

for the net warming and drying caused by flow over upstream terrain, and considerably more precipitation falls in DT than in CTL (cf. Figs. 3.9a,e). This finding is consistent with Kristovich and Laird (1998), who find lake-effect intensity to be particularly sensitive to upstream moisture conditions. Although upstream terrain reduces the intensity of the 27 Oct 2010 event, the overall effects of downstream terrain are much more substantial, and are investigated extensively in the next section.

Downstream Orographic Influences

Past work on orographic modification of lake effect has primarily dealt with enhancement through microphysical processes and increased vertical motions during ascent of a downstream slope (e.g., Hjelmfelt 1992; Saito et al. 1996; Kusunoki et al. 2004). The situation in the 27 Oct 2010 GSLE event calls for the consideration of other processes, including blocking, horizontal moisture contrasts, and flow into an orographic concavity (the Salt Lake Valley). These orographic influences combine to produce almost 16 times more precipitation in CTL (mean 1.10 mm) than in a simulation with no terrain (FLAT; mean 0.07 mm), suggesting a strong synergistic interaction between lake and mountain processes (cf. Figs. 3.9a,c; Table 3.1).

A convergence zone develops over southeast portions of the GSL, and is much stronger in simulations with terrain than those without. This convergence zone occurs along the boundary between moderate northwest winds over the western half of the GSL, and very weak flows along the eastern shore of the GSL and the northern Wasatch Front. For the majority of the event, both simulated (CTL) and observed winds are light and variable along the northern Wasatch Front, northerly along eastern portions of the GSL, and west–northwest over the western half the GSL and Bonneville Salt Flats (Figs. 3.5

and 3.8). The confluence zone between the light northerly and moderate northwesterly flow is collocated with the GSLE band at 0700 UTC, and is convergent at the lowest sigma level in the CTL simulation (Fig. 3.13a).

Weak northerly low-level flow along the Wasatch Mountains is not an inherent attribute of the background flow, as evidenced by the uniform, northwesterly flow in FLAT-NL at 0700 UTC (Fig. 3.13b). In FLAT, the thermal contrast between the land surface and the relatively warm GSL drives weak convergence over the GSL (Fig. 3.13c). FLAT, however, produces only weak precipitation far downstream of the GSL at 0700 UTC. In WAS, the low-level flow is very weak and northerly along the northern Wasatch Front, with precipitation forming along a convergence zone from mid-lake to the southeast shore (Fig. 3.13d). Precipitation in WAS is similar to CTL in distribution and intensity, suggesting that the Wasatch Mountains alone exert a particularly important orographic influence. Weak flows along the northern Wasatch Front in CTL, WAS and DT are attributable to a number of processes, which include blocking by the Wasatch Mountains, flow stagnation in the lee of upstream terrain, and thermally driven flows. The specific mechanisms at work in this area are not identified in this dissertation, but future analysis is expected to provide further insight.

The Oquirrh Mountains result in flow deflection that further enhances convergence in the Salt Lake Valley in a manner similar to that found in idealized studies of concave ridges. Watson and Lane (2012) show that in idealized scenarios, a concave ridge produces more precipitation than straight or convex ridges, due to a so-called "funneling mechanism." Flow deflection is evident in CTL at 0700 UTC around the northern end of the Oquirrh Mountains, with nearly calm or weak southerly winds in the

Salt Lake Valley coincident with the GSLE band (Fig. 3.13a). In their idealized simulations, Watson and Lane (2012) show that outer portions of the ridge deflect flow inward to yield flow deceleration, confluence and enhanced upward motions. A comparison of the low-level flows in WAS and DT supports this conceptual model. In DT, northwest flow approaching the Oquirrh Mountains is deflected eastward into the Salt Lake Valley, producing an area of strong confluence (Fig. 3.13e). This confluence zone is shifted eastward from WAS (i.e., Fig. 3.13d), and is collocated with the lake-effect precipitation. Although the simulated reflectivity is similar in WAS and DT at 0700 UTC, the mean event precipitation in DT is more than twice as much as in WAS. Simulations of a GSLE event on 7 Dec 1998 also show some confluence due to deflection of flows into both the Salt Lake and Tooele Valleys, however the simulated band might have formed too far west to be aligned with the confluence zone in either valley (Onton and Steenburgh 2001; cf. their Fig. 15).

The flow pattern along the Wasatch Mountains is likely influenced by the presence of low-level moisture contrasts. In CTL, the airmass adjacent to the northern Wasatch Mountains exhibits a lapse rate less than dry-adiabtic and dewpoint depressions near 5°C below 500-hPa (Figs. 3.14a-b). Within the GSLE band over the Salt Lake Valley, the atmosphere is saturated and moist-adiabatic (Fig. 3.14c). Hence the air to the north of the Salt Lake Valley is stable with respect to moist and dry motions and is deflected southward along the Wasatch Mountains. Conversely, the airmass within the GSLE band is saturated, with near-neutral moist stability, such that some flow over the barrier is possible. Where this occurs, the confluence of blocked and partially-unblocked airmasses might enhance precipitation within the GSLE band. A similar scenario is

described on a larger scale by Rotunno and Ferretti (2001) in the Piedmont region of the Alps. There subsaturated air is deflected along a barrier and converges with saturated air able to flow over the barrier, thus producing enhanced vertical motion and more intense precipitation. A complicating factor in this scenario is that although the moist Brunt-Väisälä frequency is near zero within the precipitation band, the low-level flow direction is perpendicular to, or even away from the barrier. Although static stability does not inhibit flow the central Wasatch Mountains, the near-surface pressure gradient drives low-level southerly flow within the Salt Lake Valley, and Froude number calculations below 750 hPa do not indicate across-barrier flow. Thus the contribution of horizontal moisture contrasts to downstream convergence is expected to be small, although blocking along the northern Wasatch Front is certainly reinforced by dry air below crest level.

Thermally driven flows associated with topography do not appear to play a significant role in the 27 Oct 2010 GSLE event. In a scenario where steep topography is located in close proximity to a water body and large-scale flows are weak, thermally driven downslope flows may help to initiate and enhance nocturnal land breezes (e.g., McGowan et al. 1995). In a benign weather pattern when thermally driven flows dominate, combined downslope-land-breeze wind systems have been observed around the GSL, notably the Tooele Valley (Stewart et al. 2002). We examined the potential role of thermal driven flows associated with the Wasatch Mountains by comparing observed surface winds near the lake with those further to the east at the base of the mountains. The moderate large-scale flow on 27 Oct 2010 appears to prevent the development of localized thermally driven downslope winds. A weak land breeze is observed along the eastern shore at QSY, indicated by east winds of 3–6 m $s^{-1}$ after 0600 UTC (Fig. 3.15a).

Winds at PWR in Weber Canyon, however, remain out of the west at 3–8 m $s^{-1}$ throughout the event (Fig. 3.15b), indicating that nocturnal downslope and gap flows are unlikely to be contributing to overlake convergence. The observed up-canyons flows are likely forced by a northeast–southwest-oriented mean-sea-level pressure gradient across the domain (not shown). Heating by the GSL creates localized low pressure and drives weak low-level onshore flows, as evident in mesonet observations and the 1500-m wind fields of CTL, FLAT, WAS and DT (c.f. Figs. 3.14a,c,d,e), but there is no indication that these flows are enhanced by nocturnal downslope or gap flows from the terrain along the northern Wasatch Front.

When orographically-induced convergence enhances convective updrafts within a lake-effect precipitation band, increased latent heating results from increases in condensation. This further enhances both the convective updrafts and adjacent land breezes, yielding stronger convergence at low levels (i.e., lake-effect as a "self-maintaining system"; Passarelli and Braham 1981). Thus a portion of the sensitivity of precipitation amounts to orography is due to this diabatic feedback, rather than convergence due to blocking and flow deflection alone.

Observed precipitation in the 27 Oct 2010 event increases considerably with elevation, from 7 mm at KSLC to 23 mm at CLN, both of which lie directly downstream of the long axis of the GSL. These data reflect a precipitation-altitude relationship that has been observed in other in lake-effect scenarios. Hill (1971) found a 25-50 cm increase in annual snowfall for every 100 m increase in elevation in the modest topography downstream of Lakes Erie and Ontario, and Saito et al. (1996) note substantial increases in precipitation efficiency over the mountains of Japan. Sources of

orographic enhancement include, but are not limited to: (1) increased vertical motions forced by steep terrain, (2) sub-cloud evaporation and/or sublimation over adjacent lowland areas, (3) advection of slow-falling hydrometeors from overlake convection into downstream terrain, and (4) increased precipitation efficiency due to higher nucleation rates when parcels are lifted to colder temperatures (e.g., Saito et al. 1996).

The largest contributor to orographic enhancement in CTL appears to be hydrometeor advection. Along a cross-section from Antelope Island to the east side of the Wasatch Mountains, the strongest vertical motions in CTL occur over the GSL, rather than the high terrain, and subcloud sublimation over the Salt Lake Valley is likely small because the relative humidity is greater than 90% from the surface to 4 km (Fig. 3.16a). The depth of the storm in fact decreases downstream along the cross-section line, and thus the Wasatch Mountains do not produce a region where temperatures are colder and ice nucleation is more likely than over the valley (e.g. Saito et al. 1996). The largest snow mixing ratios are noted over the GSL at 0700 UTC, and most 1-h hydrometeor trajectories from this area lead directly to high elevations of the Wasatch Mountains (Fig. 3.16b). This is a reasonable calculation, with an approximate 30-km horizontal transport in 1 h at an elevation of 5 km, where observed and modeled winds were ~10 m $s^{-1}$ (~36 km $h^{-1}$). Therefore, although the majority of snow formation takes place over the GSL, a large fraction of these hydrometeors are advected past the Salt Lake Valley before reaching the ground. An important caveat is that these conclusions are subject to the manner in which the WRF model simulates low-level moisture, vertical motions and hydrometeor transport within a narrow convective band at 1.33-km horizontal resolution. On 27 Oct 2010 and in other GSLE events, some of the other aforementioned orographic

enhancement processes could play a much larger role than depicted in CTL. Nonetheless, CTL presents a reasonable scenario in which orographic enhancement at the microphysical level is due more to the fortuitous position of the mountain range relative to the most intense convection rather than the processes described in past studies.

## Orographic Influences in a Lake-Enhanced Event

### Observed Evolution

We classify the 5 Nov 2011 as a lake-enhanced event rather than a pure lake-effect event, owing to the relatively large contribution of orographic precipitation, and smaller role of the GSL. As shown in a later section, significant mountain (and some valley) precipitation occurs in a simulation with no GSL. The 5 Nov 2011 event was shorter in duration and produced much less precipitation than on 27 Oct 2010. However we call attention to this event due to the availability of supplemental sounding and mesonet observations, and the profound simulated effect of orography on its evolution.

As on 27 Oct 2010, the 5 Nov 2011 event developed in association with a baroclinic trough that affected northern Utah after 0000 UTC 5 Nov 2011. At 1200 UTC 5 Nov 2011, a 500-hPa longwave trough was centered over Utah and northern Arizona, while the axis of an embedded shortwave trough had reached the Utah-Nevada border (Fig. 3.17a). Beneath the main trough, Utah was within a 700-hPa baroclinic zone, with cold advection occurring in northwest flow (Fig. 3.17b). By 1200 UTC, the 700-hPa temperature at KSLC had fallen to –9.5°C, which yielded a lake–700-hPa temperature difference of 19.7°C and, together with a layer-mean 850-700-hPa relative humidity above 80%, was sufficient for GSLE (Fig. 3.17b,c; Alcott et al. 2012). Saturated, moist-

adiabatic conditions dominated below 650-hPa in the 1200 UTC sounding at KSLC (Figs. 3.17c).

Widespread transient and orographic precipitation occurred around the GSL from 0200–1000 UTC. Around 1015 UTC an apparent mid-lake lake-effect band developed and began contributing to concurrent orographic precipitation generated by the Oquirrh Mountains (not shown). By 1200 UTC the band had become more organized, but still coincided with orographic precipitation (Fig. 3.18a). At 1330 UTC, transient and orographic precipitation diminished, and backing low-level winds caused the band to shift eastward and affect the Salt Lake Valley and central Wasatch Mountains (Fig. 3.18b). By 1500 UTC the band was already weakening and most other areas of precipitation had dissipated (Fig. 3.18c). The band itself dissipated shortly after 1700 UTC as low-level winds continued to back and fetch over the GSL decreased (Fig. 3.18d).

During the 5 Nov 2011 event (1015–1730 UTC) 3–8 mm of precipitation fell over the Salt Lake Valley and adjacent mountain ranges, based on gauge observations and radar estimation (Fig. 3.19). A portion of these totals are attributable to non-lake-effect processes, necessitating the phrase lake enhanced, rather than lake effect, to describe this event. Although precipitation totals were light, snowfall rates within the band were briefly heavy. Visibility was occasionally reduced to 0.25 mi (400 m) at KSLC in heavy snow (not shown). Mountain and valley areas received similar precipitation totals (e.g., 5 mm at KSLC and 5–7 mm in the Wasatch Mountains), a precipitation–altitude relationship that differed considerably from that observed on 27 Oct 2010.

Simulated Evolution

The WRF model simulation for 5 Nov 2011 produces a precipitation distribution similar to the observed event, albeit with subtle differences in structure and timing (Fig. 3.20). At 1200 UTC, the WRF simulated reflectivity indicates an area of precipitation along the south shore of the GSL, although it is unclear how much of this precipitation is driven by the GSL (Fig. 3.20a). By 1330 UTC, the WRF reflectivity accurately depicts a band in the Salt Lake Valley, distinct from areas of orographic and transient precipitation (Fig. 3.20b). The band briefly moves over the Wasatch Mountains and dissipates in backing low-level flow, then reforms around 1700 UTC further north (Fig. 3.20c-d).

Sensitivity to Orography

The 5 Nov 2011 event, although fairly minor, is another example of the synergistic interactions between lake-effect and orographic processes. Simulated precipitation amounts in CTL were similar to the observed values, with a mean of 0.56 mm, a maximum of 10.7 mm, and an area of 9 $km^2$ receiving more than 10 mm (Fig. 3.21a; Table 3.2). As in the 27 Oct 2010 event, removal of terrain around the GSL reduces precipitation amounts almost to zero. In the most basic case with no terrain and no GSL (FLAT-NL), the mean precipitation during the event is less than 0.01 mm, with a maximum of 0.3 mm (Fig. 3.21b; Table 3.2). In FLAT, the mean precipitation is also less than 0.01, with a maximum of 0.9 mm (Fig. 3.21c; Table 3.2). With only the Wasatch Mountains in WAS, the mean precipitation was 0.46 mm, 18% less than in CTL, with a maximum of 7.3 mm (Fig. 3.21d; Table 3.2). An area of banded precipitation still developed directly south of the GSL in WAS, despite the absence of the Oquirrh Mountains. With full downstream orography (DT), the mean precipitation nearly

doubled from WAS to 0.87 mm, 55% more than CTL, with a maximum of 16.3 mm and 265 $km^2$ receiving more than 10 mm (Table 3.2). Differences between CTL and DT are largest over the Salt Lake Valley and Oquirrh Mountains (Fig. 3.21e). Mean precipitation in NL is 0.19 mm, 67% less than CTL, with a maximum of 4.3 mm (Table 3.2). NL yields primarily orographic precipitation at high elevations, but still produces an area of banded precipitation along the far western side of the Salt Lake Valley (Fig. 3.21f). The band in NL however is more limited in areal coverage and produces only 0.2–1 mm of precipitation, versus 3–5 mm in CTL. Thus while the simulated lowland precipitation on 5 Nov 2011 cannot be described as entirely lake-driven, the GSL does play a significant role.

Upstream Orographic Influences

As on 27 Oct 2010, upstream barriers lead to considerable drying and modification of the low-level flow in the 5 Nov 2011 event. Model diagnostics show lowest-sigma-level relative humidity is 15-25% lower over northern portions of the GSL than over the Snake River Plain (Fig. 3.22a), although the drying is limited to the lowest 800 m above the GSL level (Fig. 3.22b). The difference in low-level potential temperature between the Snake River Plain and north shore of the GSL is approximately 3 K. Although the low-level relative humidity is higher than on 27 Oct 2010, very dry air is present at only 3 km in the 5 Nov 2011 simulation.

The upstream flow pattern at 1230 UTC on 5 Nov 2011, the approximate time of peak intensity, is similar to that observed during the 27 Oct 2010 event (Fig. 3.23a). Flow is blocked by the Albion, Raft River and adjacent mountain ranges and deflected along the Snake River Plain. A well-developed wake is located southeast of the Raft

River Mountains, with a curved zone of confluence over the north arm of the GSL (Fig. 3.23a). Model diagnostics (not shown) indicate that this zone is convergent. Convergence here is likely enhanced, as on 27 Oct 2010, by acceleration of flow through Moburg Canyon and other gaps in the upstream barrier, and by blocking and deflection along the Promontory Mountains. Removal of the upstream terrain in DT leaves a uniform northwest flow pattern over the north arm of the GSL (Fig. 3.23b).

IOP6 observations support the features identified in CTL. The 1200 UTC sounding at Kelton (KEL1; see Fig. 3.1 for location) shows a flow reversal from the surface to 800 hPa, with near-surface southerly winds of 5 m $s^{-1}$ (Fig. 3.24). Downstream of the Raft River Mountains, observations from mesonet sites indicate light (5–7 m $s^{-1}$) northwest or northerly flow, with the winds at KEL1 becoming southeasterly at 1700 UTC (cf. Fig. 3.18d).

Downstream Orographic Influences

Downstream orographic influences are a crucial factor in the 5 Nov 2011 event. Light northerly flow along the Wasatch Mountains meets northwesterly flow over the GSL along a convergence zone from the Promontory Mountains to the northeast edge of the Oquirrh Mountains. In CTL, the simulated GSLE enhancement is collocated with this convergence zone and is affecting the Oquirrh Mountains and western portions of the Salt Lake Valley (Fig. 3.25a). Kinematic effects along the Wasatch Front are further supported by the 1200 UTC IOP6 sounding near Syracuse (Fig. 3.26; QSY; see Fig. 3.1 for location). Winds are northwesterly at mid levels and north-northwesterly below 700 hPa, with speeds near 10 m $s^{-1}$ at the surface. Near-saturated, moist-adiabatic conditions below 700 hPa are capped by a stable layer from 700–670 hPa, which increases the

likelihood of blocking. Convergence over the Salt Lake Valley is further enhanced by deflection of the low-level flow around the Oquirrh Mountains (Fig. 3.25a), although the effect is not as apparent as on 27 Oct 2010.

As on 27 Oct 2010, orographically induced convergence on 5 Nov 2011 is necessary for the development of an organized, lake-enhanced band. Neither of the simulations with flat topography produces more than 1 mm of precipitation anywhere in the domain. FLAT-NL shows near uniform northwest flow (Fig. 3.25b), while FLAT produces thermally driven confluence near the southeast shore of the GSL (Fig. 3.25c). WAS develops a precipitation band along a confluence zone extending south-southeast from Antelope Island at 1230 UTC, in addition to orographic precipitation over the Wasatch Mountains (Fig. 3.25d). In DT, a similar precipitation band forms, but covers a larger area and is more intense (Fig. 3.25e). As in the 27 Oct 2010, deflection around the northern Oquirrh Mountains in DT yields an effect similar to that of idealized concave ridges, and nearly doubles mean precipitation relative to the WAS simulation. NL is dominated by orographic precipitation, with some cellular structures in the Salt Lake Valley (Fig. 3.25f). Despite some flow deflection along the Wasatch Mountains and north of the Oquirrh Mountains, removing the GSL inhibits the formation of organized valley precipitation. Wind speeds are also much weaker in NL, presumably due to the increase in surface friction when replacing the GSL with land, which may limit the strength of orographically-generated convergence zones.

On 5 Nov 2011, observed precipitation totals were only slightly higher in the Wasatch Mountains than the Salt Lake Valley, which raises questions regarding the differing precipitation-altitude relationships between the two events in this study. The 5

Nov 2011 CTL simulation, however, does not produce a semiorganized band directly affecting the Wasatch Mountains, as was observed from about 1300–1700 UTC. Model errors in evolution and position of the band in CTL therefore prevent a proper analysis of the roles of subcloud evaporation, hydrometeor advection and other microscale processes. Analysis of Doppler-on-Wheels data collected during the 5 Nov 2011 event will provide further insight regarding these orographic factors, but at the time of writing the data has not yet been fully processed.

## Summary

We have examined two GSLE events where analysis of observations and numerical sensitivity studies indicate a synergistic, nonlinear interaction between lake and orographic effects. Within the spectrum of lake-dominated to terrain-dominated precipitation, these events occur at a point where lake–air interactions and orographic flow modification are together crucial to the development of precipitation. The major orographic influences are shown graphically in Fig. 3.27, and summarized below. Although these processes are presented in a sequential manner, it must be emphasized that they are occurring simultaneously:

- A foehn-like flow over the upstream terrain leads to adiabatic warming and lower relative humidity at low-levels, which reduces the intensity of both events.
- A convergence zone forms over the north arm of the GSL, in the lee of the Raft River Mountains. This feature may help to organize lake-effect precipitation bands downstream.
- A secondary convergence zone develops over southern portions of the GSL between weak northerly flow along the northern Wasatch Front and moderate

northwest flow over the GSL. Blocking of the low-level flow by the Wasatch Mountains or flow stagnation in the lee of terrain northeast of the GSL may contribute to this convergence zone.

- The Oquirrh Mountains deflect the low-level flow into the Salt Lake Valley, acting as a "funneling mechanism" similar to idealized concave ridges in Watson and Lane (2012).
- Where orographically induced convergence zones enhance GSLE bands, a diabatic feedback mechanism may significantly increase the degree of enhancement.
- Observed and modeled precipitation amounts on 27 Oct 2010 were considerably higher in the Wasatch Mountains than over adjacent lowland regions. Based on CTL, we attribute this to the transport of hydrometeors from the more intense overlake convection into high terrain downstream. Subcloud sublimation and orographically enhanced vertical motions are believed to play smaller roles in this event, but our results are subject to the accuracy of the model simulation.

Low-level drying in the foehn-like upstream flow and the development of convergence zones in the lee of isolated obstacles are two independent effects that work against one another in both events. Our results indicate that low-level drying offsets any enhancement of GSLE by lee convergence zones, with upstream terrain yielding a net reduction in precipitation amounts. However, it is conceivable that changes in the upstream thermodynamic and kinematic structure could produce a case in which the superposition of these effects yields little or no sensitivity of precipitation amounts to upstream terrain.

In both events, model sensitivity studies involving the removal of either the lake or the surrounding terrain produce much less precipitation than the control cases. Thus our results demonstrate two situations where the relatively warm lake and high mountain ridges act together to yield significant precipitation episodes that would have been negligible without one or both of the lake and mountain components. These results, however, are not necessarily applicable to events that lie near the ends of the lake-orographic forcing spectrum. For example, in a case of abundant lake-induced instability and low-level moisture, the co-location of orographic convergence zones with lake-effect convection is unlikely to greatly enhance precipitation amounts. On the other end of the spectrum, when the primary driver of precipitation is orographic uplift, the presence of an upstream water body might have limited influence on precipitation amounts. As is often a characteristic of complex mesoscale environments, subtle changes in the low-level thermodynamic profile or background flow direction can have a large impact on these non-linear lake–orographic interactions. Steenburgh and Onton (2001) describe a more northerly-flow, lake-dominated case on 7 Dec 1998, and domain-average precipitation amounts in this event were not significantly reduced in a simulation with flat terrain (Onton and Steenburgh 2001). In the 7 Dec 1998 event, precipitation was largely driven by the lake and displaced from areas where blocking and deflection of the low-level flow by orography was likely to produce convergence. Thus the removal of terrain had a small impact on the precipitation field, a finding that is perhaps applicable to other northerly-flow GSLE events, but contrasts greatly with the results of this study.

The lake-mountain environment in northern Utah is unusual by North American standards, but the results of this study retain broader applicability to the smaller terrain of

the Laurentian Great Lakes, Lake Champlain, and the Finger Lakes. While the more simplistic model of orographic enhancement (i.e., increased vertical motion due to direct ascent) is perhaps not as appropriate for these regions, low-level blocking and channeling by small obstacles may play a larger role than has been previously considered. The superposition of orographically generated convergence zones with thermally driven lake circulations is likely to have a significant impact on lake effect associated with small water bodies, where fetch is limited and sensible and latent heat fluxes are small. In a larger context, lake-effect storms associated with the Sea of Japan and Black Sea occur near terrain similar in scale to the Wasatch Mountains and nearby ranges. The size and shape of downstream terrain in these areas, particularly where orographic concavities are present, may play an important kinematic role in the development of heavy precipitation.

Table 3.1

Sensitivity of 0230–1700 UTC 27 Oct 2010 simulated precipitation amounts to orography, for the domain shown in Figs. 3.9 and 3.21.

| Event | Experiment | Description | Mean precip. (mm) | Change from CTL | Max. precip. (mm) | Area of ≥10 mm precip. ($km^2$) |
|---|---|---|---|---|---|---|
| 27 Oct 2010 | FLAT-NL | Flat, no lake | 0.00 | –100% | 0.0 | 0 |
| 27 Oct 2010 | FLAT | Flat domain | 0.07 | –94% | 3.2 | 0 |
| 27 Oct 2010 | WAS | Wasatch only | 0.80 | –27% | 21.6 | 214 |
| 27 Oct 2010 | DOWN | Downstream only | 1.77 | +61% | 41.9 | 1703 |
| 27 Oct 2010 | CTL | Real topography | 1.10 | - | 26.8 | 731 |
| 27 Oct 2010 | NL | No lake | 0.11 | –90% | 2.5 | 0 |

Table 3.2

Sensitivity of 1015–1730 UTC 5 Nov 2011 simulated precipitation amounts to orography, for the domain shown in Figs. 3.9 and 3.21.

| Event | Experiment | Description | Mean precip. (mm) | Change from CTL | Max. precip. (mm) | Area of ≥10 mm precip. ($km^2$) |
|---|---|---|---|---|---|---|
| 5 Nov 2011 | FLAT-NL | Flat, no lake | <0.01 | –100% | 0.3 | 0 |
| 5 Nov 2011 | FLAT | Flat domain | <0.01 | –100% | 0.9 | 0 |
| 5 Nov 2011 | WAS | Wasatch only | 0.46 | –18% | 7.3 | 0 |
| 5 Nov 2011 | DOWN | Downstream only | 0.87 | +55% | 16.3 | 265 |
| 5 Nov 2011 | CTL | Real topography | 0.56 | - | 10.7 | 9 |
| 5 Nov 2011 | NL | No lake | 0.19 | –67% | 4.3 | 0 |

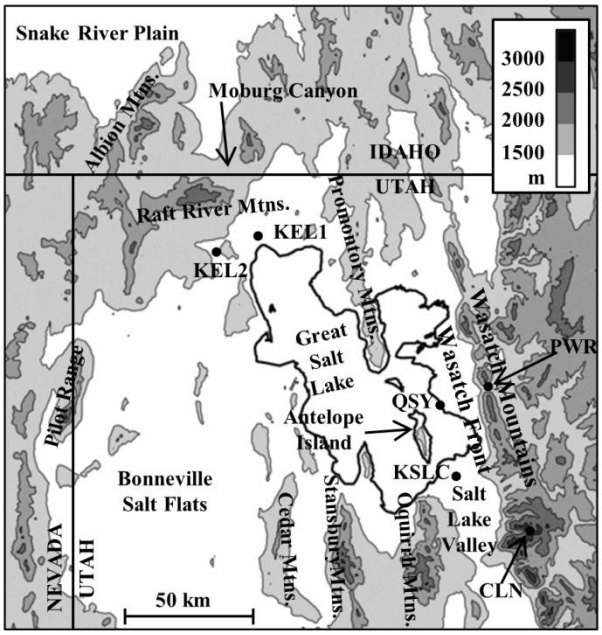


Fig. 3.1. Elevation (m; shaded according to scale at upper right) and landmarks of the study region.

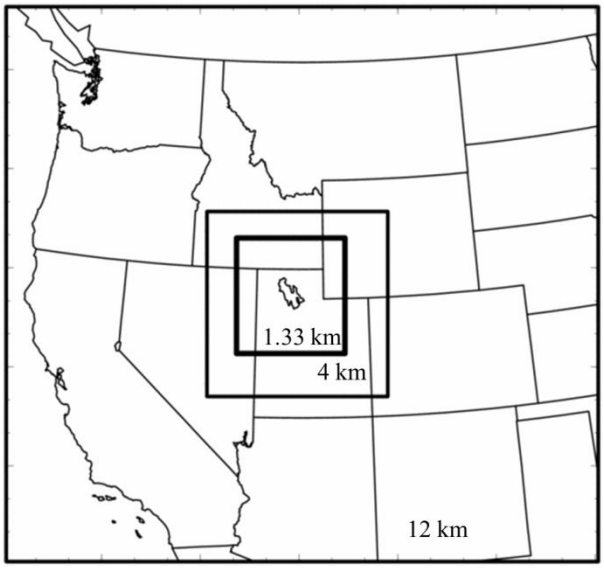


Fig. 3.2. Locations of the three nested WRF domains.

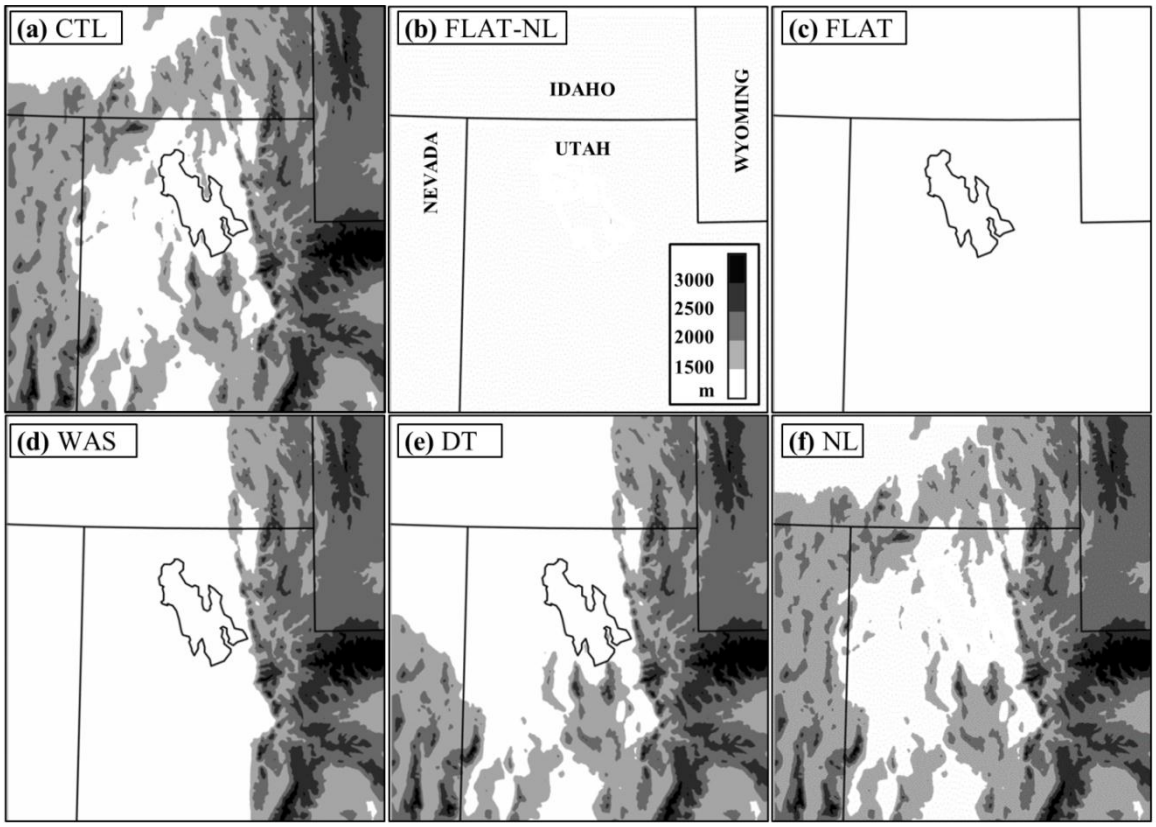


Fig. 3.3. WRF model terrain elevations (m; shaded according to scale in [a]) for the (a) CTL; (b) FLAT-NL; (c) FLAT; (d) WAS; (e) DT; and (f) NL simulations.

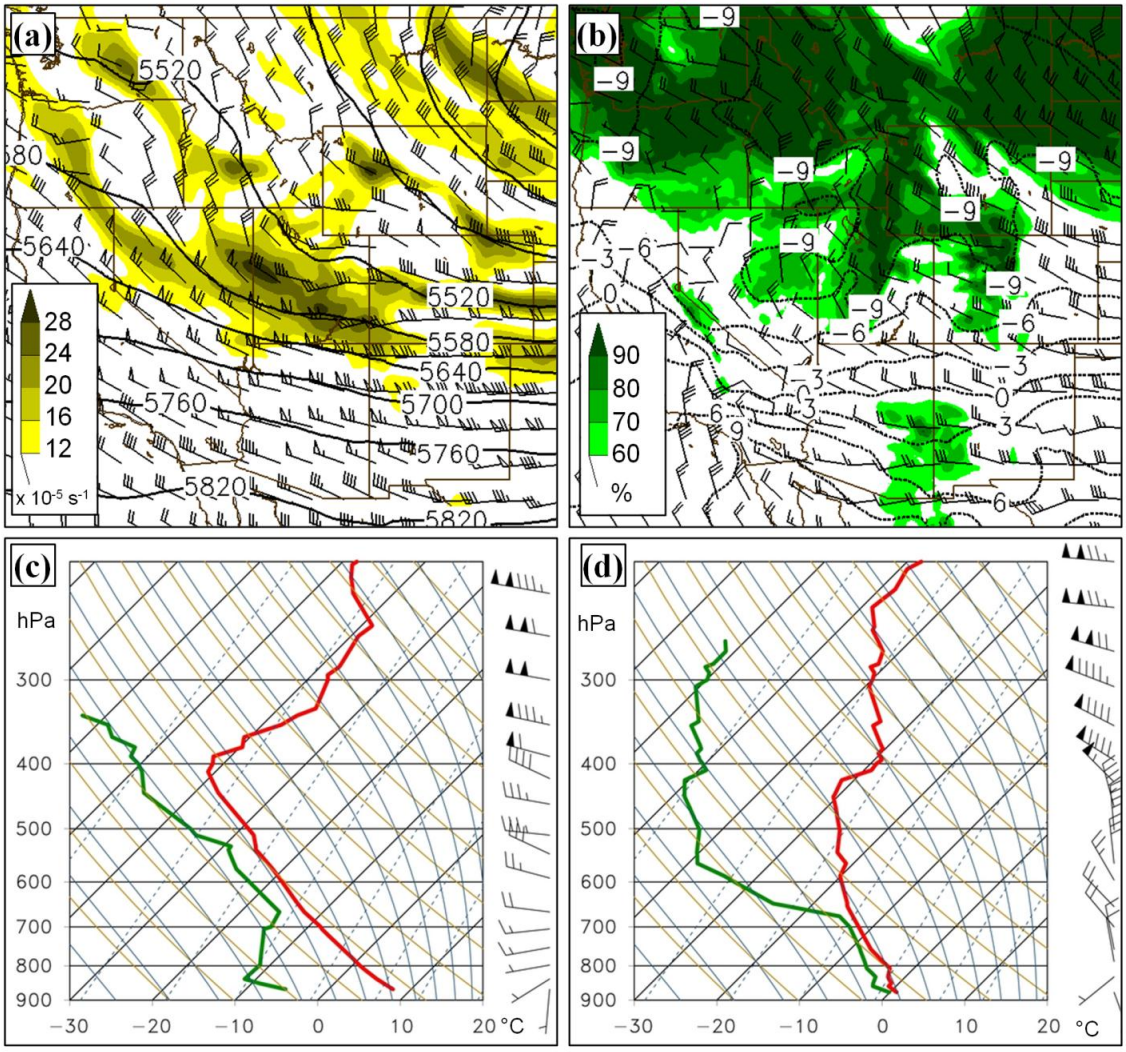


Fig. 3.4. Environmental conditions for 27 Oct 2010: a) 500-hPa geopotential height (black contours), wind barbs (full barb = 5 m $s^{-1}$, half barb= 2.5 m $s^{-1}$), and absolute vorticity (x$10^{-5}$ $s^{-1}$, shaded according to scale at left) at 0600 UTC; b) 700-hPa temperature (black contours, dashed where negative), 700-hPa wind barbs, and 850–700-hPa mean relative humidity (%, shaded according to scale at left) at 0600 UTC; c) Salt Lake City Skew *T*-log*p* [temperature, dewpoint, and wind barbs (full and half barbs denote 5 and 2.5 m $s^{-1}$, respectively)] diagram for 0000 UTC; d) Same as (c) except for 1200 UTC.

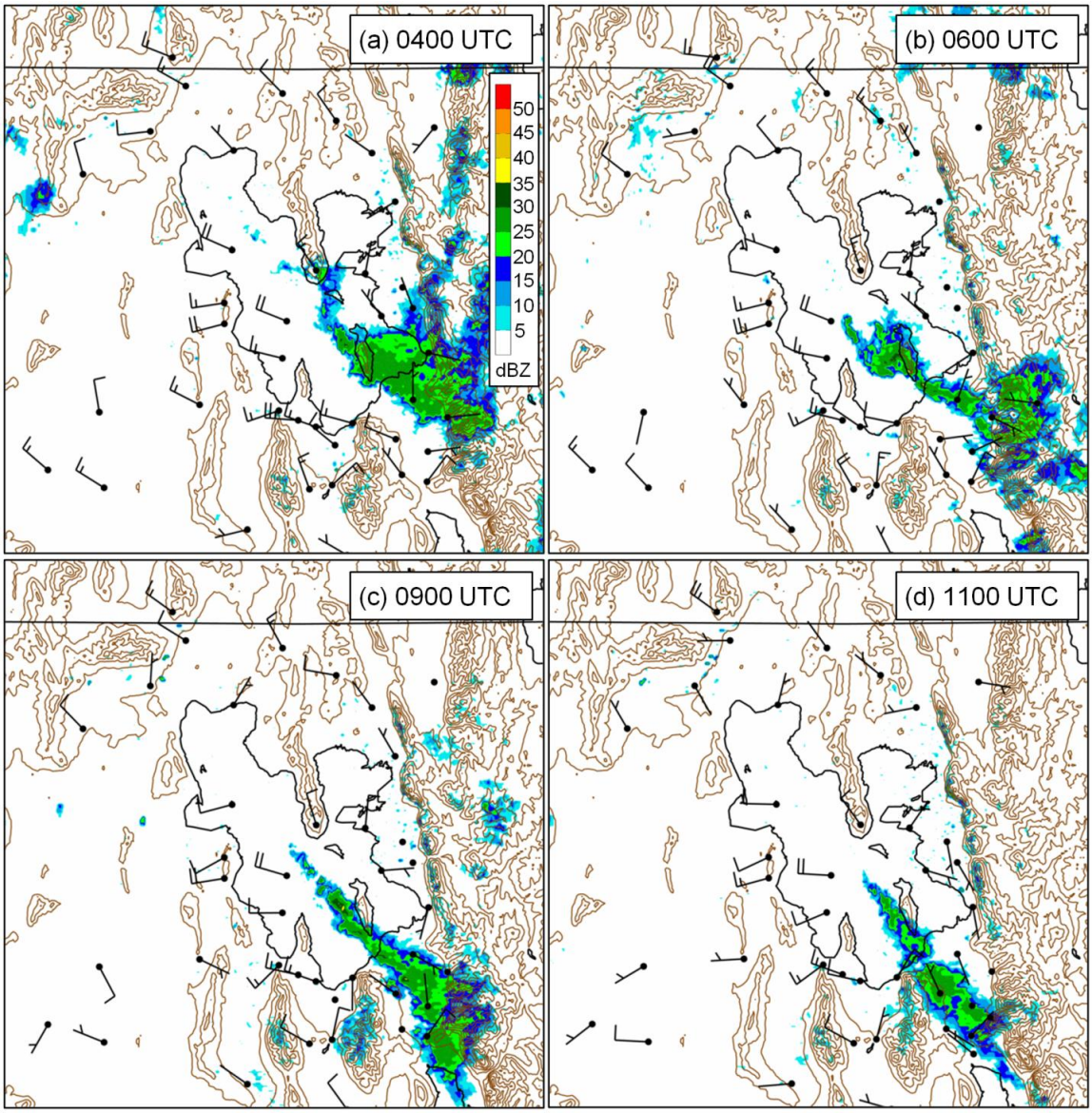


Fig. 3.5. Terrain (brown contours every 200 m), KMTX radar reflectivity [dBZ, shaded according to scale in (a)] and mesonet winds (full barb = 5 m $s^{-1}$, half barb = 2.5 m $s^{-1}$) on 27 Oct 2010 at (a) 0400 UTC, (b) 0600 UTC, (c) 0900 UTC, and (d) 1100 UTC.

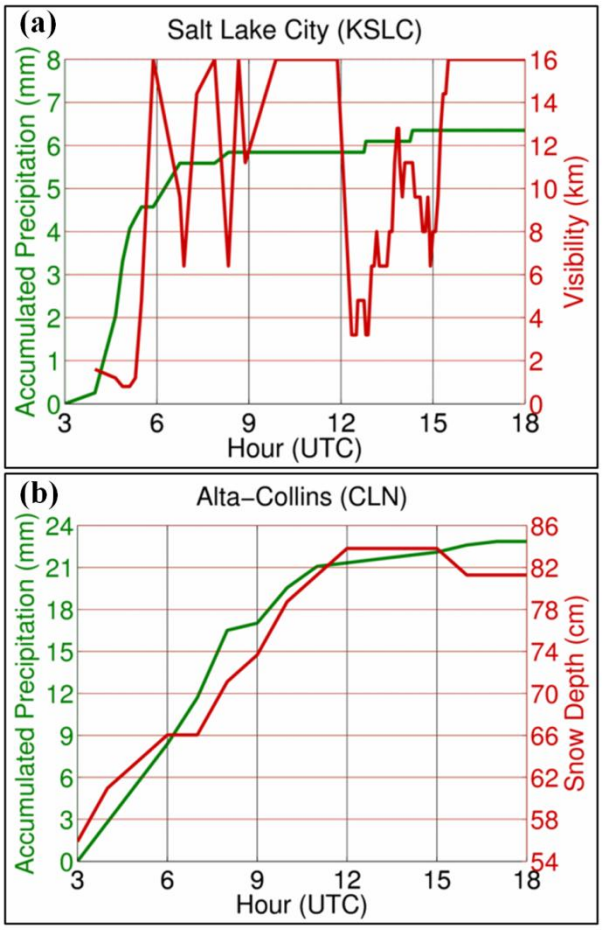


Fig. 3.6. Observed conditions during the 27 Oct 2010 GSLE event. (a) KSLC accumulated precipitation (mm; green line), and visibility (km; red line). (b) CLN accumulated precipitation (snow-water-equivalent; mm; green line), and snow depth (cm; red line).

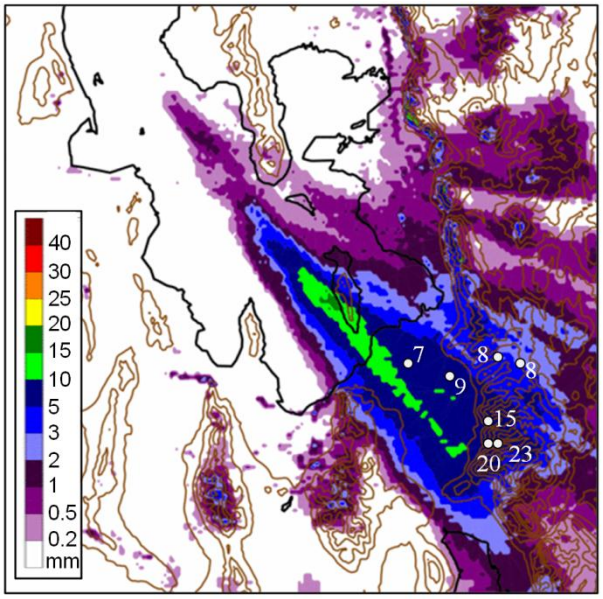


Fig. 3.7. Terrain (brown contours every 200 m) and precipitation totals during the 27 Oct 2010 GSLE event, with radar estimated totals shaded according to scale at left and observed totals annotated in white text (mm).

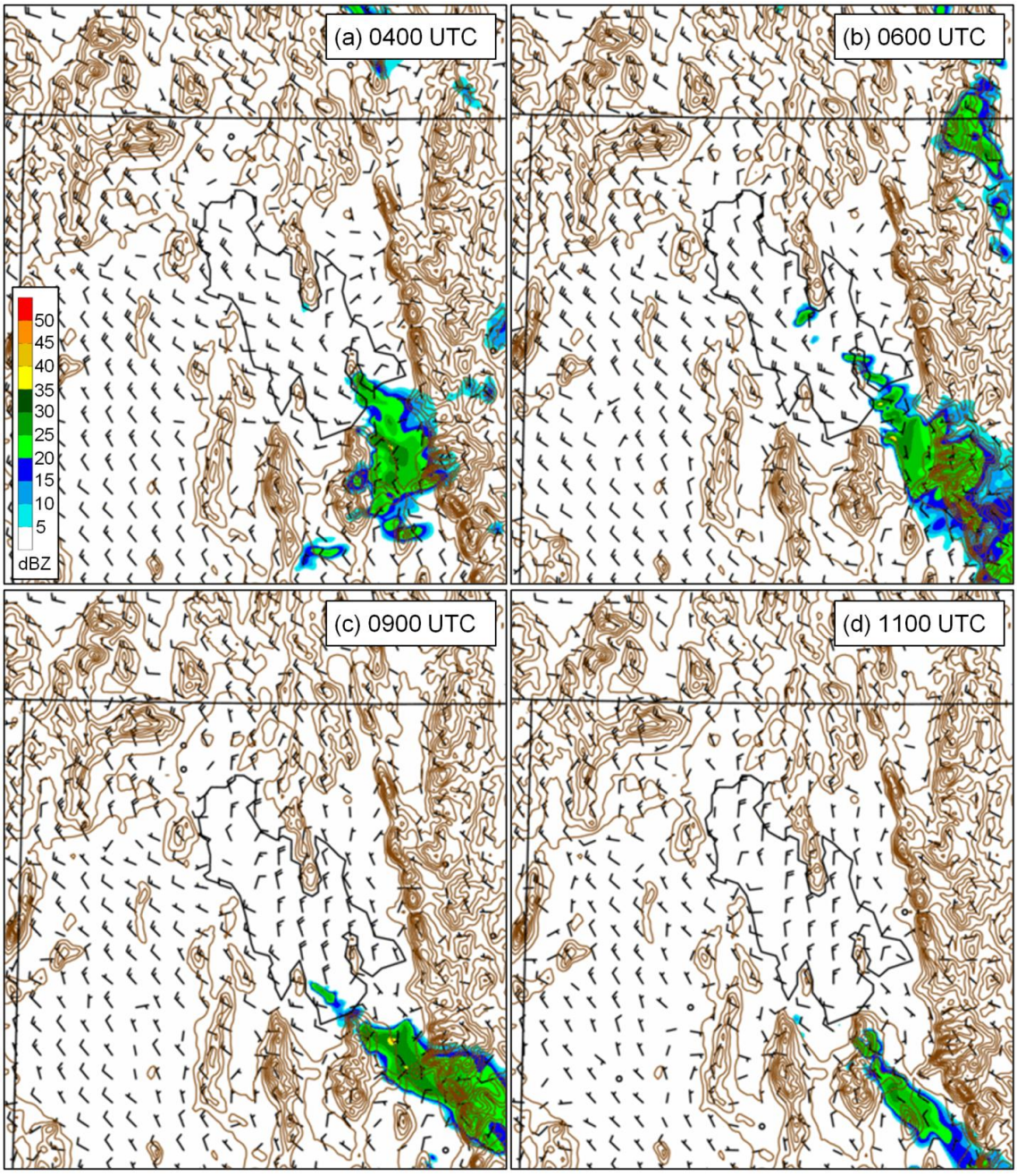


Fig. 3.8. Model terrain (brown contours every 200 m), simulated 10-m wind speed (full barb = 5 m $s^{-1}$, half-barb = 2.5 m $s^{-1}$) and radar reflectivity (dBZ, shaded according to scale in [a]) at (a) 0400, (b) 0600, (c) 0900, and (d) 1100 UTC on 27 Oct 2010.

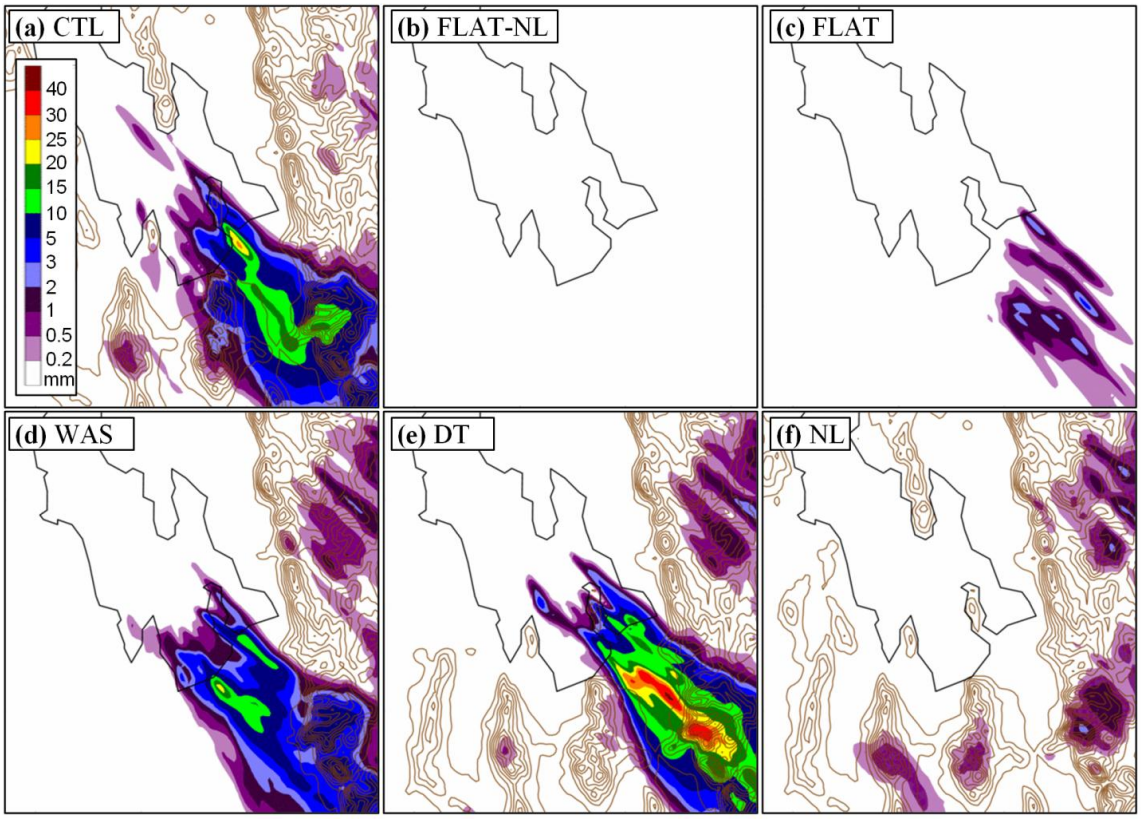


Fig. 3.9. Model terrain (brown contours every 200 m) and simulated precipitation (mm, shaded according to scale in [a]) from the (a) CTL, (b) FLAT-NL, (c) FLAT, (d) WAS, (e) DT, and (f) NL simulations for 0230–1700 UTC 27 Oct 2010. Lake outlines in (b) and (f) are shown for reference only.

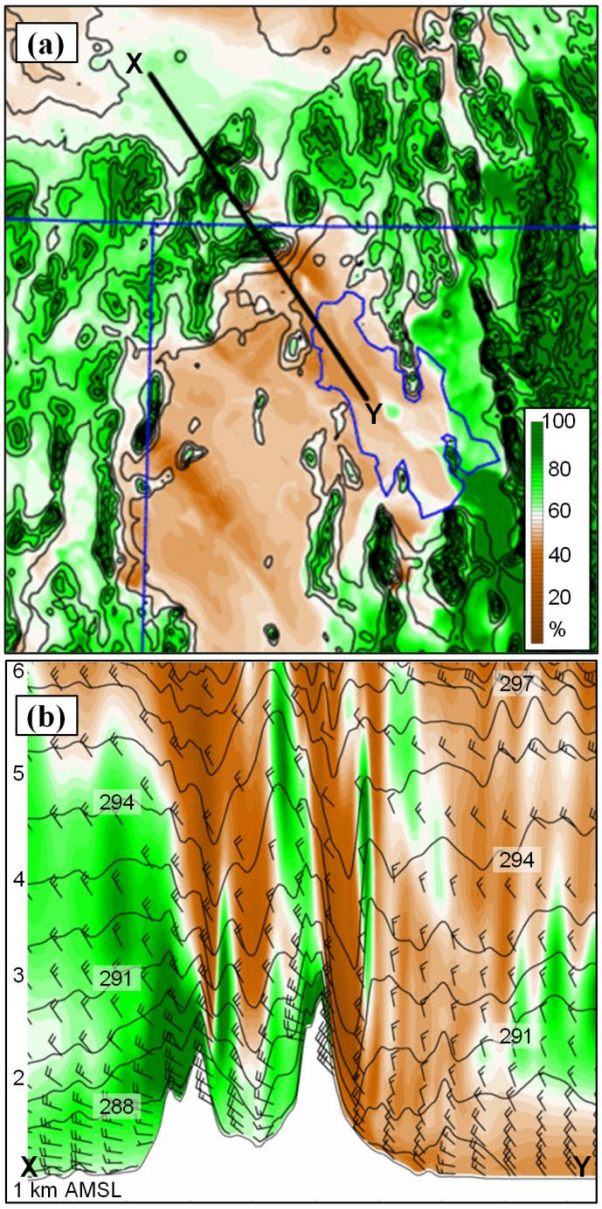


Fig. 3.10. Upstream modification. (a) Lowest sigma-level relative humidity (%, shaded according to scale at right) and terrain contours (200-m intervals) at 0700 UTC 27 Oct 2010. (b) Cross-section relative humidity (%, shaded according to scale in [a]), potential temperature (contoured at 1 K intervals) and winds (full barb = 5 m $s^{-1}$, half-barb = 2.5 m $s^{-1}$) averaged over 5 km either side of the thick black line in [a], at 0700 UTC 27 Oct 2010.

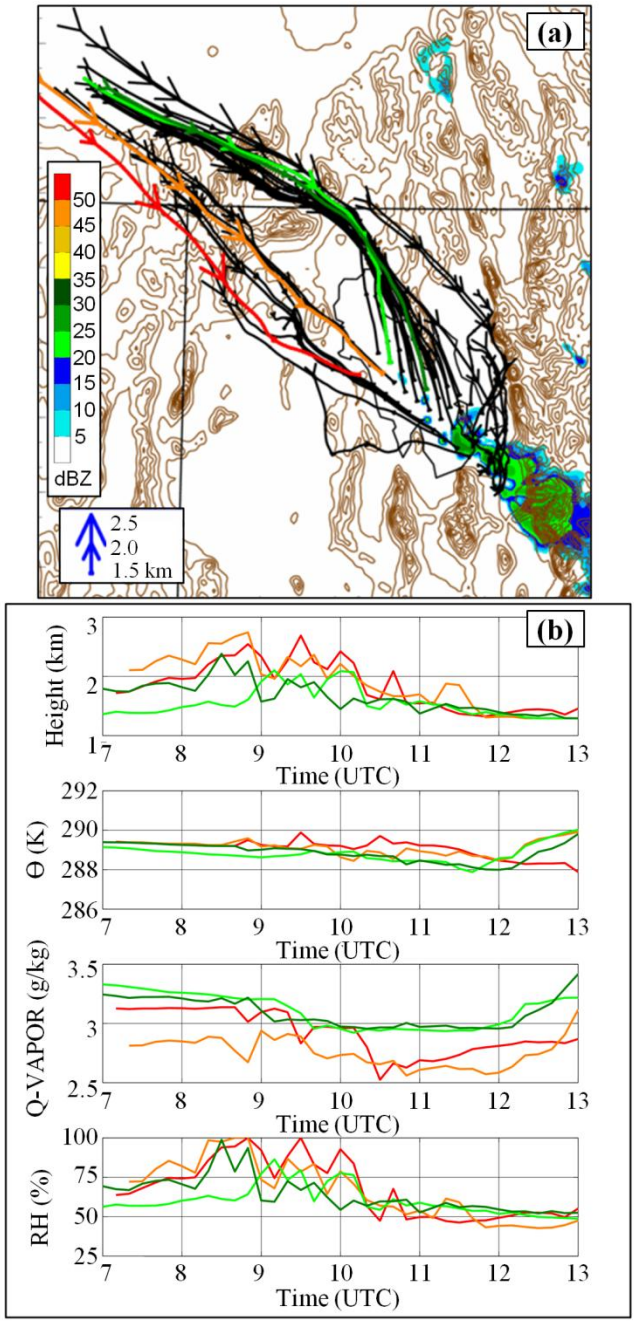


Fig. 3.11. Upstream kinematics. (a) Simulated trajectory paths beginning 0100 UTC and ending 0700 UTC 27 Oct 2010 in CTL, and simulated radar reflectivity (dBZ, shaded according to scale at left). Trajectory height (AMSL) indicated by arrow size, with scale at left. (b) Height, potential temperature, water vapor mixing ratio and relative humidity along selected trajectory paths in [a].

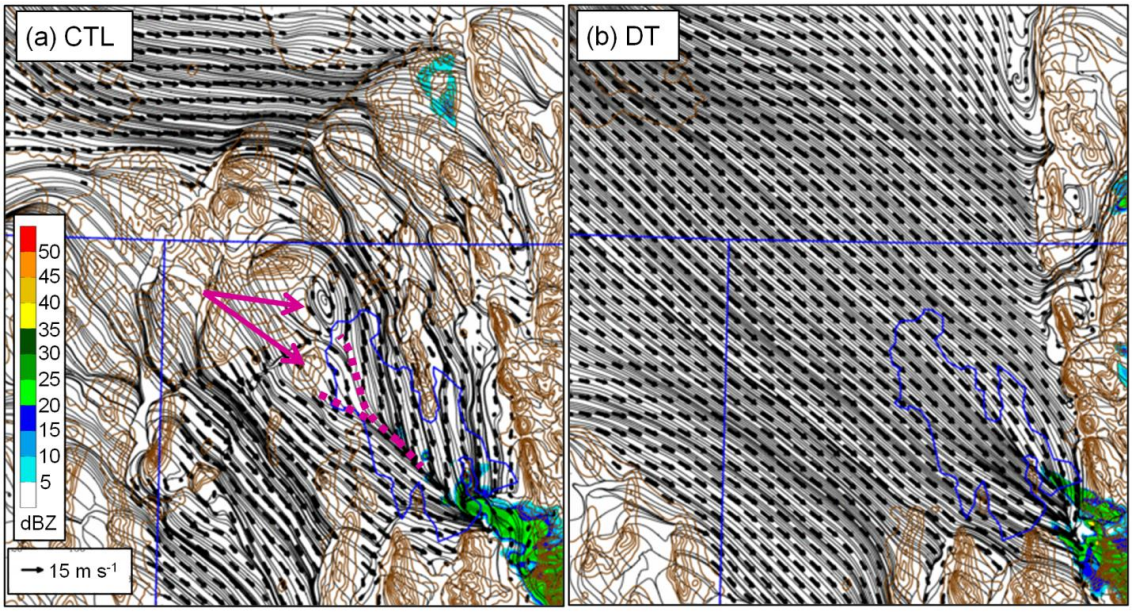


Fig. 3.12. Model terrain (brown contours every 200 m), 1500-m streamlines, wind vectors (length relative to sample vector in [a], and simulated reflectivity (dBZ, shaded according to scale in [a]) at 0700 UTC on 27 Oct 2010 for the (a) CTL; and (b) DT simulations. Purple arrows and dashed lines indicate wakes and confluence zones, respectively.

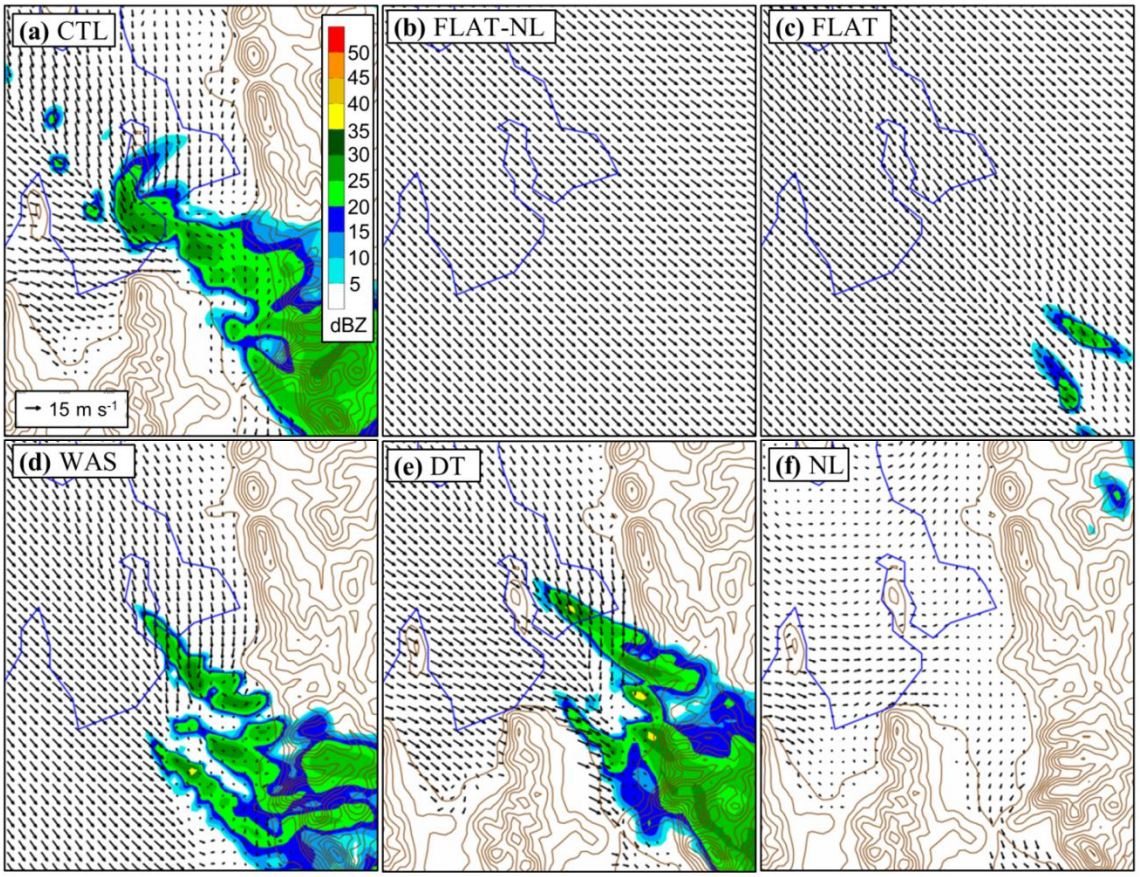


Fig. 3.13. Wind vectors (relative length according to scale in [a]) and simulated reflectivity (dBZ, shaded according to scale in [a]) for 0700 UTC 27 Oct 2010 in the (a) CTL, (b) FLAT-NL, (c) FLAT, (d) WAS, (e) DT, and (f) NL simulations. Lake outlines in (b) and (f) are shown for reference only.

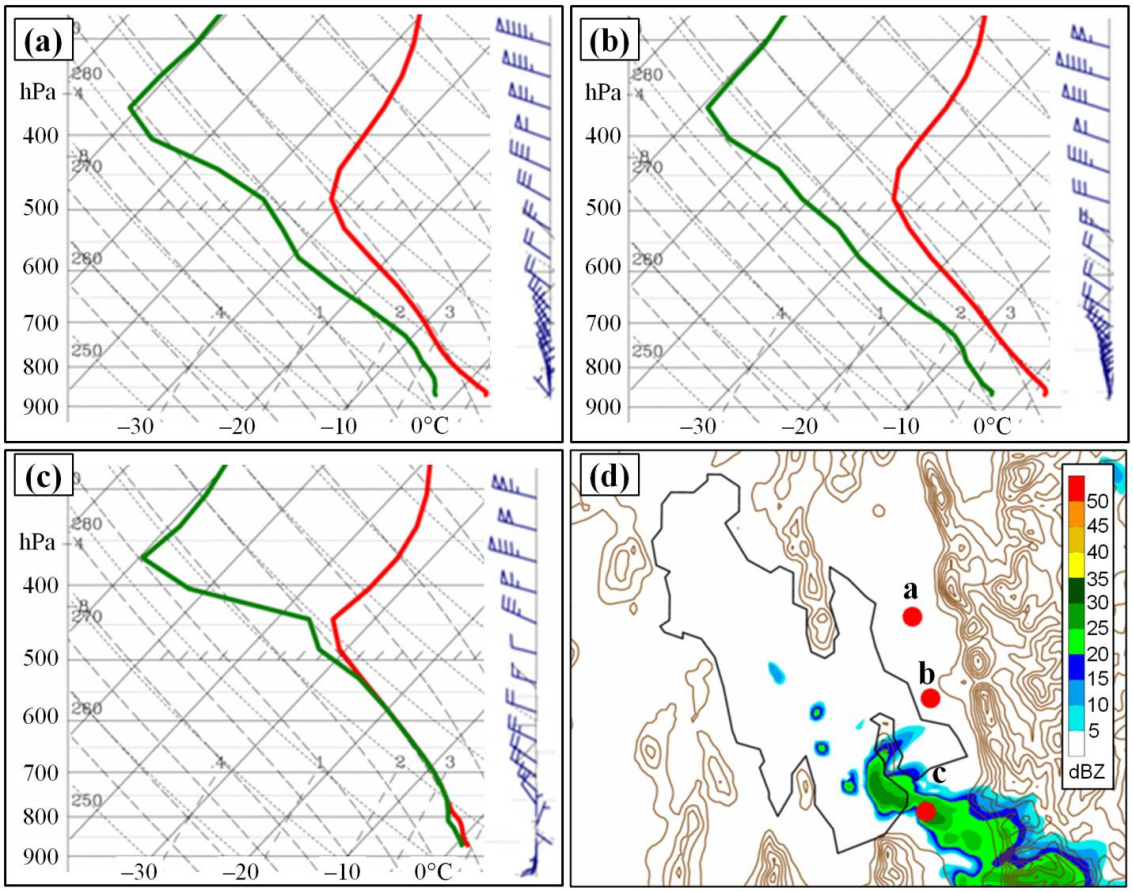


Fig. 3.14. Model thermodynamic profiles at 0700 UTC 27 Oct 2010 in CTL. Locations of profiles in (a), (b), and (c) indicated on map in (d). Simulated reflectivity in (d) shaded according to scale at right, with terrain height contoured every 200 m.

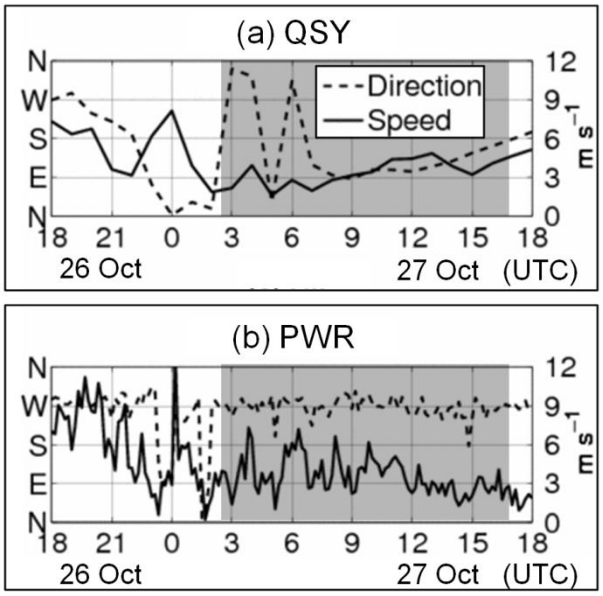


Fig. 3.15. Observed wind speed and direction at (a) Syracuse (QSY) and (b) PWR (see Fig. 3.1 for locations). Grey-shaded area indicates the time range of the 27 Oct 2010 GSLE event.

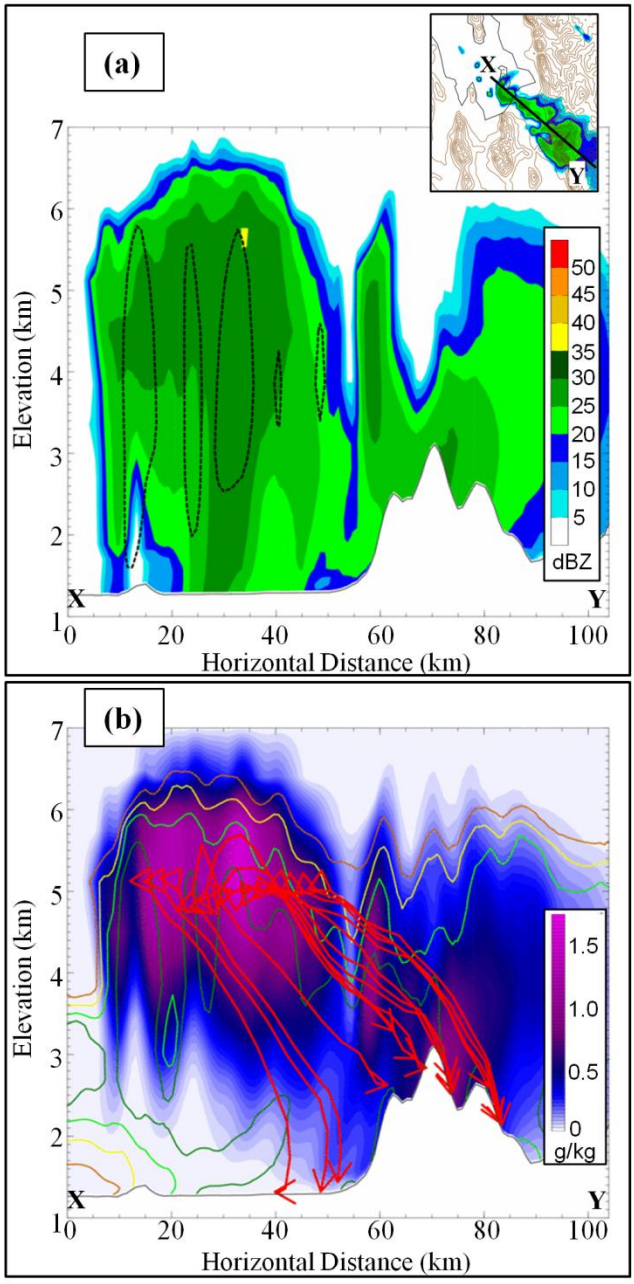


Fig. 3.16. Cross-sections for CTL at 0700 UTC 27 Oct 2010, with fields averaged over 5 km either side of the line indicated by inset in (a). (a) Simulated reflectivity (dBZ, shaded according to scale at right), and upward vertical velocity (dashed black contours where greater than 1 m $s^{-1}$). (b) Snow mixing ratio (g $kg^{-1}$, shaded according to scale at right), relative humidity (brown, yellow, light green, dark green contours indicate 60, 70, 80 and 90%), and 0700–0800 UTC hydrometeor trajectories (red lines).

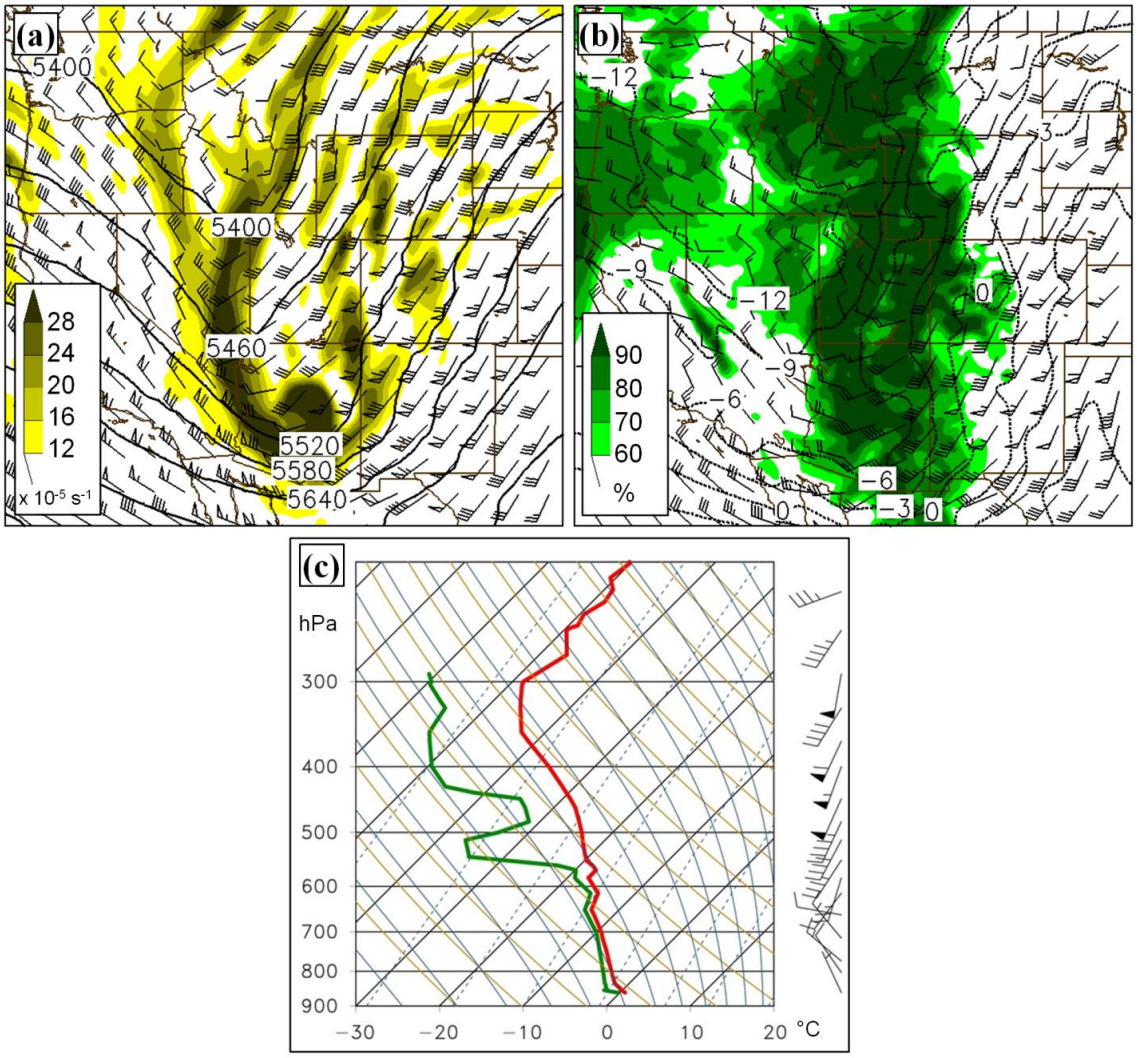


Fig. 3.17. Environmental conditions for 5 Nov 2011: (a) 500-hPa geopotential height (black contours), wind barbs (full barb = 5 m $s^{-1}$, half barb= 2.5 m $s^{-1}$), and absolute vorticity (x$10^{-5}$ $s^{-1}$, shaded according to scale at left) at 0600 UTC; (b) 700-hPa temperature (black contours, dashed where negative), 700-hPa wind barbs, and 850–700-hPa mean relative humidity (%, shaded according to scale at left) at 0600 UTC; (c) Salt Lake City Skew *T*-log*p* [temperature, dewpoint, and wind barbs (full and half barbs denote 5 and 2.5 m $s^{-1}$, respectively)] diagram for 0000 UTC.

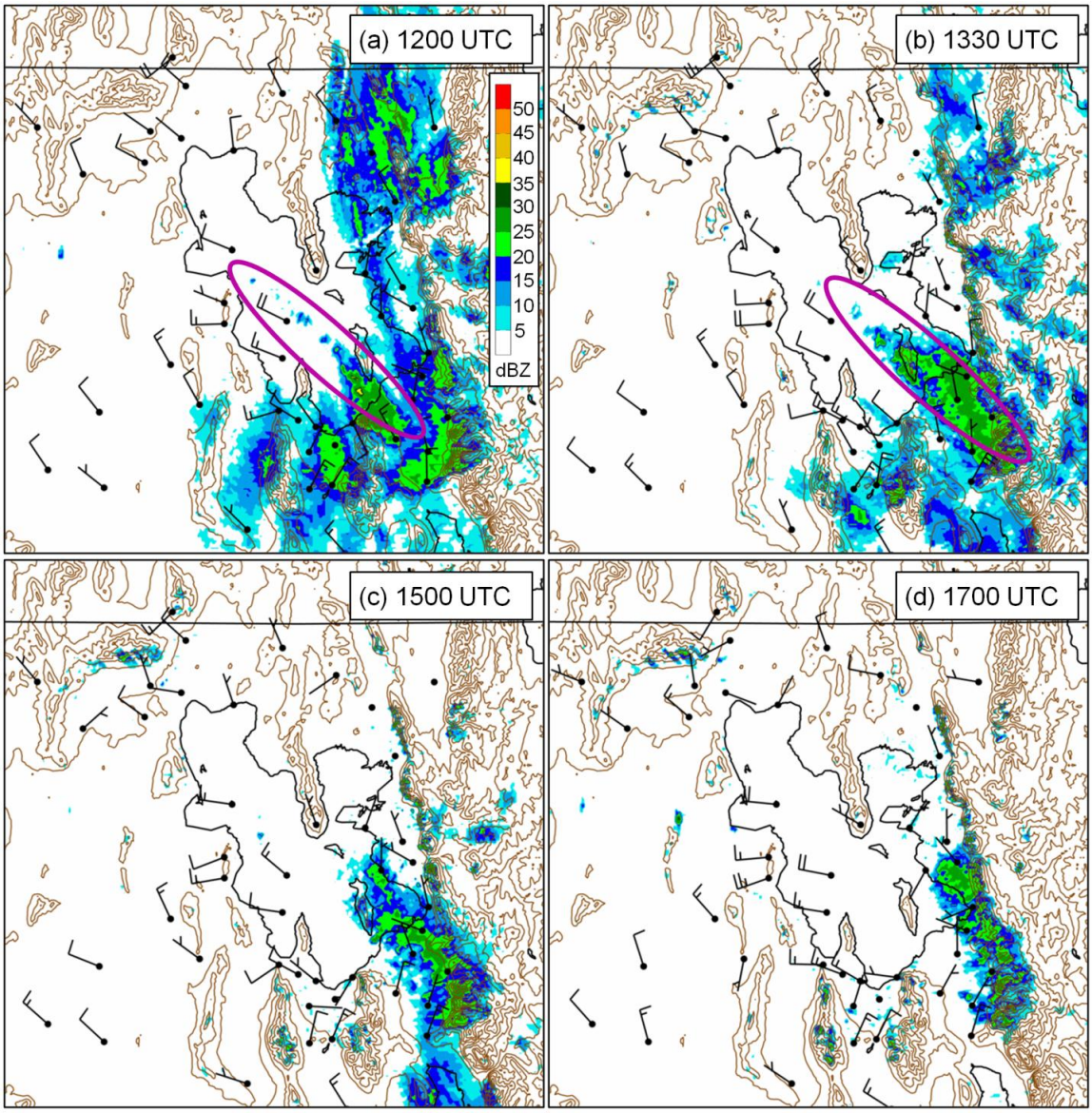


Fig. 3.18. Terrain (brown contours every 200 m), KMTX radar reflectivity [dBZ, shaded according to scale in (a)] and mesonet winds (full barb = 5 m $s^{-1}$, half barb = 2.5 m $s^{-1}$) on 5 Nov 2011 at (a) 1200 UTC, (b) 1330 UTC, (c) 1500 UTC, and (d) 1700 UTC. Apparent lake-effect band circled in purple in (a) and (b).

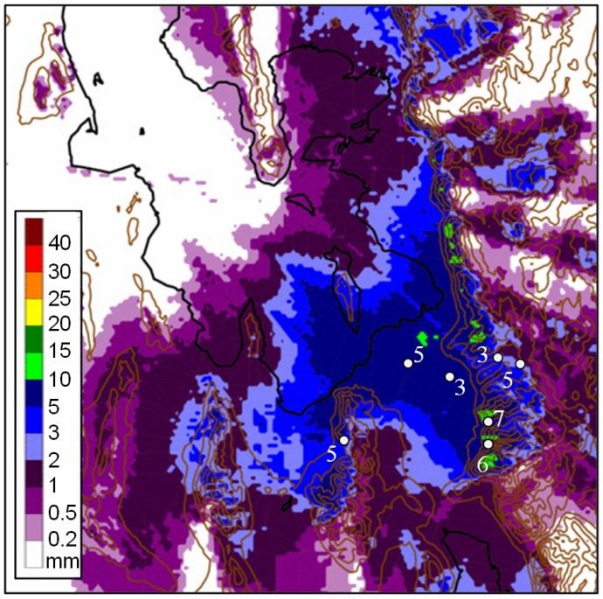


Fig. 3.19. Terrain (brown contours every 200 m) and precipitation totals during the 5 Nov 2011 GSLE event, with radar estimated totals shaded according to scale at left and observed totals annotated in white text (mm)..

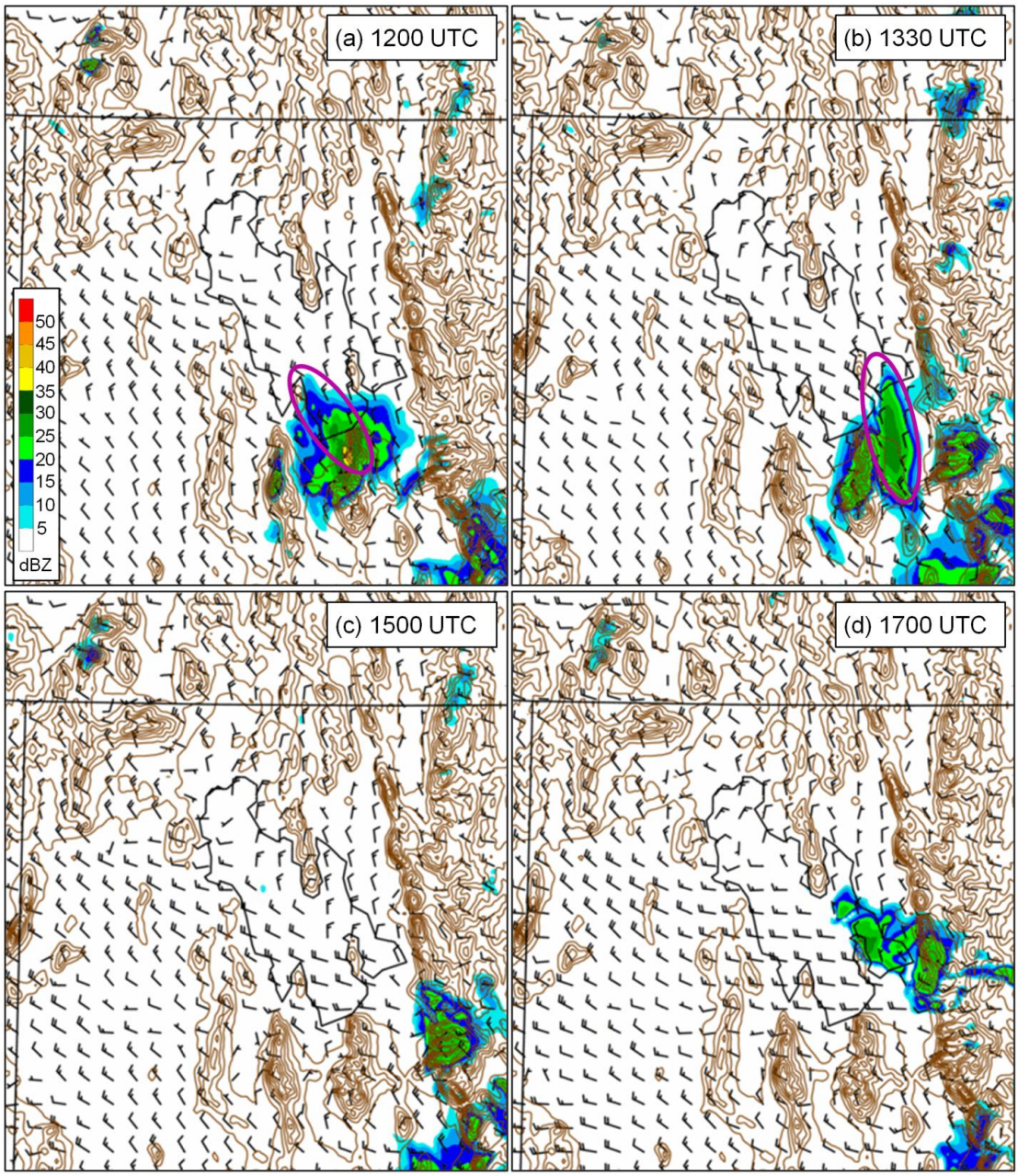


Fig. 3.20. Model terrain (brown contours every 200 m), simulated 10-m wind speed (full barb = 5 m $s^{-1}$, half-barb = 2.5 m $s^{-1}$) and radar reflectivity (dBZ, shaded according to scale in [a]) at (a) 1200, (b) 1330, (c) 1500, and (d) 1700 UTC on 5 Nov 2011. Lake-effect band circled in purple in (a) and (b).

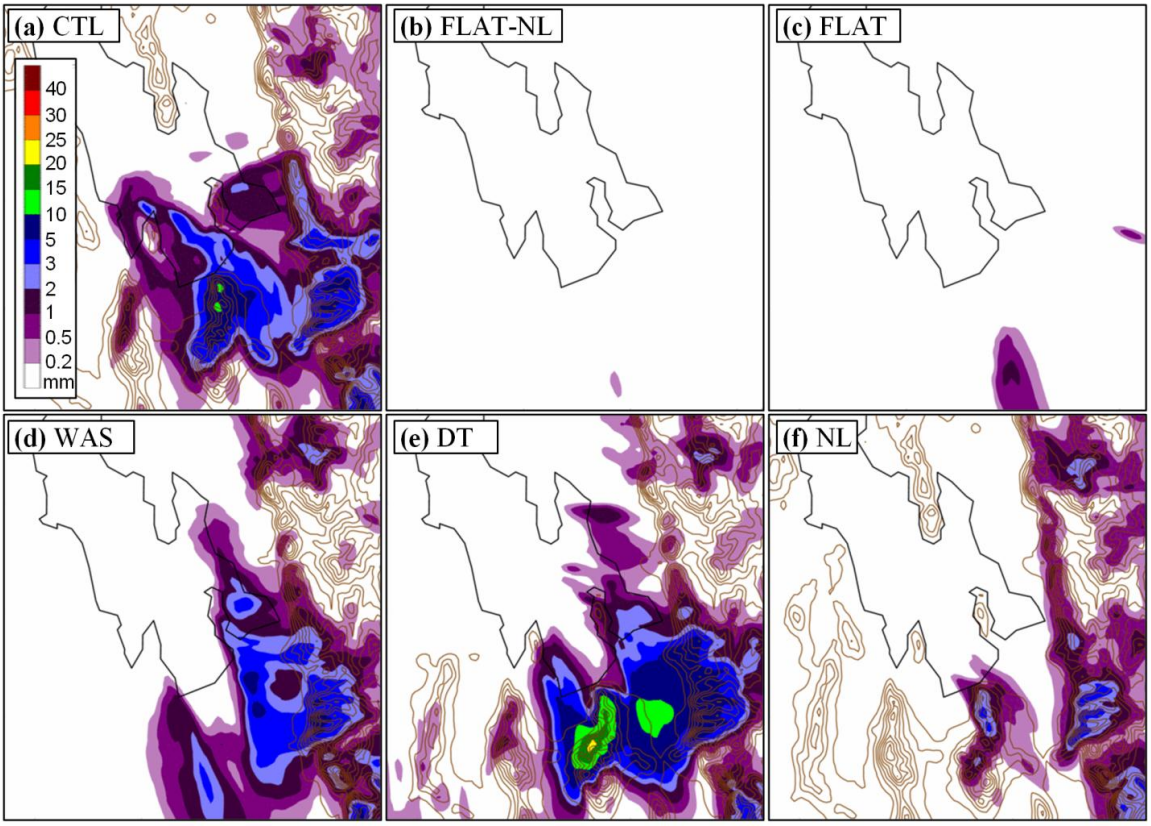


Fig. 3.21. Model terrain (brown contours every 200 m) and simulated precipitation (mm, shaded according to scale in [a]) from the (a) CTL, (b) FLAT-NL, (c) FLAT, (d) WAS, (e) DT, and (f) NL simulations for 1000–1800 UTC 5 Nov 2011. Lake outlines in (b) and (f) are shown for reference only.

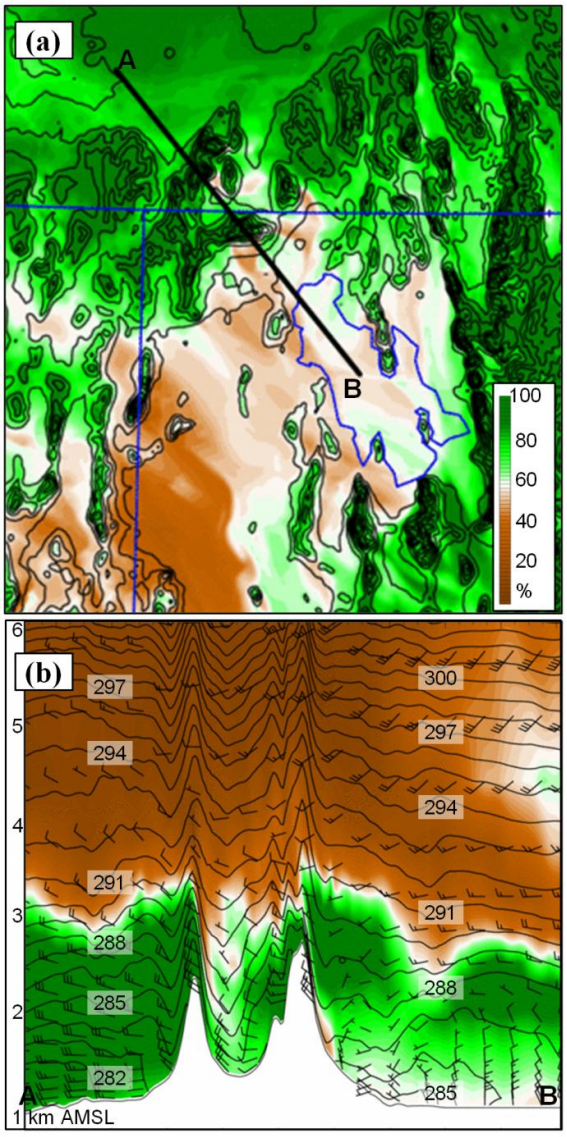


Fig. 3.22. Upstream modification. (a) Lowest sigma-level relative humidity (%, shaded according to scale at right) and terrain contours (200-m intervals) at 1230 UTC 5 Nov 2011. (b) Cross-section relative humidity (%, shaded according to scale in [a]), potential temperature (contoured at 1 K intervals) and winds (full barb = 5 m $s^{-1}$, half-barb = 2.5 m $s^{-1}$) averaged over 5 km either side of the thick black line in [a].

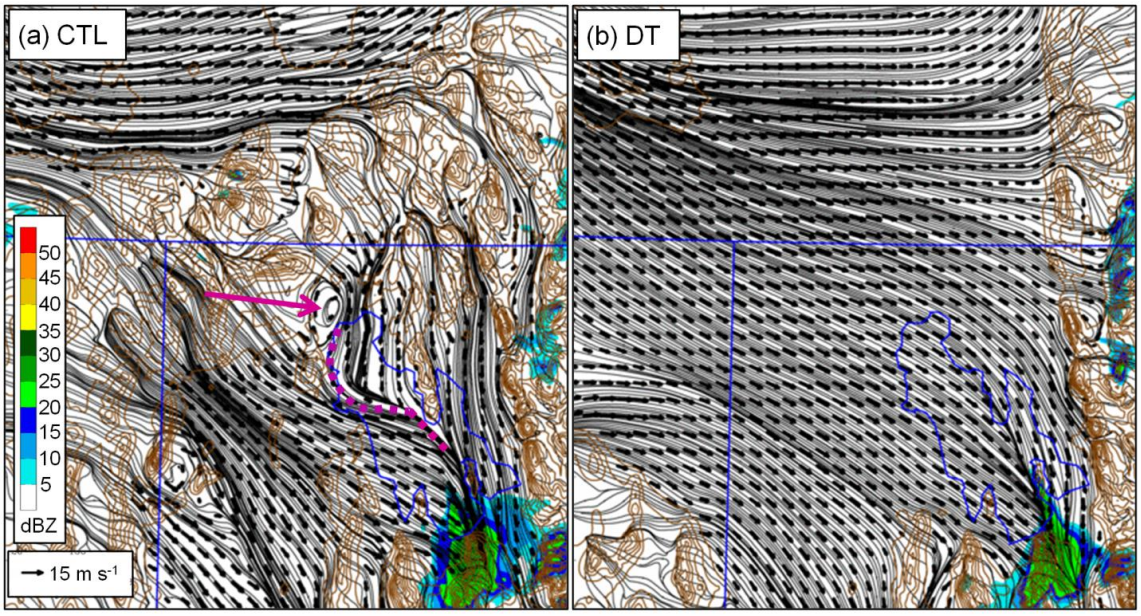


Fig. 3.23. Model terrain (brown contours every 200 m), 1500-m streamlines, wind vectors (length relative to sample vector in [a], and simulated reflectivity (dBZ, shaded according to scale in [a]) at 1230 UTC on 5 Nov 2011 for the (a) CTL; and (b) DT simulations. Purple arrows and dashed lines indicate wakes and confluence zones, respectively.

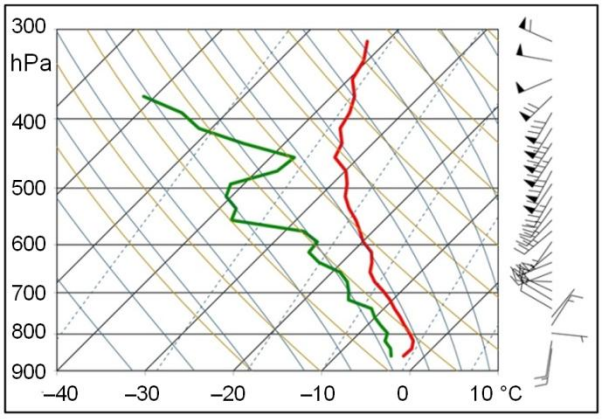


Fig. 3.24. Observed 1200 UTC sounding at KEL.

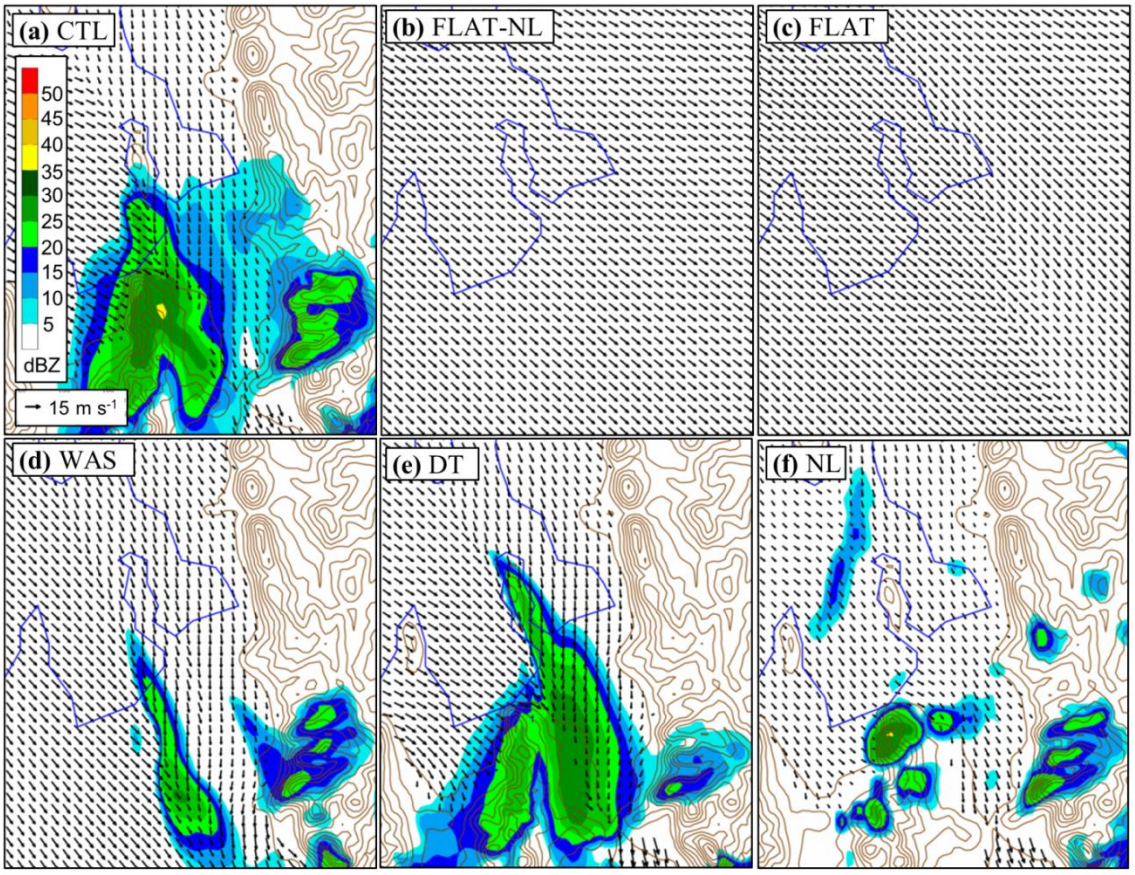


Fig. 3.25. Wind vectors (relative length according to scale in [a]) and simulated reflectivity (dBZ, shaded according to scale in [a]) for 1230 UTC 5 Nov 2011 in the (a) CTL, (b) FLAT-NL, (c) FLAT, (d) WAS, (e) DT, and (f) NL simulations. Lake outlines in (b) and (f) are shown for reference only.

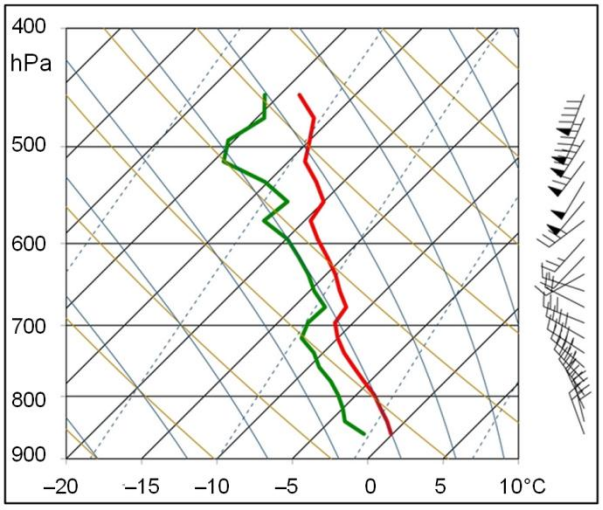


Fig. 3.26. Observed 1200 UTC sounding at ANT.

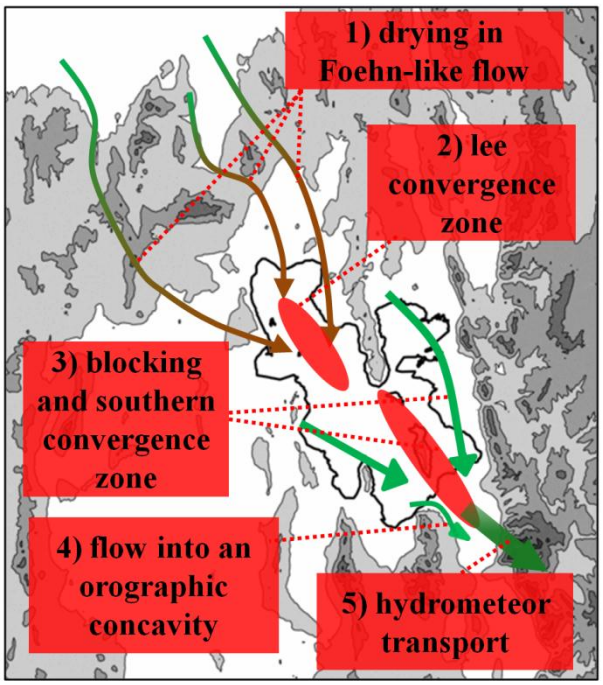


Fig. 3.27. Summary of orographic influences.

# CHAPTER 4

# CONCLUDING REMARKS

## Summary of Findings

For the updated climatology, 149 GSLE events were identified from analysis of radar data over the 13-year period from 1997/98 – 2009/10. The distribution of events over the period showed large interannual variability, which was more strongly correlated with atmospheric factors than the area of the GSL. GSLE events exhibited fall and spring peaks in frequency, and were less common in mid-winter when the lake temperature fell to near freezing. In fall and spring, however, GSLE occurs only at values of lake–700-hPa temperature difference ($\Delta T$) that greatly exceed the commonly used operational threshold of 16°C. A seasonally varying threshold ($\Delta T_{min}$), calculated from a quadratic curve fit to the monthly minimum $\Delta T$ values for GSLE soundings, is considered more appropriate for use in forecast applications than a single threshold value.

Our results suggest that low-level moisture is a crucial secondary ingredient for GSLE, even when large $\Delta T$ values are present. Alignment of the 700-hPa flow along the long axis of the GSL (i.e., near 325°) also substantially increases the likelihood of lake effect above that observed with westerly or northeasterly flow. GSLE only occurred when the lake temperature was greater than the average temperature at adjacent land stations, suggesting the importance of thermally driven land breezes in the initiation and maintenance of convection.

Banded GSLE, which tends to be associated with higher snowfall rates and thus greater transportation impacts, was more common than widespread, nonbanded convection when low-level (750-hPa) winds were strong (> 7 m $s^{-1}$) and when the lake temperature was much warmer than adjacent land stations. However, it remains an issue that there is substantial overlap in the conditions associated with these GSLE modes.

We propose a probabilistic approach to forecasting the occurrence of GSLE that considers $\Delta T_{excess}$, 850–700-hPa relative humidity, and 700-hPa wind direction. Although not a perfect indicator, the 700–500-hPa lapse rate and 700–500-hPa relative humidity can be used to anticipate the areal coverage of GSLE precipitation. Forecast errors in current 12-km operational NAM (and other) model guidance provide an additional source of uncertainty, and could lead forecasters to overestimate (in the case of the NAM) the probability of GSLE.

In our investigation of orographic influences, we examined two GSLE events where analysis of observations and numerical sensitivity studies indicate a synergistic, non-linear interaction between lake and orographic processes. Within the spectrum of lake-dominated to terrain-dominated precipitation, these events occur at a point where lake-air interactions and orographic flow modification are together crucial to the development of heavy precipitation. The major orographic influences include, but are not limited to: (1) low-level drying in a foehn-like flow over upstream terrain; (2) development of a convergence zone in the lee of isolated upstream obstacles; (3) overlake convergence due to blocking by the Wasatch Mountains; and (4) enhancement of convergence in the Salt Lake Valley due to the Oquirrh Mountains forming an orographic concavity. The role of orographic enhancement due to increased vertical motions over

high terrain was considered minimal in both events, although errors in the 5 Nov 2011 model simulation precluded a full evaluation.

In both events, model sensitivity studies involving the removal of either the lake or the surrounding terrain produce much less precipitation than the control cases. Thus our results demonstrate two situations where the relatively warm lake and high mountain ranges act together to yield significant precipitation episodes that would have been negligible without one or both of the lake and mountain components. These results, however, are not necessarily applicable to events that lie near the ends of the lake-orographic forcing spectrum (e.g., those that are exclusively dominated by either lake *or* orographic processes). As is often the case in a complex mesoscale environment, subtle changes in the low-level thermodynamic profile or background flow direction can have a large impact on these nonlinear lake-orographic interactions.

The results of the climatology and investigation of environmental influences are particularly pertinent to operational forecasting, and have already been incorporated into the lake-effect forecasting methodology at the National Weather Service in Salt Lake City. The work herein regarding orographic influences, although not directly applicable to weather prediction, provides useful insight into the complex mesoscale characteristics of GSLE storms. These events reflect synergistic interactions between lake-driven moist convection and orographically modified flows, bringing an added degree of complexity to the conceptual model of lake-effect precipitation developed for the Laurentian Great Lakes and small lakes such as Lake Champlain and the Finger Lakes.

## Future Work

The Center for Severe Weather Research Doppler-on-Wheels (DOW) mobile radar was operated continuously in the Salt Lake Valley during the 5 Nov 2011 event. Data from the DOW was not fully processed at the time of writing, but will eventually provide a unique perspective on a GSLE storm, with high vertical and temporal resolution. The DOW data, supplemented with observations from the SOLPEX field program could be utilized in a more observational examination of the 5 Nov 2011 event, with an emphasis on low-level kinematics and orographic microphysics.

The effectiveness numerical models in simulating the two case studies suggests some potential for improved operational forecasts of GSLE using high-resolution local models. I recommend a joint effort between the University of Utah and the National Weather Service to develop an operational local model, run at sub-2-km horizontal resolution, for northern Utah. Although the National Weather Service has subjectively identified an overprediction of GSLE by a previous 4-km model, improvements since then in the global models (e.g. the Global Forecast System) that supply initial and boundary conditions are expected to translate into improved high-resolution forecasts.

The Mountain Meteorology Group at the University of Utah has expressed an interest in the proposed Ontario Winter Lake-effect Storms project (OWLeS), which would utilize DOWs, mobile sounding units and mesonet stations. Our interest is in the influences of the Tug Hill Plateau on the evolution of these storms, representing a continuation of current research. We intend to compare the influences of steep terrain on a small lake (e.g., the GSL) to those for gently sloping terrain and a large lake, thereby generalizing results of the current study to a broader range of lake-mountain scenarios.

REFERENCES


Alcott, T. I., W. J. Steenburgh, and N. F. Laird, 2012: Great Salt Lake-effect precipitation: Observed frequency, characteristics and associated environmental factors. *Mon. Wea. Rev*., in press.

Andersson, T., and N. Gustafsson, 1994: Coast of departure and coast of arrival: Two important concepts for the formation and structure of convective snowbands over seas and lakes. *Mon. Wea. Rev.*, **122**, 1036–1049.

Andretta, T. A., D. S. Hazen, 1998: Doppler radar analysis of a Snake River Plain convergence event. *Wea. Forecasting*, **13**, 482–491.

Braham, R. R., and M. J. Dungey, 1984: Quantitative estimates of the effect of Lake Michigan on snowfall. *J. Climate Appl. Meteor.*, **23**, 940–949.

Browning, K. A., A. J. Eccleston, and G. A. Monk, 1985: The use of satellite and radar imagery to identify persistent shower bands downwind of the North Channel. *Q. J. R. Meteor. Soc.*, **114,** 325–331.

Carpenter, D. M., 1993: The lake effect of the Great Salt Lake: overview and forecast problems. *Wea. Forecasting*, **8**, 181–193.

Chen, F., and J. Dudhia, 2001: Coupling an advanced land surface-hydrology model with the Penn State-NCAR MM5 modeling system. Part I: Model implementation and sensitivity. *Mon. Wea. Rev.*, **129,** 569–585.

Chien, F.-C., and C. Mass, 1997: Interaction of a warm-season frontal system with the Coastal Mountains of the western United States. Part II: Evolution of a Puget Sound convergence zone. *Mon. Wea. Rev.*, **125,** 1730–1752.

Colle, B. A., and coauthors, 2005: High-resolution simulations and microphysical validation of an orographic precipitation event over the Wasatch Mountains during IPEX IOP3. *Mon. Wea. Rev.*, **133,** 2947–2971.

Cooper, K. A., M. R. Hjelmfelt, R. G. Derickson, D. A. R. Kristovich, and N. F. Laird, 2000: Numerical simulation of transitions in boundary layer convective structures in a lake-effect snow event. *Mon. Wea. Rev.*, **128**, 3283–3295.

Cordeira, J. M., and N. F. Laird, 2008: The influence of ice cover on two lake-effect snow events over Lake Erie. *Mon. Wea. Rev.*, **136**, 2747–2763.

Cosma, S., E. Richard, and F. Miniscloux, 2002: The role of small-scale orographic features in the spatial distribution of precipitation. *Q. J. R. Meteorol. Soc.*, **128,** 75–92

Cox, J. A. W., W. J. Steenburgh, D. E. Kingsmill, J. C. Shafer, B. A. Colle, O. Bousquet, B. F. Smull, H. Cai, 2005: The kinematic structure of a Wasatch Mountain winter storm during IPEX IOP3. *Mon. Wea. Rev.*, **133**, 521–542.

Crosman, E. T., and J. D. Horel, 2010: MODIS-derived surface temperature of the Great Salt Lake, 2008. *Remote Sensing of Environment*, **113,** 73–81.

Crum, T. D., R. L. Alberty, and D. W. Burgess, 1993: Recording, archiving, and using WSR-88D data. *Bull. Amer. Meteor. Soc.*, **74**, 645–653.

Dickson, D. R., J. H. Yepsen, and J. V. Hales, 1965: Saturated vapor pressures over Great Salt Lake brine. *J. Geophys. Res.*,**70,** 500–503.

Eichenlaub, V. L., 1970: Lake-effect snowfall to the lee of the Great Lakes: Its role in Michigan. *Bull. Amer. Meteor. Soc.*, **51**, 403–412.

Eito, H., T. Kato, M. Yoshizaki, and A. Adachi, 2005: Numerical simulation of the quasi-stationary snowband observed over the southern coastal area of the Sea of Japan on 16 January 2001. *J. Meteor. Soc. Japan*, **83,** 551–576.

Fuhrer, O., and C. Schär, 2005: Embedded cellular convection in moist flow past topography. *J. Atmos. Sci.*, **62**, 2810–2828.

Fuhrer, O., and C. Schär, 2007: Dynamics of orographically triggered banded convection in sheared moist orographic flows. *J. Atmos. Sci.*, **64**, 3542–3561.

Hill, J. D., 1971: Snow squalls in the lee of Lakes Erie and Ontario. NOAA Tech. Memo., NWS ER-43.

Hjelmfelt, M. R., and R. R. Braham, 1983: Numerical simulation of the airflow over Lake Michigan for a major lake-effect snow event. *Mon. Wea. Rev.*, **111**, 205–219.

Hjelmfelt, M. R., 1990: Numerical study of the influence of environmental conditions on lake-effect snowstorms over Lake Michigan. *Mon. Wea. Rev.*, **118**, 138–150.

Hjelmfelt, M. R., 1992: Orographic effects in simulated Lake-Effect snowstorms over Lake Michigan. *Mon. Wea. Rev.*, **120**, 373–377.

Holroyd, E. W., 1971: Lake-effect cloud bands as seen from weather satellites. *J. Atmos. Sci.*, **28**, 1165–1170.

Hong, S.-Y., Y. Noh, and J. Dudhia, 2006: A new vertical diffusion package with an explicit treatment of entrainment processes. *Mon. Wea. Rev.,* **134,** 2318–2341.

Horel, J., and coauthors, 2002: Mesowest: Cooperative mesonets in the western United States. *Bull. Amer. Meteor. Soc.*, **83**, 211–225.

Hozumi, K., and C. Magono, 1984: The cloud structure of convergent cloud bands over the Japan Sea in winter monsoon period. *J. Meteor. Soc. Japan*, **62,** 522–533.

Iacono, M. J., J. S. Delamere, E.J. Mlawer, M. W. Shephard, S. A. Clough, and W. D. Collins, 2008: Radiative forcing by long-lived greenhouse gases: Calculations with the AER radiative transfer models, *J. Geophys. Res.*, **113,** D13103, doi:10.1029/2008JD009944.

Kain, J. S., 2004: The Kain-Fritsch convective parameterization: an update. *J. Appl. Meteor.*, **43,** 170–181.

Kindap, T., 2010: A severe sea-effect snow episode over the city of Istanbul. *Nat. Hazards,* **54,** 707–723.

Kirshbaum, D. J., and D. R. Durran, 2004: Factors governing cellular convection in orographic precipitation. *J. Atmos. Sci.,* **61,** 682–698.

Kirshbaum, D. J. and D. R. Durran, 2005a: Atmospheric factors governing banded orographic convection. *J. Atmos. Sci.,* **62,** 3758–3774.

Kirshbaum, D. J. and D. R. Durran, 2005b: Observations and modeling of banded orographic convection. *J. Atmos. Sci.,* **62,** 1463–1479.

Kristovich, D. A., 1993: Mean circulations of boundary-layer rolls in lake-effect snow storms. *Bound.-Layer Meteor.*, **63,** 293–315.

Kristovich, D. A. R., and N. F. Laird, 1998: Observations of widespread lake-effect cloudiness: Influences of lake surface temperature and upwind conditions. *Wea. Forecasting*, **13**, 811–821.

Kristovich, D. A. R., N. F. Laird, M. R. Hjelmfelt, R. G. Derickson, and K. A. Cooper, 1999: Transitions in boundary layer meso-γ convective structures: An observational case study. *Mon. Wea. Rev.*, **127**, 2895–2909.

Kristovich, D. A. R., and M. L. Spinar, 2005: Diurnal variations in lake-effect precipitation near the western Great Lakes. *J. Hydrometeor.*, **6,** 210–218.

Kusunoki, K., and Coauthors, 2004: The characteristics and evolution of orographic snow clouds under weak cold advection. *Mon. Wea. Rev.*, **132,** 174–191.

Laird, N. F., 1999: Observation of coexisting mesoscale lake-effect vortices over the western Great Lakes. *Mon. Wea. Rev.*, **127**, 1137–1141.

Laird, N. F., D. A. R. Kristovich, and J. E. Walsh, 2003a: Idealized model simulations examining the mesoscale structure of winter lake-effect circulations. *Mon. Wea. Rev.*, **131**, 206–221.

Laird, N. F., J. E. Walsh, and D. A. R. Kristovich, 2003b: Model simulations examining the relationship of lake-effect morphology to lake shape, wind direction, and wind speed. *Mon. Wea. Rev.*, **131**, 2102–2111.

Laird, N. F., and D. A. R. Kristovich, 2004: Comparison of observations with idealized model results for a method to resolve winter lake-effect mesoscale morphology. *Mon. Wea. Rev.*, **132**, 1093–1103.

Laird, N. F., J. Desrochers, and M. Payer, 2009a: Climatology of lake-effect precipitation events over Lake Champlain. *J. Appl. Meteor. Climatol.*, **48**, 232–250.

Laird, N., R. Sobash, and N. Hodas, 2009b: The frequency and characteristics of lake-effect precipitation events associated with the New York State Finger Lakes. *J. Appl. Meteor. Climatol.*, **48**, 873–886.

Laird, N., R. Sobash, and N. Hodas, 2010: Climatological conditions of lake-effect precipitation events associated with the New York State Finger Lakes. *J. Appl. Meteor. Climatol.*, **49**, 1052–1062.

Lavoie, R. L., 1972: A mesoscale numerical model of lake-effect storms. *J. Atmos. Sci.*, **29,** 1025–1040.

Magono, C., K. Kikuchi, T. Kimura, S. Tazawa, and T. Kasai, 1966: A study on the snowfall in the winter monsoon season in Hokkaido with special reference to low land snowfall. *J. Fac. Sci., Hokkaido Univ., Ser. VII*, **11,** 287–308.

Markowski, P., and Y. Richardson, 2010: *Mesoscale Meteorology in Midlatitudes*. Wiley-Blackwell. 407 pp.

Mass, C., 1981: Topographically forced convergence in western Washington State. *Mon. Wea. Rev.*, **109,** 1335–1347.

Mass, C., and D. P. Dempsey, 1985: A topographically forced convergence line in the lee of the Olympic Mountains. *Mon. Wea. Rev.*, **113,** 659–663.

Mayr, G. J., and T. B. McKee, 1995: Observations of the evolution of orogenic blocking. *Mon. Wea. Rev.*, **123**, 1447–1464.

Matsuura, S., K. Matsuyama, S. Asano, T. Okamoto, and Y. Takeuchi, 2005: Fluctuation of the seasonal snowpack in a mountainous area of the heavy-snow district in the warm-temperate zone of Japan. *J. Glaciol.,* **51,** 547–554.

McGowan, H. A., I. F. Owens, A. P. Sturman, 1995: Thermal and dynamic characteristics of alpine lake breezes, Lake Tekapo, New Zealand. *Boundary-Layer Meteorol.,* **76,** 3–24.

Mesinger, F., and Coauthors, 2006: North American Regional Reanalysis. *Bull. Amer. Meteor. Soc.,* **87**, 343–360.

Mitchell, C. L., 1921: Snow flurries along the eastern shore of Lake Michigan. *Mon. Wea. Rev.*, **49,** 502-503.

Murphy, A. H., 1991: Probabilities, odds, and forecasts of rare events. *Wea. Forecasting*, **6**, 302–307.

Niziol, T. A., 1987: Operational forecasting of lake-effect snowfall in western and central New York. *Wea. Forecasting*, **2**, 310–321.

Niziol, T. A., W. R. Snyder, and J. S. Waldstreicher, 1995: Winter weather forecasting throughout the eastern United States. Part IV: Lake-effect snow. *Wea. Forecasting*, **10**, 61–77.

Onton, D. J., and W. J. Steenburgh, 2001: Diagnostic and sensitivity studies of the 7 December 1998 Great Salt Lake–effect snowstorm. *Mon. Wea. Rev.*, **129**, 1318–1338.

Passarelli, R. E., and R. R. Braham, 1981: The role of the winter land breeze in the formation of Great Lake snow storms. *Bull. Amer. Meteor. Soc.*, **62**, 482–492.

Payer, M., J. Desrochers, and N. F. Laird, 2007: A lake-effect snowband over Lake Champlain. *Mon. Wea. Rev.*, **135**, 3895–3900.

Phillips, D. W., 1972: Modification of surface air over Lake Ontario in winter. *Mon. Wea. Rev.*, **100**, 662–670.

Saito, K., M. Murakami, T. Matsuo, and H. Mizuno, 1996: Sensitivity experiments on the orographic snowfall over the mountainous region of northern Japan. *J. Meteor. Soc. Japan,* **74,** 797–813.

Sinclair, M. R., 1994: A diagnostic model for estimating orographic precipitation. *J. Appl. Meteor.,* **33,** 1163–1175.

Smith, R. B., Q. Jiang, M. G. Fearon, P. Tabary, M. Dorninger, J. D. Doyle, and R. Benoit, 2003: Orographic precipitation and air mass transformation: An Alpine example. *Quart. J. Roy. Meteor. Soc.,* **129,** 433–454.

Smith, R. B., I. Barstad, and L. Bonneau, 2005: Orographic precipitation and Oregon's climate transition. *J. Atmos. Sci.*, **62,** 177–191

Splitt, M. E., and J. D. Horel, 1998: Use of multivariate linear regression for meteorological data analysis and quality assessment in complex terrain. Preprints, *10th Symp. on Meteorological Observations and Instrumentation*, Phoenix, AZ, Amer. Meteor. Soc., 359–362.

Steenburgh, W. J., S. F. Halvorson, and D. J. Onton, 2000: Climatology of lake-effect snowstorms of the Great Salt Lake. *Mon. Wea. Rev.*, **128**, 709–727.

Steenburgh, W. J., and D. J. Onton, 2001: Multiscale analysis of the 7 December 1998 Great Salt Lake–effect snowstorm. *Mon. Wea. Rev.*, **129**, 1296–1317.

Steenburgh, W. J., 2003: One hundred inches in one hundred hours: Evolution of a Wasatch Mountain winter storm cycle. *Wea. Forecasting*, **18**, 1018–1036.

Stewart, J. Q., C. D. Whiteman, W. J. Steenburgh, and X. Bian, 2002: A climatological study of thermally driven wind systems of the U. S. Intermountain West. *Bull. Amer. Meteor. Soc.*, **83,** 699–708.

Thompson, G., P. R. Field, R. M. Rasmussen, and W. D. Hall, 2008: Explicit forecasts of winter precipitation using an improved bulk microphysics scheme. Part II: Implementation of a new snow parameterization. *Mon. Wea. Rev.*, **136,** 5095–5114.

Tripoli, G. J., 2005: Numerical study of the 10 January 1998 lake-effect bands observed during Lake-ICE. *J. Atmos. Sci.*, **62**, 3232–3249.

U. S. Census Bureau, cited 2011: 2010 Census Data. [Available online at http://2010.census.gov/2010census/data/.]

U. S. Geological Survey (USGS), cited 2012: Great Salt Lake, Utah. [Available online at http://ut.water.usgs.gov/greatsaltlake/.]

Varney, B. M., 1920: Monthly variations of the precipitation–altitude relation in the central Sierra Nevada of California. *Mon. Wea. Rev.*, **48,** 648–650.

Watson, C. D., and T. P. Lane, 2012: Sensitivities of orographic precipitation to terrain geometry and upstream conditions in idealized simulations. *J. Atmos. Sci.*, submitted.

Weckwerth, T. M., J. W. Wilson, R. M. Wakimoto, and N. A. Crook, 1997: Horizontal convective rolls: determining the environmental conditions supporting their existence and characteristics. *Mon. Wea. Rev.*, **125**, 505–526.

Wiggin, B. L., 1950: Great snows of the Great Lakes. *Weatherwise*, **3,** 123–126.

Wilson, J. W., 1977: Effect of Lake Ontario on precipitation. *Mon. Wea. Rev.*, **105**, 207–214.

Wood, V. T., R. A. Brown, and S. V. Vasiloff, 2003: Improved detection using negative elevation angles for mountaintop WSR-88Ds. Part II: Simulations of the three radars covering Utah. *Wea. Forecasting*, **18**, 393–403.

Yeager, K. N., W. J. Steenburgh, and T. I. Alcott, 2013: Contributions of lake-effect periods to the cool-season hydroclimate of the Great Salt Lake basin. *J. Appl. Meteor.*, submitted. [Available at http://www.inscc.utah.edu/~steenburgh/papers/DLEclimo.pdf]